AN ABSTRACT OF THE THESIS OF

Mitchell Lyle for the degree of Doctor of Philosophy

in Oceanography presented on June 21, 1978

Title: THE FORMATION AND GROWTH OF FERROMANGANESE OXIDES ON THE NAZCA PLATE

Redacted for privacy

Abstract Approved: John B. Corliss

Redacted for privacy

Jack Dymond

Marine ferromanganese oxides form four major ferromanganese deposits: Hydrothermal crusts, ferromanganese coatings on basalt, ferromanganese nodules, and a mixture of micronodules and other dispersed hydroxyoxides within marine sediments.

Hydrothermal crusts grow only near active marine hydrothermal systems that cool newly emplaced basaltic crust. The crusts are characterized by rapid growth rates, extreme fractionation of Mn from Fe, low accessory element concentrations, and well crystallized manganese minerals.

Ferromanganese coatings on basalt can receive an Fe-rich component from hydrothermal source but are mainly composed of ferromanganese oxides grown by direct precipitation from seawater (hydrogenous formation). They have δ-MnO_2 mineralogy, have almost equal Mn and Fe abundances, are relatively enriched in the rare earth elements, highly en-

riched in Ce and Co, and have relatively low Cu, Ni, and Zn abundances. Coatings with a large hydrothermal component are more enriched in Fe, and generally have lower trace element contents.

Nodule and micronodule compositional variations resulting from different sources of transition metals may be further modified by diagenetic reactions within the sediments. The most extreme of these is preferential reductive mobilization of manganese within the sediment column by oxidation of organic carbon and subsequent Mn diffusion to the seawater-sediment interface. Because supply of organic carbon to marine sediments comes primarily from biological productivity in the surface waters and to a lesser extent from terrigenous sources, ferromanganese oxides formed or altered by this process lie beneath highly productive surface waters or near continents. They are characterized by relatively pure well-crystallized manganese oxides, generally the 7 Å mineral birnessite, and by rapid growth rates. Mn/Fe ratios are 5 or greater, and accessory element contents are low.

Ferromanganese deposits enriched in Mn relative to hydrogenous precipitates are also found in the Bauer Deep and other areas along the fringes of the most highly productive regions, where sediments are not reducing enough to remobilize Mn. Oxic diagenetic reactions, such as Fe-smectite formation from biogenic opal, fractionate Fe from ferromanganese hydroxyoxides. The released Mn precipitates as nodules and micronodules.

Iron and manganese that form the ferromanganese deposits have only two ultimate sources: runoff from the continents and hydrothermal fluids that have interacted with cooling basalts formed on the mid-ocean ridges. Seawater acts as a reservoir and mixing chamber for these two sources and currents carry the added metals far from their input point. The relative magnitudes of terrigenous and hydrothermal input are roughly equal on the Nazca Plate, although terrigenous input may dominate worldwide.

THE FORMATION AND GROWTH OF FERROMANGANESE OXIDES ON THE NAZCA PLATE

by

Mitchell Lyle

A THESIS

submitted to

Oregon State University

in partial fulfillment of
the requirements for the
degree of

Doctor of Philosophy

Completed June 1978

Commencement June 1979

APPROVED:

Redacted for privacy

Redacted for privacy

Professors of Oceanography in Charge of Major

Redacted for privacy

Acting Dean of School of Oceanography

Redacted for privacy

Dean of Graduate School

Date thesis is presented June 21, 1978

Typed by Cheryl Schurg for Mitchell Lyle

ACKNOWLEDGEMENTS

There are always a great number of people that help to make a thesis possible. I wish to first thank my two advisors, Jack Dymond and Jack Corliss, whose support and advice made the job so much easier. I would also like to thank the rest of my committee, Erwin Suess, Julius Dasch, Arthur Chen, and Carroll DeKock for their help and their criticism on various thesis drafts.

Pat Price, Libby Asbury, Mark Hower, Bobbi Conard, and Andy Ungerer were all valuable help during the gathering and analysis of the data while Cheryl Schurg and Lindy Zeeman slaved long hours at the typewriter to finish the thesis.

I would finally like to thank my other friends who helped me get through, either by their direct aid on the thesis or by various and other means: Chris Moser, Debbie Stakes, Roger Hart, Margaret Leinen, Chiye Wenkam, Connie Sancetta, Terry and Heidi Chriss, John Toth, Bruce Selk, Ralph Moore, Gail Davis, Greg Malstaff, Frances Stilwell, Ron Stillinger, and a certain A.G. Tanner.

My support was provided by an International Nickel Company Fellowship and by the NSF/IDOE Nazca Plate Project.

III.

science walks in beauty:

nets are many knots
skin is border-guard, a pelt is borrowed warmth;
a bow is the flex of a limb in the wind
a giant downtown building
    is a creekbed stood on end.

detritus pathways. "delayed and complex ways
to pass the food through webs."

maturity. stop and think. draw on the mind's
stored richness. memory, dream, half-digested
image of your life. "detritus pathways"--feed
the many tiny things that feed an owl.
send heart boldly travelling,
on the heat of the dead & down.

Gary Snyder

'Towards Climax'

FOR MY PARENTS

TABLE OF CONTENTS

TABLE OF CONTENTS (continued)

LIST OF FIGURES

LIST OF FIGURES (continued)

LIST OF FIGURES (continued)

LIST OF TABLES

CHAPTER 1

COPPER-NICKEL-ENRICHED FERROMANGANESE NODULES AND ASSOCIATED CRUSTS FROM THE BAUER BASIN, NORTHWEST NAZCA PLATE

Mitchell Lyle

School of Oceanography
Oregon State University
Corvallis, OR 97331

Earth and Planetary Science Letters, 35 (1977) 55–64

[1]

COPPER-NICKEL-ENRICHED FERROMANGANESE NODULES AND ASSOCIATED CRUSTS FROM THE BAUER BASIN, NORTHWEST NAZCA PLATE

MITCHELL LYLE, JACK DYMOND

School of Oceanography, Oregon State University, Corvallis, Ore. 97331 (USA)

and

G. ROSS HEATH

Graduate School of Oceanography, University of Rhode Island, Kingston, R.I. 02881 (USA)

Received November 29, 1976
Revised version received February 14, 1977

Analysis of a suite of ferromanganese nodules and crusts from the dredge Y73-3-22D in the Bauer Deep (13°40'S, 102°08'W) shows distinct differences between the nodules and crusts. Ultra-slow-scan X-ray diffraction shows that the nodules are more enriched in todorokite while the crusts are more enriched in δMnO_2. Both have phillipsite and smectite as accessory minerals as well as minor amounts of apatite, barite, and quartz. Chemical analyses show that the nodules also have higher abundances of Mn, Ni, Cu, Zn, and Ba, while crusts are more enriched in Fe, Co, and Ca. We suggest that normal authigenic precipitation of ferromanganese oxyhydroxides from seawater controls the mineralogy and chemistry of the crusts, while nodule mineralogy and chemistry are governed by small-scale diagenetic reactions in the sediment. Todorokite may form because iron in the Fe-Mn oxyhydroxide material dispersed in the sediment reacts with amorphous silica to form iron-rich smectites. The remaining oxyhydroxide material recrystallizes as todorokite.

1. Introduction

Nodules enriched in Cu and Ni have long been known from a zone parallel to the equator in the northeastern Pacific (Fig. 1) [1,2]. The Cu and Ni enrichments have been ascribed to: (1) a high influx of these elements in biogenic debris [3]; (2) high porosity of the radiolarian clay substrate, allowing free upward diffusion of metal ions [4]; (3) enhanced upward migration of the metals in sediments enriched in organic matter (i.e. in sediments beneath productive surface waters [5]); and (4) repeated burial and exhumation of nodules in the dynamic depositional regime where bottom waters flow into the North Pacific southeast of Hawaii [6]. The lack of metal-enriched nodules beneath the equator, in apparent defiance of 1 and 3 above, can be attributed to rapid deposition of calcareous ooze [7] which inhibits the development of the slowly growing concretions [8].

If hypothesis 1, 2 or 3 is correct, then the belt of enriched nodules at about 10°N should be matched by an equivalent belt south of the equator. Hypothesis 4 does not require such a southern zone. Recent analyses have identified Cu-Ni-enriched nodules around 12°S, 80–90°W and 135–145°W (Fig. 1). This paper describes similarly enriched nodules from the Bauer Deep, east of the East Pacific Rise, at about 14°S. These nodules are of particular interest because they are associated with sediments rich in hydrothermal components derived from the nearby rise crest [9,10].

Our samples were collected from R/V "Yaquina" during cruise YALOC-73 of Oregon State University. Nodules were recovered at 5 of 18 stations within the Bauer Deep. Four of these were piston core stations, at each of which more than one nodule was recovered. The fifth, a dredge station (Y73-3-22D; 13°40'S, 102°8'W) collected 834 ferromanganese nodules, as well as numerous ferromanganese crusts attached to or broken from highly altered basalts.

The sediment in the Bauer Basin is unusually en-

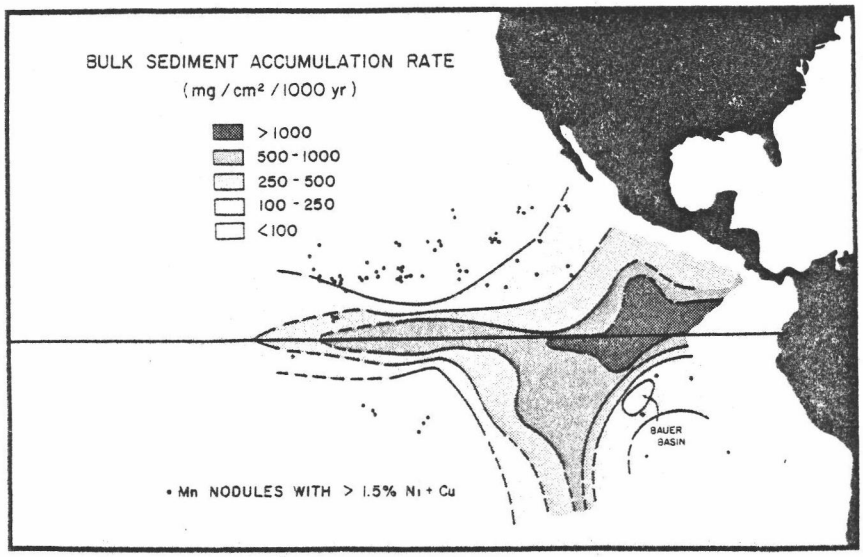

Fig. 1. Bulk sediment accumulation rates in the eastern Pacific. Accumulation rate data from references 16–20. Dots represent stations between 20° N and 20° S where nodules that contain greater than 1.5% (Cu + Ni) have been collected. Mn nodule data from Mero [1] and Monget et al. [21].

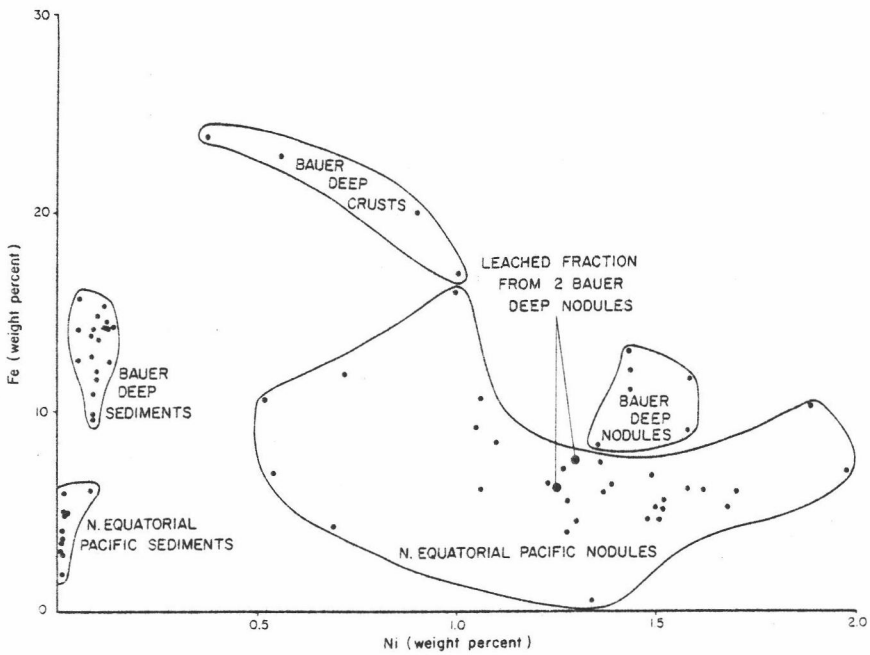

Fig. 2. Fields of Bauer Deep and north equatorial Pacific sediments, nodules and crusts in a Ni–Fe coordinate system. North equatorial Pacific sediment analyses from Cronan [22]; equatorial Pacific nodule analyses from Mero [1] and Monget et al. [21].

riched in transition metals [10]. The Fe contents of these sediments are nearly double those in northern equatorial Pacific sediments (Fig. 2). Mn, Ni, and Cu are also enriched. If the composition of the sedimentary substrate controls nodule composition, the Bauer Basin nodules might be expected to have distinctive compositions. We have determined the mineralogy and chemical composition of a suite of nodules and associated crusts from the Bauer Basin to test this possibility, and to further constrain the conditions that govern the chemical composition of equatorial Pacific nodules.

2. Description of nodules and crusts

Ferromanganese nodules recovered in Y73-3-22D can be divided into six morphological types. Six samples of four of these morphologies were studied in this paper (see Table 1 for a description of morphologic types and for a list of samples studied).

In addition to the nodules, four samples of ferromanganese crust were also analyzed to determine whether the chemistry and mineralogy of the ferromanganese phases depend on the mode of occurrence. Two of the samples were from the surfaces of altered basalt fragments. The other two were from competent pieces of

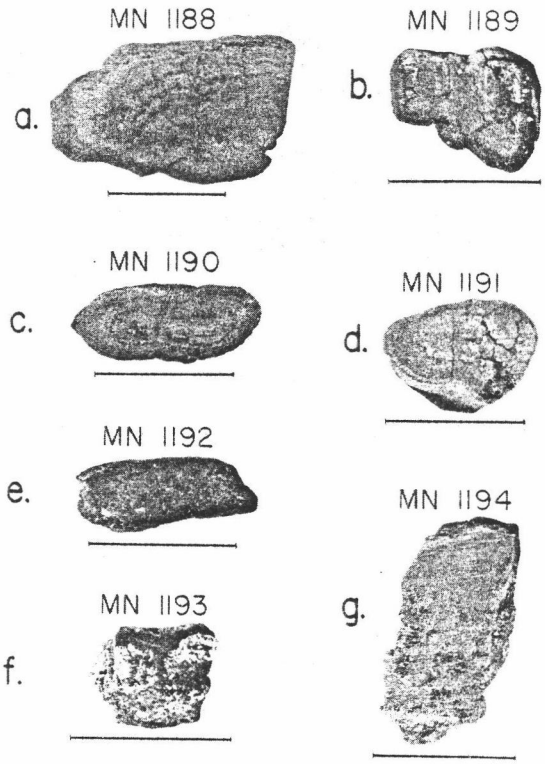

Fig. 3. Photographs of nodules included in this study. Scale bar is 2 cm in each case.

TABLE 1

Manganese nodule types in Y73-3-22D

Type	Size (cm)	Percentage of total nodules recovered of a given type	Samples in study	Description
1	0.5–2	33	MN 1191 HN 1440	Ellipsoidal to subspherical shape. Entire surface simple, somewhat grainy, slightly abraded (during dredging?). Core of ferromanganese material. Fig. 3d
2		41	MN 1189	Multicentered nodules, mostly type 1, grown together. Simple, somewhat grainy surface. Core of ferromanganese material. Fig. 3b
3	0.5–3	14	MN 1190	Discoidal nodules grading to flat ellipsoids (type 4) and to type 1. Simple, grainy surface. Core in MN 1190 a fragment of an older nodule. Fig. 3c.
4	0.5–8	5	MN 1188	Flat ellipsoidal nodules. Surface generally smooth, simple surface on one side, botryoidal on other. Nodules grade into type 3. Core in MN 1188 a fragment of older nodules. Fig. 3a
5	0.5–8	3		Highly irregular botryoidal nodules. Similar to masses of type 1 nodules or perhaps crusts overgrowing basalt fragments. Grades to types 4 and 2
6		3		Abraded and often angular fragments, possibly exposed scree

crust lacking attached substrates. MN 1192 is a sample from the surface 1 cm of a 2–3-cm crust that completely covers a 20-cm highly altered basalt fragment. There is no visible layering in the crust (Fig. 3e) and it contains minimal amounts of light-colored silicate phases. In contrast, MN 1193 contains a major amount of the light-colored phases. The sample, from a 1–3-cm crust on a 15-cm fragment of highly altered basalt, consists of regularly layered ferromanganese oxides surrounding yellow lobes (Fig. 3f). MN 1194 and HN 1442 are both samples of dense crusts. They are quite competent, fracture conchoidally, and exhibit no layering (Fig. 3g). They appear to have broken off a basalt pillow or other object with a radius of curvature of some tens of centimeters.

3. Methods of analysis

The six nodules and four crusts from Y73-3-22D were analyzed both chemically and mineralogically. One cross-section through each sample was ground in an agate mortar, dissolved with hydrofluoric acid and aqua regio under pressure, and analyzed by atomic absorption spectrophotometry for Fe, Mn, Cu, Ni, Zn, Co, Ba, Ca, Si, and Al (see Dymond et al. [9] for complete methodology). Splits of two nodules and one crust were leached with ammonium oxalate-oxalic acid [11]. This leach preferentially attacks poorly crystalline iron and manganese oxyhydroxides, leaving behind well crystalline Fe phases such as goethite. It also strongly attacks Mn minerals such as todorokite or δMnO_2. The dissolved material was analyzed for Fe, Mn, Cu, Ni, Zn, Co, Ba, Si, and Al to determine the partitioning of these elements between the oxyhydroxides and the more refractory phases. Ca was not analyzed in the leachate because it forms an insoluble oxalate precipitate. Results of all the chemical analyses are given in Table 2.

A second cross-section of each nodule was ground under liquid nitrogen to less than 200 mesh for X-ray diffraction analysis using Cu radiation (graphite crystal monochromator). Random mounts of the ground material were scanned from 5° to 70° 2θ using an ultra-slow-scan rate of 500 seconds per degree. Three representative diffractograms are shown in Fig. 4. They represent end member samples as defined by both chemical and mineralogical analysis. X-ray diffraction analyses were also performed on the residues left after the ammonium oxalate leach of nodule HN 1441 and crust HN 1442, to identify the non-oxide phases included in the nodules and crusts of the Bauer Deep.

4. Results

4.1. Mineralogy

Following the classification scheme outlined by Burns and Burns [12] two manganese minerals, δMnO_2 and todorokite can be identified in the bulk-sample diffractograms (Fig. 4). The lack of a 3.60-Å reflection indicates that birnessite is not present, even though there are 7-Å diffractions (due to phillipsite plus the 002 reflection of a poorly crystalline smectite) in most of the samples.

The relative abundance of todorokite and δMnO_2 in each sample can be estimated from the ratio of the 9.8-Å todorokite peak area to the 1.42-Å peak area common to both todorokite and δMnO_2. If δMnO_2 dominates the sample, this ratio should approach zero. If todorokite dominates, the ratio will approach a finite upper limit reflecting the relative intensity of these two peaks in pure todorokite. The observed ratio differs significantly from nodules to crusts (Fig. 5 and Table 2). Nodules are relatively enriched in todorokite and have an average 9.8 Å/1.42 Å ratio of 2.2. Crusts, on the other hand, with an average ratio of only 0.6, must contain more δMnO_2. Diffractograms of the two extreme samples, the nodule MN 1188 and the crust Mn 1194, are shown in Fig. 4. Their 9.8 Å/1.42 Å peak area ratios are 3.5 and 0.0, respectively.

Accessory minerals identifiable in the bulk-sample diffractograms are phillipsite, quartz, and smectite. Only in crust MN 1193 do phillipsite peaks dominate the diffractogram. This is consistent with the macroscopic descriptions of major inclusions of yellow non-oxide phases (Fig. 3f). Most of the samples contain only minor amounts of accessory minerals. Residual phases comprise about 20 wt.% of the two nodules and one crust that were leached by the ammonium oxalate-oxalic acid technique. Diffractograms of the residue from this leach again show phillipsite, quartz

TABLE 2

Composition of nodules and crusts in the Bauer Basin (in wt.%)

Sample	9.8 Å/1.42 Å peak area ratio	Al	Si	Si/Al	Ca	Mn	Fe	Co	Ni	Cu	Zn	Ba
Nodules												
MN 1188	3.5	1.36	3.67	2.71	1.35	33.8	8.26	0.064	1.36	0.801	0.239	0.371
MN 1188 top surface	–	1.69	4.10	2.44	1.77	28.7	11.5	0.103	1.51	0.622	0.178	0.285
MN 1188 bottom surface	–	1.14	3.23	2.85	1.91	32.3	10.1	0.109	1.37	0.697	0.230	0.277
MN 1189	2.2	1.76	4.08	2.31	1.54	28.5	12.1	0.111	1.44	0.658	0.149	0.270
MN 1190	2.1	1.65	3.70	2.25	1.65	31.8	9.06	0.093	1.58	0.829	0.193	0.238
MN 1191	1.7	1.60	3.91	2.45	1.55	27.9	11.7	0.113	1.59	0.625	0.160	0.230
HN 1440	1.7	1.78	4.23	2.38	1.81	27.0	13.1	0.103	1.43	0.730	0.162	0.224
HN 1441	2.0	1.91	5.06	2.65	1.86	27.6	11.0	0.093	1.44	0.702	0.169	0.197
Average bulk composition	2.2	1.68	4.11	2.45	1.63	29.5	10.9	0.096	1.47	0.724	0.179	0.255
Average north equatorial Pacific composition (Ni + Cu > 1.5%)	–	2.94	7.29	2.48	1.24	28.1	6.22	0.22	1.49	1.17	0.133	0.406
Crusts												
MN 1192	0.8	1.42	4.23	2.97	1.72	21.9	20.1	0.144	0.903	0.305	0.091	0.170
MN 1193	1.2	2.92	8.76	3.01	1.04	16.8	17.0	0.078	1.05	0.444	0.095	0.125
MN 1194	0	1.49	5.46	3.66	1.95	17.8	23.9	0.132	0.378	0.174	0.063	0.167
HN 1442	0.4	1.18	5.01	4.24	2.17	19.5	22.9	0.149	0.561	0.250	0.069	0.149
Average bulk composition	0.6	1.76	5.86	3.34	1.72	19.0	21.0	0.126	0.723	0.293	0.080	0.153
Ammonium oxalate leach (wt.% of original sample leached)												
HN 1440	–	1.06	1.07	–	–	25.0	7.49	0.099	1.30	0.651	0.128	0.073
HN 1441	–	0.849	0.799	–	–	24.4	6.08	0.086	1.25	0.607	0.126	0.061
HN 1442	–	0.719	1.94	–	–	18.9	15.1	0.156	0.546	0.214	0.063	0.063

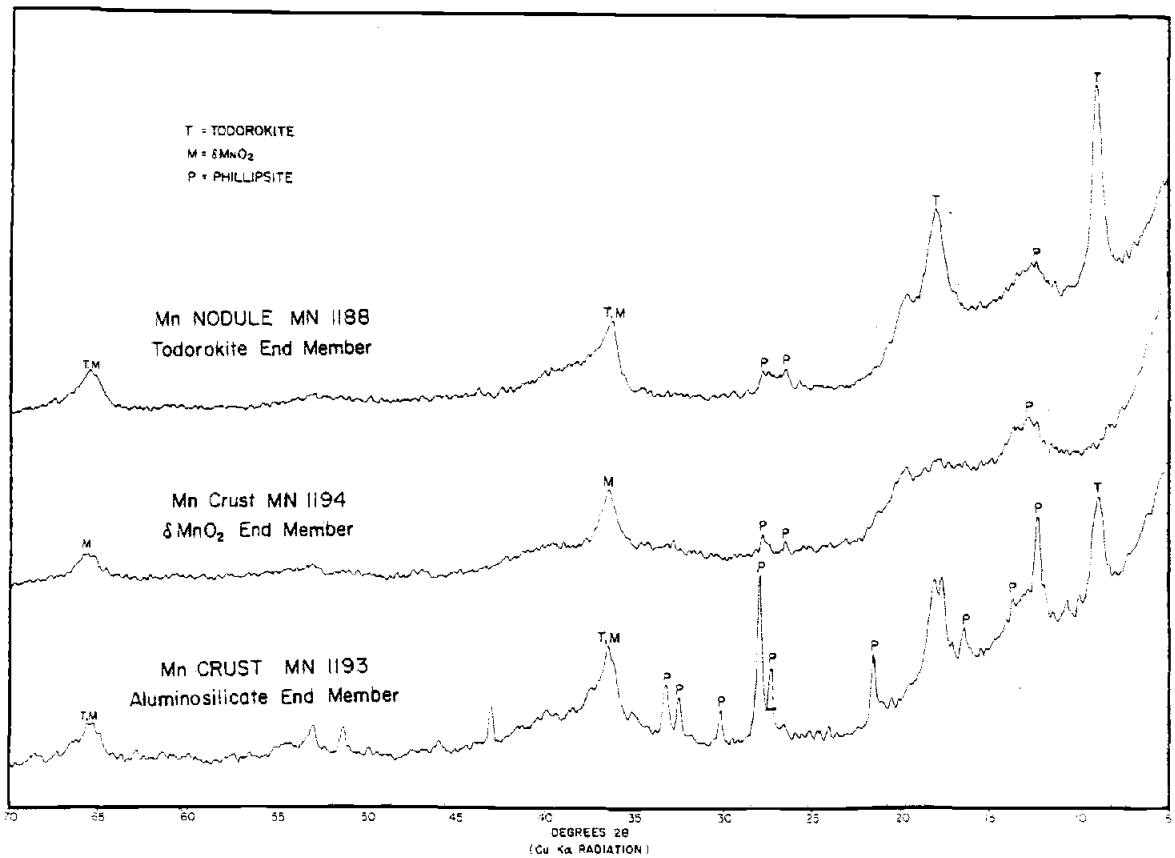

Fig. 4. Three representative X-ray diffractograms of Bauer Deep ferromanganese nodules and crusts (Cu-K_α radiation). They show *MN 1188, the sample most highly enriched in todorokite; MN 1194, the most highly enriched in* δMnO_2; *and MN 1193, the sample most highly enriched in phillipsite.*

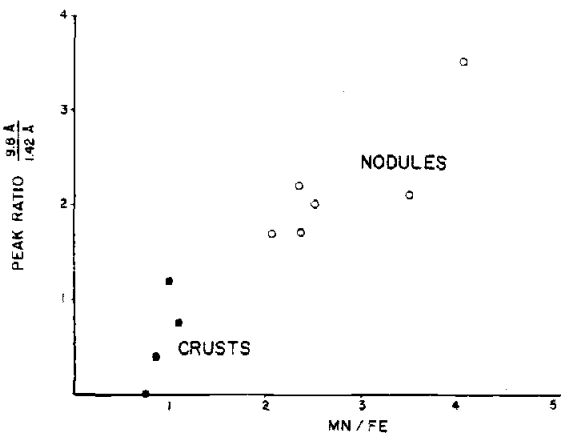

and smectite, but also show the presence of apatite and minor amounts of barite. Although the ammonium oxalate leach will not attack goethite or other crystalline Fe phases, no sign of these minerals was seen in the leach residue.

Fig. 5. Chemical and mineralogical distinction between Bauer Deep nodules and crusts shown by plotting the 9.8 Å/1.42 Å peak area ratio versus Mn/Fe ratio. The higher the 9.8 Å/1.42 Å ratio, the more highly enriched the sample is in todorokite.

4.2. Chemical composition

The chemical compositions of the Bauer Deep manganese nodules are not radically different from north equatorial Pacific nodules (Table 2, although the former appear to have higher Fe relative to Ni contents (Fig. 2). The compositions of material leached from two nodules by the ammonium oxalate-oxalic acid extraction lie well within the range of north equatorial Pacific nodules. Much of the Fe remains behind in a residual phase, presumably smectite; there is no X-ray evidence for other major residual Fe phases. The bulk-sediment composition thus seems to exert little control over the composition of the oxyhydroxide phases in the nodule.

The mineralogic distinction between nodules and crusts is also evident in the chemical data. Nodules have more Mn, Ni, Cu, Zn, and Ba, whereas crusts have more Fe and Co. With the exception of Ba, the same trends persist in the leach data, indicating that the chemical differences between nodules and crusts reflect differences in the composition of the poorly crystalline oxyhydroxide phases. Ba is consistently more abundant in the nodules even though it does

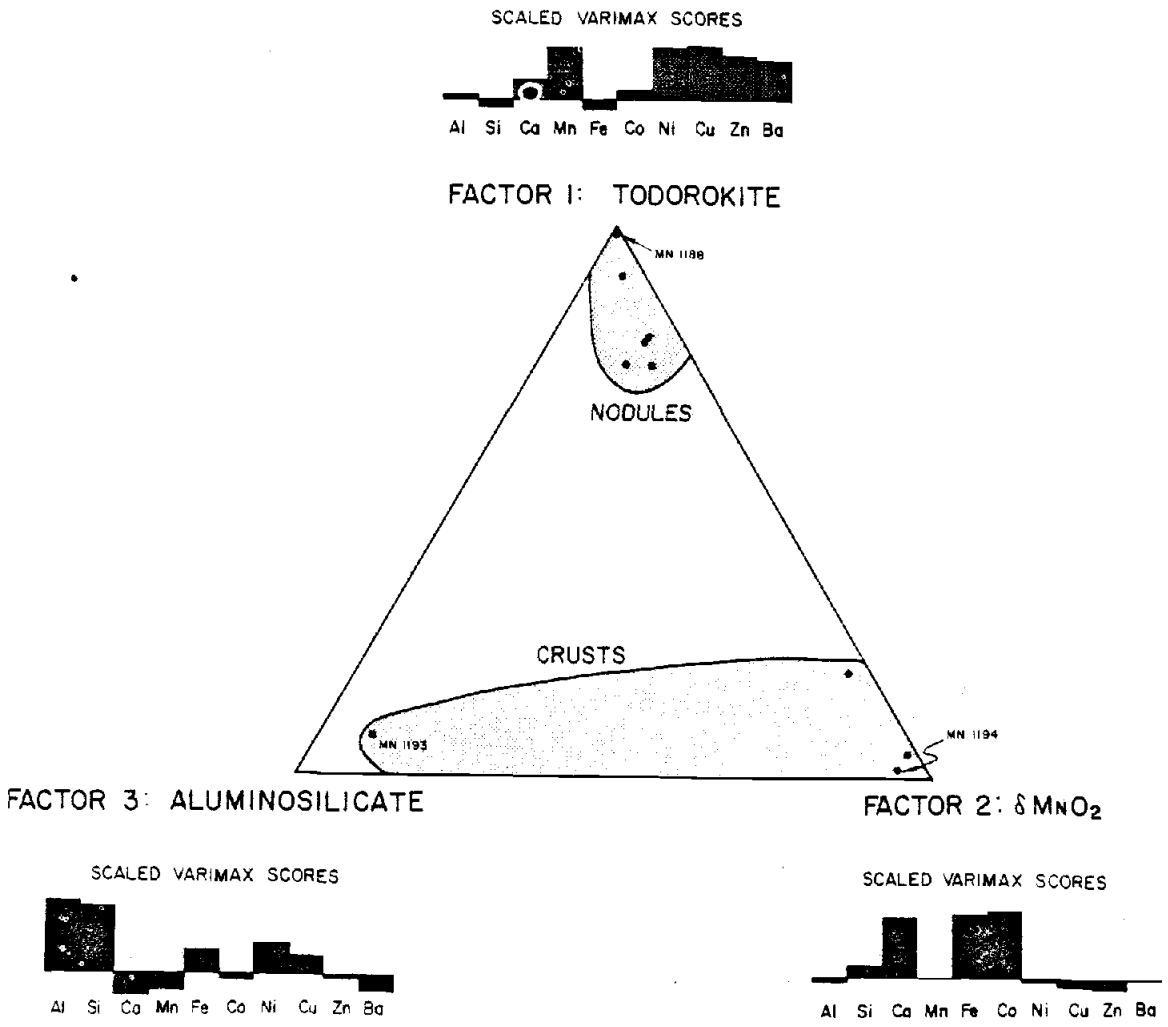

Fig. 6. Elemental loadings of each factor and relative abundance of factors in Bauer Deep nodules and crusts.

not reside in the oxyhydroxide phases. One possible explanation for this may be that it is found in a residual phase that forms more readily in the presence of todorokite or that barite formed at the sediment-water interface during breakdown of biogenic debris is accidently incorporated in growing nodules.

Another striking difference between nodules and crusts is the Si/Al ratio (Table 2). The average nodule ratio is 2.5 versus 3.4 for the crusts, with no overlap between values in the two populations. The crust value is consistent with the value in bulk-sediment surface samples from the region [10], suggesting accidental incorporation of detrital grains in the growing crusts. The nodules, however, are clearly enriched in Al, suggesting incorporation of Al^{3+} in the todorokite lattice. The Si/Al ratios in the material leached from the nodules in HN 1440 and HN 1441 clearly demonstrate the Al enrichment in the oxyhydroxide phase.

The distinction between nodule and crust compositions can be summarized through the statistical technique of factor analysis. Factor analysis describes most of the variance in a complex data set in terms of a few statistically independent linear combinations of the original variables, known as factors. The algorithm used in this paper is described by Klovan and Imbrie [13]. Since all the elements which we analyzed are of roughly equal geochemical interest in this study, we scaled the concentration of each element in each sample (Table 1) to the fraction of its concentration range in the data set so that abundant elements would not dominate the resultant factors as they would if raw data were used.

Three factors that together explain 98% of the variance in the scaled data set were generated by the factor analysis. The elemental loadings for each factor and the compositions of each sample in terms of these factors are shown in Fig. 6. Factor 1, which is dominated by Mn, Ni, Cu, Zn, and Ba, is most abundant in todorokite-rich samples. The nodule with the highest 9.8 Å/1.42 Å peak area ratio (MN 1188) is most highly loaded in this factor. Factor 2 is primarily a Fe, Co, Ca Factor, and is most abundant in δMnO_2-enriched samples. Again, the sample with extreme (lowest) 9.8 Å/1.42 Å peak area ratio (MN 1194) is most highly loaded in this factor. The final factor, dominated by Al and Si, represents alumino-silicate residual phases. Only the phillipsite-rich sample, MN 1193, shows high loadings in this factor.

The enrichment of Ni, Cu, and Zn in todorokite is possible because of its structure, which is presumed to be similar to hollandite or psilomelane in having frameworks of MnO_6 octahedra and large tunnel structures where large cations or hydrated metal ions needed to balance charge can be fitted [12]. It is also possible that the metal cations replace octahedrally coordinated Mn^{II}.

δMnO_2 does not have the room for these cations in its structure and, therefore, is not enriched in them. The enrichment of Fe and Co is attributed to random intergrowths of $FeOOH \cdot H_2O$ with sheets of edge-shared MnO_6 octahedra in the disordered birnessite structure of δMnO_2 [20]. This would account for the correlation between Fe content and the presence of δMnO_2 [20]. The replacement of Mn^{IV} by Co in octahedral sites of the mineral [12] would also account for Co enrichment in this phase.

5. Discussion and conclusions

Our data indicate that ferromanganese crusts from the Bauer Basin are richer in δMnO_2 and contain more Fe, Co and Ca than nodules from the same area which are richer in todorokite and contain more Mn, Cu, Ni, Zn and Na. Accessory minerals found in both crusts and nodules are phillipsite, quartz, iron-rich smectite, apatite, and barite.

Because crusts grow only in contact with normal bottom waters, we conclude that they must form by direct precipitation of ferromanganese oxyhydroxides from seawater. Incorporation of detritus settling through the water column or resuspended particles captured from the near-bottom nepheloid layer introduce accessory minerals and possibly add more ferromanganese phases (colloidal material of hydrothermal origin, for example). Crystallization of amorphous ferromanganese oxyhydroxides in seawater produces δMnO_2.

In contrast, the nodules appear to have accreted within the surficial sediments. They show no features [14] that suggest they grow partially above the sediment-water interface. Nodules recovered in cores from the same area typically show nodules buried at a depth of about 5 cm.

We believe that the markedly lower Fe/Mn ratio in nodules is a result of small-scale diagenetic process-

es within the sediment. Segregation of Fe into a smectite during the diagenetic formation of the clay is suggested by recent work on northwest Nazca plate sediments by Heath and Dymond [10]. They found that hydrothermal Fe-Mn oxyhydroxides formed at the crest of the East Pacific Rise are transformed into iron-rich smectite by reaction with biogenic silica (opal) after they are transported to the Bauer Deep. The Mn originally associated with the iron oxyhydroxide is not accepted by the smectite structure and crystallizes as very pure todorokite micronodules [15]. An analogous scenario can be visualized for the Bauer Deep nodules: the presence of reactive silica (opal) leads to the formation of sedimentary iron-rich smectite. The incompatible Mn is incorporated into the nodule and crystallizes to todorokite, which also accepts Ni, Cu and Zn (perhaps derived in part from the opal) in the process. The process can be summarized as:

opal (Cu, Ni, Zn) + Fe-MnO(OH) → Fe smectite

+ todorokite (Cu, Ni, Zn)

This diagenetic process does not require large-scale remobilization of manganese. It can be adequately supplied from sediments close to the nodule. Some of the ferromanganese components in the nodules may be seawater-derived. From existing data, it is impossible to establish what fraction of the ferromanganese oxyhydroxides was derived directly from seawater, and what fraction was accreted during transformation and early diagenetic reactions within the sediment. In either case, the resultant nodules are markedly enriched in Mn and depleted in Fe relative to the crusts.

If the diagenetic process we envision actually occurs and is globally applicable, it explains many enigmatic features of nodule compositions. In particular, todorokite-Cu-Ni-enriched nodules will only be found where biogenic opal is available to react with and fractionate Fe from Mn. Such opal is available in the zone of Cu-Ni-rich nodules north of the equator, for example. In contrast, nodules from red clay areas where surface productivity is low will show less Fe depletion and will grade in composition to the crusts, which retain the original Mn/Fe ration of the authigenic oxyhydroxides. Fig. 7 is a schematic diagram that summarizes the pathways by which we visualize

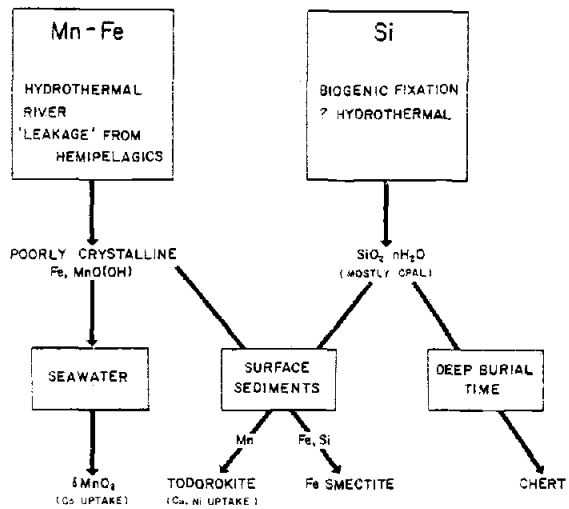

Fig. 7. Pathways by which Fe, Mn, and Si are transferred from their sources to their final pelagic phases.

Fe, Mn and Si being transferred from their sources to their final pelagic phases.

Acknowledgements

We would like to thank Chi Muratli for performing some of the analyses included in this paper. This study was funded by the NSF/IDOE Nazca Plate Project, grant number IDO 71-04208.

References

1 J.L. Mero, The Mineral Resources of the Sea (Elsevier, Amsterdam, 1965) 311 pp.
2 D.R. Horn, B.M. Horn and M.N. Delach, Distribution of ferromanganese deposits in the world ocean, in: Papers from a Conference on Ferromanganese Deposits on the Ocean Floor, D.R. Horn, ed. (NSF-IDOE, Washington, D.C., 1972) 9.
3 J.L. Greenslate, J.Z. Frazer and G. Arrhenius, Origin and deposition of selected transition elements in the seabed, in: Papers on the Origin and Distribution of Manganese Nodules in the Pacific and Prospects for Exploration, Symposium by Hawaii Institute of Geophysics and Valdivia Manganese Exploration Group, M. Morgenstein, ed. (1973) 45–71.
4 D.R. Horn, B.M. Horn and M.N. Delach, Copper and

nickel content of ocean ferromanganese deposits and their relation to properties of the substrate, in: Papers on the Origin and Distribution of Manganese Nodules in the Pacific and Prospects for Exploration, Symposium by Hawaii Institute of Geophysics and Valdivia Manganese Exploration Group, M. Morgenstein, ed. (1973) 77–85.

5 N.B. Price and S.E. Calvert, Compositional variation in Pacific Ocean ferromanganese nodules and its relationship to sediment accumulation rates, Mar. Geol. 9 (1970) 145–171.

6 J.D. Craig, The distribution of ferromanganese nodule deposits in the north equatorial Pacific, M.S. Thesis, Univ. of Hawaii, Honolulu, Hawaii (1975) unpublished.

7 J.D. Hays, T. Saito, N.D. Opdyke and L.H. Burckle, Pliocene-Pleistocene sediments of the equatorial Pacific: their paleomagnetic, biostratigraphic, and climatic record, Geol. Soc. Am. Bull. 80 (1969) 1481–1514.

8 S. Krishnaswami, B.L.K. Somayajulu and W.S. Moore, Dating of manganese nodules using beryllium-10, in: Papers from a Conference on Ferromanganese Deposits on the Ocean Floor, D.R. Horn, ed. (NSF-IDOE, Washington, D.C., 1972) 117, and references therein.

9 J. Dymond, J.B. Corliss, G.R. Heath, C.W. Field, E.J. Dasch and H.H. Veeh, Origin of metalliferous sediments from the Pacific Ocean, Geol. Soc. Am. Bull. 84 (1973) 3355–3372.

10 G.R. Heath and J. Dymond, Genesis and transformation of metalliferous sediments from the East Pacific Rise, Bauer Deep and Central Basin, northwest Nazca Plate, Geol. Soc. Am. Bull. (1976) in press.

11 E.R. Landa and R.G. Gast, Evaluation of crystallinity in hydrated ferric oxides, Clays Clay Miner. 21 (1973) 121–130.

12 R.G. Burns and V.M. Burns, Mineralogy of ferromanganese nodules, in: Marine Manganese Deposits, G.P. Glasby, ed. (Elsevier, 1977) in press.

13 J.E. Klovan and J. Imbrie, An algorithm analysis and calculation of factor scores, Math. Geol. 3 (1971) 61–67.

14 W. Raab, Physical and chemical features of Pacific deep sea manganese nodules and their implications to the genesis of nodules, In: Papers from a Conference on Ferromanganese Deposits on the Ocean Floor, D.R. Horn, ed. (NSF-IDOE, Washington, D.C., 1972) 31.

15 W.A. Eklund, A microprobe study of metalliferous sediment components, M.S. Thesis, Oregon State Univ., Corvallis, Ore. (1974) unpublished, 77 pp.

16 T.L. Ku, W.S. Broecker and N. Opdyke, Comparison of sedimentation rates measured by paleomagnetic and the ionium methods of age determination, Earth Planet. Sci. Lett. 4 (1968) 1–16.

17 Tj.H. van Andel, G.R. Heath and T.C. Moore, Jr., Cenozoic history and paleoceanography of the central equatorial Pacific Ocean, Geol. Soc. Am., Mem. 143 (1975).

18 P.R. Thompson and T. Saito, Pacific Pleistocene sediments: planktonic foraminifera, dissolution cycles, and geochronology, Geology 2 (1974) 333–339.

19 G.R. Heath, T.C. Moore, Jr., B.L.K. Somayajulu and D.S. Cronan, Sediment budget in a deep-sea core from the central equatorial Pacific, J. Mar. Res. 28 (1970) 225–234.

20 J. Dymond and H.H. Veeh, Metal accumulation rates in the southeast Pacific and the origin of metalliferous sediments, Earth Planet. Sci. Lett. 28 (1975) 13–22.

21 J.M. Monget, J.W. Murray and J. Mascle, A world-wide compilation of published multicomponents analyses of ferromanganese concretions, IDOE/NSF Manganese Nodule Project Tech. Rep. No. 12 (1976).

22 D.S. Cronan, Average abundances of Mn, Fe, Ni, Co, Cu, Pb, Mo, V, Cr, Ti, and P in Pacific pelagic clays, Geochim. Cosmochim. Acta 33 (1969) 1562–1565.

CHAPTER 2

THE EARLY DIAGENESIS OF METALLIFEROUS SEDIMENTS IN THE BAUER DEEP, NAZCA PLATE

Mitchell Lyle

School of Oceanography
Oregon State University
Corvallis, OR 97331

The Bauer Deep forms a catchment basin for hydrothermal ferromanganese hydroxyoxide precipitates that drift from the East Pacific Rise. This process results in an unusually high concentration of amorphous, reactive iron and manganese-rich phases due to the low input of other sedimentary components. As a result, the Bauer Deep provides a unique opportunity to examine the processes that form ferromanganese nodules, micronodules, and Fe-rich smectites, since the authigenic and diagenetic phases will not be as easily masked by sediment phases common in more normal pelagic basins. Lyle et al. (1977) suggest that formation of smectites by the reaction of poorly crystalline ferromanganese hydroxyoxides with biogenic silica is a means to form economically valuable Cu,. Ni, and manganese-enriched nodules in oxidizing marine sediments. In this letter I will examine evidence of diagenetic reorganization of ferromanganese hydroxyoxides and opal in a core from the Bauer Deep to evaluate the extent to which these reactions occur.

Y73-3-20P (13°36.8'S 102°31'W) recovered 10.6 meters of sediment in a water depth of 4396 meters. The upper 5 meters are a microfossil-poor dark reddish-brown metalliferous sediment as has been described by Dymond et al. (1973) and grades into reddish-brown calcareous foram-nanno ooze of Late Miocene age (D. Bukry, written communication). Manganese nodules up to 5 cm in diameter were found at the top of the core and in the trigger weight cores. Another nodule about 1 cm in diameter was discovered at 71 cm depth. Two catastrophic sedimentation events are indicated by a turbidite layer of silicified forams at 409-411 cm and by a relatively pure foram sand turbidite from 670 to 716 cm.

Bulk samples were analyzed by atomic absorption spectrophotometry (AA) for Mg, Al, Ca, Si, Mn, Fe, Co, Ni, Cu, and Zn after dissolution in hydrofluoric acid and aqua regia. A second split was leached with oxalic acid buffered with ammonium oxalate (Landa and Gast, 1973) to separate the oxide fraction of the sediment, filtered, and the leachate analyzed by AA for all elements except Ca (it forms an insoluble oxalate precipitate). A third split was sieved at 44 microns while rubbing gently under flowing water and washed with acetic acid buffered at pH 5 to separate a micronodule-rich concentrate free of dispersed oxides. Micronodules were separated from this coarse fraction by the oxalic acid leach and filtration, and also analyzed by AA.

Silica exhibits the most pronounced diagenetic mobility of any species in this core. Despite the poor preservation of silica microfossils at this site, Fe-stained Si-replaced forams are common in the coarse fraction of the sediment. Clay aggregates, possibly loosely bound with silica, are abundant. The percentage of opaline silica, determined by the normative technique of Leinen (1977) and confirmed by the x-ray diffraction technique described by Molina-Cruz and Price (1977), remains relatively constant throughout the first 3 meters of the metalliferous sediment section (Figure 1).

The x-ray diffraction technique estimates a higher opal abundance in the surface sediment that decreases in parallel with the decrease in carbonate abundance, however. Both techniques estimate that opal increases dramatically in the lower 2 meters of the metalliferous sediment section and within the carbonate ooze, correlated to the increasing

carbonate content of the sediment. Quartz abundance (Figure 1), estimated by x-ray diffraction, has a similar distribution. It is most abundant in the surface, decreases downcore as carbonate decreases, and increases slightly in the carbonate ooze. Dilution by opal masks its increase within the carbonate ooze. Kastner et al. (1977) have shown experimentally that calcium carbonate increases the rate at which biogenic opal is diagenetically altered to chert. I suggest that the correlation between x-ray determined opal and quartz abundances and calcium carbonate in the core in this study are due to similar interactions between carbonate and biogenic silica. The carbonate enhances the conversion of silica to more ordered forms, such as quartz or secondary opal. If true, much of the quartz in this core must be authigenically formed; its variation in abundance are not produced by processes of sedimentation. If quartz were truly of detrital origin, lowest abundances would occur in the more quickly deposited carbonate-rich sediments, opposite of the pattern observed here.

Although Bauer Deep sediments are relatively similar to East Pacific Rise sediments (Dymond et al., 1973), they are enriched in silica, most probably from dissolution of biogenic debris. The average Si/Fe ratio of East Pacific Rise sediment is about 0.15 (J. Dymond, personal communication) compared with a ratio of about 1 throughout Y73-3-20P. Even when Si bound in opal and in quartz are subtracted from the sediment, Si is about twice as abundant in Bauer Deep sediments as in those from the Rise Crest. Si released from dissolving biogenic debris must also be incorporated in another sedimentary component.

Kato (1969) has demonstrated that Fe, and to a lesser extent Mn, coprecipitate Si and lower its solubility from that in equilibrium with amorphous silica. Nriagu (1978) hypothesizes that such neoformed cryptocrystalline aluminosilicates fix biogenic Si in the Great Lakes. I hypothesize that a similar reaction occurs in the Bauer Deep. Fe, derived from poorly crystalline ferromanganese hydroxyoxides, will coprecipitate Si, forming an aluminosilicate that eventually ages to form an Fe-rich smectite. Although this reaction consumes Fe from the hydroxyoxide, little of the Mn is involved. Manganese can then precipitate as a separate phase.

The smectite found in the sediment is characterized by poor crystallinity along the c-axis, even though a and b reflections are relatively strong. The crystallinity of the clay is relatively constant downcore, until the metalliferous sediment-carbonate ooze boundary has been reached (see Figure 2). Where carbonate percentages increase, the 060 peak of the smectite in the carbonate-free fraction sharpens and increases dramatically, however, suggesting that its relative abundance and crystallinity have increased. Carbonate may promote smectite formation by uptake of protons released as the clay forms. Throughout the metalliferous sediment section Si and Al leachable by oxalic acid treatment decrease steadily downcore. This suggests that although the crystal size of the smectite may not increase, the constituents that make up the clay are more tightly bound with time.

Ferromanganese hydroxyoxides occur as micro-concretions and as dispersed hydroxyoxides throughout the core. Although the bulk Fe/Mn

ratio in the metalliferous sediment section is similar to a hydrothermal ration of 3 (Heath and Dymond, 1977) the leachable fraction is more highly enriched in Mn (Fe/Mn ~1.3). Most of this 'excess' Mn is contained in the micronodule fraction of the sediments, consistent with the model that Fe is partitioned into a smectite and Mn into a separate oxide phase (Lyle et al., 1977; Heath and Dymond, 1977). The Fe/Mn ratio in the micronodules rises dramatically in the lower part of the core, to greater than 1 in the carbonate ooze. The Fe enrichments may represent later overgrowths of Fe-rich oxides on the micronodules, as described by Dymond and Eklund (in press) for micronodules sieved from 470 cm at a nearby station in the Bauer Deep. The data suggests there is a second diagenetic process that mobilizes Fe during maturation of the sediment.

Enrichments in Ni, Cu, and Zn in the oxide fraction (oxalic acid leachable) of micronodules correlate with Mn content of the micronodules (Figure 1). The similar composition of the nodule at the top of the core (oxide fraction composition is Mn, 41.9%; Fe, 5.88%; Ni, 1.76%; Cu, 1.10%; Zn, 0.225%) and suggest that the processes that form nodules and micronodules at this site are similar.

The evidence contained in this core implies that the following diagenetic sequence occurs. Biogenic opal is deposited at the sediment-water interface and subsequently dissolves within the upper few centimeters of the sediment. If carbonate is present, a fraction of the silica either replaces the carbonate or precipitates in micro-environments within foraminiferal tests. Some of the silica also combines with FeMn-

hydroxyoxides to form well crystallized smectites. In metalliferous sediment devoid of carbonate, biogenic SiO_2 is fixed through the formation of poorly crystalline Fe-smectites. The observation that the measured leachable fraction Fe/Mn ratio is approximately equal to 1 suggests that the formation of smectites must consume approximately 2/3 of the available Fe in the amorphous hydroxyoxides, assuming that the original Fe/Mn ratio in ferromanganese hydroxyoxides is 3 as in Rise Crests sediments. If accumulation rates of Fe and Mn are similar in this core as in others in the Bauer Deep (1.0-2.1 mg $Mn/cm^2/100$ yr; Dymond and Veeh, 1975), approximately 0.7 to 1.4 $mg/cm^2/10^3$ yr of Mn are freed during the formation of smectites to form micronodules and nodules. In comparison, nodule accumulation rates of Mn reported by Bender et al. (1970) are from 0.2 to 1.0 $mg/cm^2/10^3$ yr.

This paper is a part of the author's Ph.D. research at Oregon State University. Funding was provided by an International Nickel Company Fellowship, and by the NSF/IDOE Nazca Plate Project.

1. Bender, M.L., Ku, T.L., and Broecker, W.S. Earth Plan. Sci. Lett., 8, 143-148 (1970).
2. Dymond, J., and Eklund, W. Earth Plan. Sci. Lett., in press.
3. Dymond, J., Corliss, J.B., Heath, G.R., Field, C.W., Dasch, E.J., and Veeh, H.H. Geol. Soc. Am. Bull. 84, 3355-3372 (1973).
4. Dymond, J., and Veeh, H.H. Earth Plan. Sci. Lett. 28, 13-23 (1975).
5. Kastner, M., Keene, J.B., and Gieskes, J.M. Geochim Cosmochim Acta 41, 1041-1059 (1977).

6. Kato, K. Geochemical J. 3, 87-97 (1969).

7. Landa, E.R., and Gast, R.G. Clays Clay Miner. 21, 121-130 (1973).

8. Leinen, M. Geochim. Cosmochim. Acta 41, 671-675 (1977).

9. Molina-Cruz, A., and Price, P. Geology 5, 81-84 (1977).

10. Nriagu, J.O. Limnol. and Oceanog. 23, 53-66 (1978).

FIGURE CAPTIONS

Figure 1: Variations of sedimentary components, bulk composition, composition of leachable fraction of the sediment and micronodule composition downcore in Y73-3-20P. Quartz, opal, and micronodule abundances, as well as the bulk and leach compositions are reported on a $CaCO_3$ and salt-free basis. Opal abundances are estimated by the technique of Leinen (1977). Leach fraction composition is reported as mg leached/kg original sample.

Figure 2: Change of smectite crystallinity downcore in Y73-3-20P, as shown by the smectite 060 peak. Shaded section is carbonate ooze.

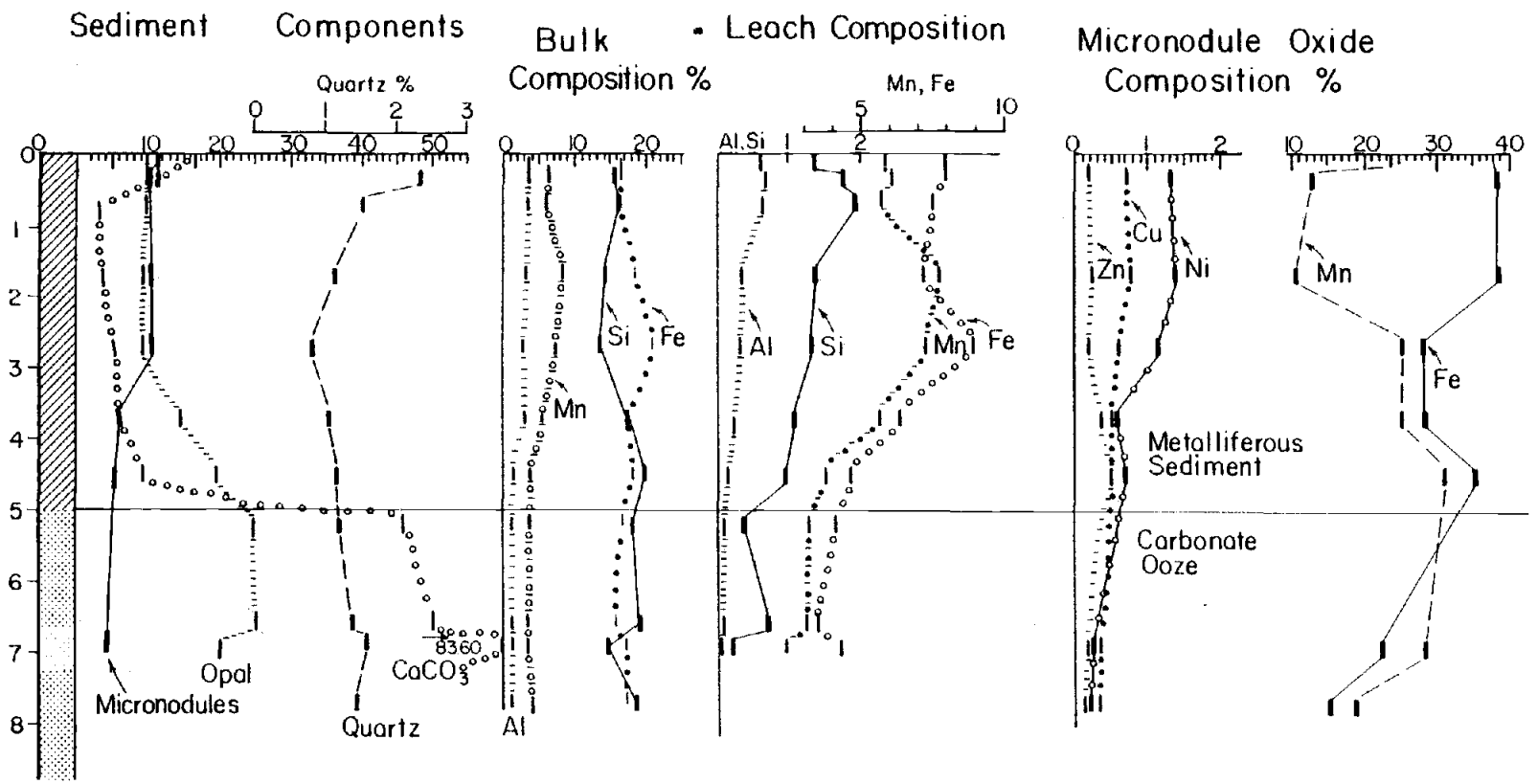
Sediment Components
Quartz %
0 2 3
0 10 20 30 40 50
Micronodules
Opal
Quartz
8360
CaCO3
Bulk Composition %
0 10 20
Mn
Si
Fe
Al
Leach Composition
Mn, Fe
5 10
Al,Si 1 2
Al
Si
Mn
Fe
Micronodule Oxide Composition %
0 1 2
Zn
Cu
Ni
10 20 30 40
Mn
Fe
Metalliferous Sediment
Carbonate Ooze
0 1 2 3 4 5 6 7 8

Figure 1

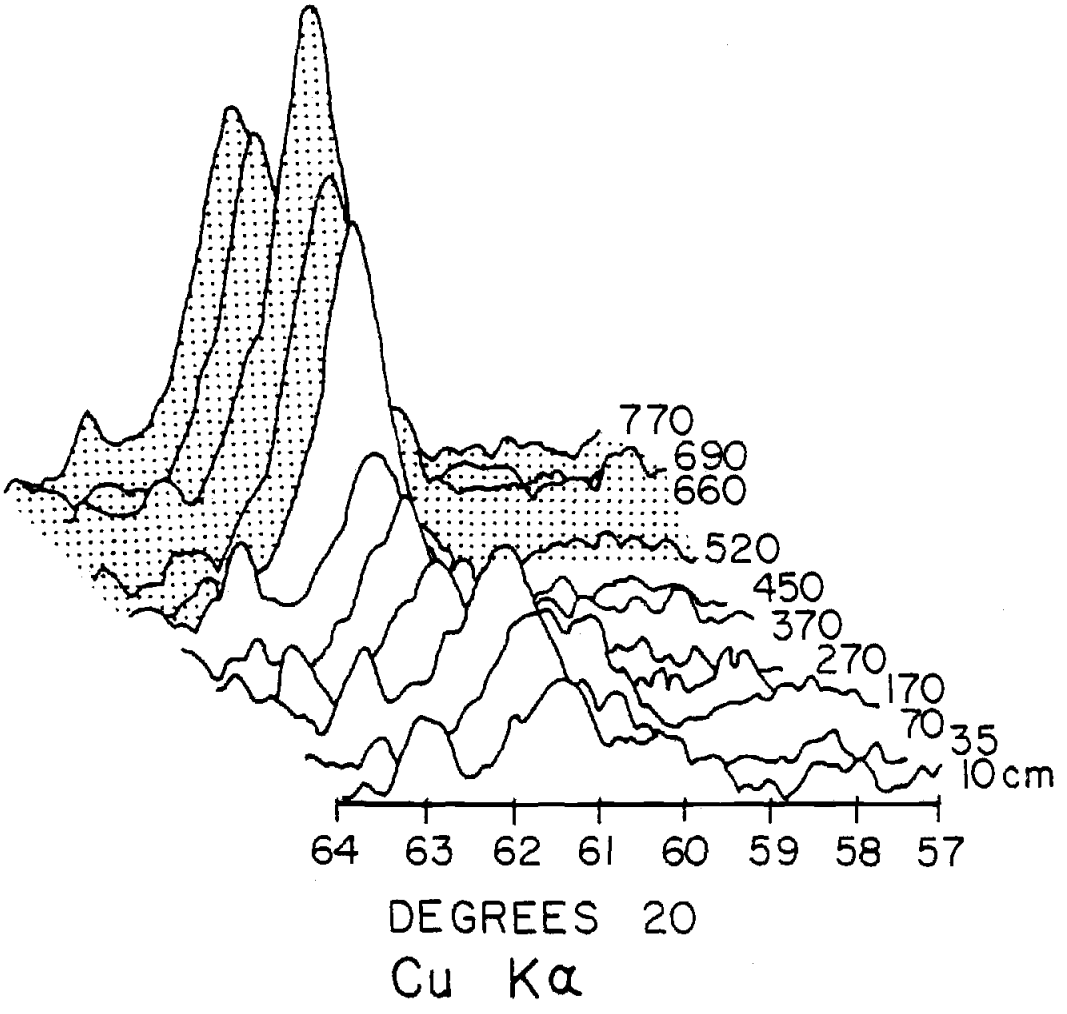
770
690
660
520
450
370
270
170
70
35
10cm
64 63 62 61 60 59 58 57
DEGREES 2θ
Cu Kα

Figure 2

CHAPTER 3

PROCESSES THAT INCORPORATE TRANSITION METALS INTO FERROMANGANESE NODULES: EVIDENCE FROM THE SOUTHEAST PACIFIC OCEAN

Mitchell Lyle

School of Oceanography

Oregon State University

Abstract

Ferromanganese nodules from the southeastern Pacific Ocean have distinct regional variations in their mineralogical and chemical compositions. Nodules from areas of low biological productivity have higher Fe and Co contents and a δMnO_2 mineralogy, while nodules that lie beneath regions of higher productivity are enriched in Mn, Ni, Cu, and Zn and formed of either todorokite or birnessite. The highest Ni and Cu abundances in nodule occur at the fringes of the productive region, as has been observed in the North Pacific, while highest manganese concentrations occur in nodules beneath waters of highest productivity. Nodules most enriched in Mn grow on sediments that become reducing at depth; the nodule must receive a component of remobilized Mn. In areas of moderate productivity, there is no evidence of reducing conditions at depth in the sediments. Other diagenetic reactions (e.g., the formation of Fe-rich smectite from ferromanganese hydroxyoxide and biogenic opal must enrich nodules in Mn. Accumulation rates of Mn, Fe, Co, Ni, Cu, and Zn were calculated by estimating growth rates of the nodules from a regression of chemical compositional data with growth rates for dated nodules. It predicts very high growth rates ($\sim$100mm/10^6 yr) for nodules underneath regions of highest productivity and rates consistent with the bulk of measured growth rates for the other nodules. Accumulation rates for Ni, Cu, and Zn in nodules increase toward regions of highest productivity, suggesting that these elements are enriched by a biogenic vector. Mn, which can be added to sediment through settling of biogenic debris to

the bottom, receives an additional component from its preferential reductive mobilization. The extra Mn flux overwhelms higher fluxes of the other transition metals and causes the nodules most highly enriched in Cu, Ni, and Zn to be found at the fringes of productive regions.

Introduction

Ferromanganese nodules and other ferromanganese oxide deposits can be classified by the processes that form them into three major types of deposits (1). The first major class are the authigenic or hydrogenous nodules. These are considered to have formed by direct precipitation from seawater, and are characterized by Mn/Fe ratios near unity and a S-MnO_2 mineralogy (2). Diagenetic nodules make up the second class of these deposits and are recognized by much higher Mn contents, due to fractionation of manganese from iron within the sediment either through remobilization of manganese by reducing conditions (3, 4) or through diagenetic formation of iron-rich minerals that reject manganese (5). The redox condition of pelagic sediments is primarily controlled by the influx of particulate biogenic debris high in organic carbon. The flux of biogenic debris also can carry significant quantities of the minor elements to the sediments (6). This produces additional compositional variations in the diagenetic nodules. Hydrothermally formed ferromanganese oxides form the third type of deposit. They form crusts on Mn and Fe precipitated on rocks and sediments from seawater solutions that have interacted at elevated temperatures with cooling basalt. Recent studies (7, 8, 9, 10) indicate that true hydrothermal ferromanganese deposits occur only locally around hydrothermal vent areas. Hydrothermal processes may be of regional importance only through the supply of Mn and Fe to seawater that may later be incorporated into a growing nodule through other processes.

Most workers agree that the relative importance of each formation mechanism will produce regional compositional differences in nodules. For instance, Calvert and Price (2) have shown that variations in nodule composition and mineralogy occur from the poorly productive central gyre regions to more highly productive equatorial Pacific sites. They suggest that central gyre nodules have compositions determined by direct precipitation from seawater (authigenic or hydrogenous formation) while nodules from the equatorial Pacific are more influenced by diagenetic reactions. Boudreau and Scott (11), using a theoretical approach, suggest that diagenetic remobilization of Mn will only be significant for nodule growth if the oxidizing layer is less than 40 cm thick. They also show that no other source than seawater is needed to supply most of the trace metals to nodules.

Work by Lyle et al (1977) demonstrates that both hydrogenous and diagenentic processes can operate at the same locality. Ferromanganese crusts that flow in contact with seawater alone have significantly different compositions than nodules growing in sediments close by. The nodules are enriched in Mn, Ni, Cu, and Zn, while the crusts have compositions that resemble authigenic nodules.

The purpose of this paper is to examine the regional variations of chemical composition and flux of elements to manganese nodules in the southeast Pacific Ocean in order to discern specific incorporation processes for Mn, Fe, Ni, Cu, Zn, and Co. I hope to further demonstrate that the interplay between hydrogenous precipitation and the range of diagenetic processes can produce striking regional variations

in manganese nodule chemistry. I also plan to demonstrate through elemental accumulation rate estimates that the enigmatic enrichment of Cu, Ni, and Zn at the edges of regions of high productivity (6, 13) in ferromanganese nodules is produced because Mn is supplied to the nodules by different processes than the minor transition metals.

PROCEDURES:

The data set described in this paper is a combination of previous analyses compiled in Monget et al (12) and new analyses of Nazca Plate nodules (Table I). A half or quarter of each nodule described in Table I was ground coarsely (to about 30 mesh) in an agate mortar and pestle. A split was dissolved in hydrofluoric acid and aqua regia as described by Dymond et al (1973) and analyzed by atomic absorption spectrophotometry for Mn, Fe, Al, Si, Mg, Cu, Ni, and Zn. A second split was irradiated three hours at one megawatt on the research reactor at Oregon State University and analyzed for Sc, Co, Ag, Sb, Ba, the rare earth elements, Hf, Th, and U by instrumental neutron activation analysis. All data except Co is discussed in a separate paper (14). Replicate precision was better than 5% for Mn, Fe, Mg, Cu, Ni, and Zn and better than 7.5% for Al and Si. Accuracy for all elements determined by in-house standards are of the same magnitude.

A third split was ground fine (less than 325 mesh) in an auto-grinder under butanol and random powder mounts were analyzed by slow scan x-ray diffractometry (500 sec/degree 2θ) using Cu-Kα radiation with graphite monochromater and Ni filtration. The data was collected

digitally and smoothed with a 13 point filter. Comparison of crystallinities from diffractograms of powdered nodule material ground under butanol and that ground under liquid nitrogen to preserve crystallinity (13) show little difference between the two techniques. The results of the x-ray diffraction analysis are also reported in Table I. The data are reported as the respective areas of the todorokite 9.6Å peak, the birnessite 3.6Å peak, and 'δ-MnO_2' 1.42Å peak (mineral usage as in Burns and Burns, 1977) over the combined peak areas. The birnessite 3.6Å peak was used instead of the primary 7.2Å peak because of possible smectite and phillipsite interference at 7.2Å. Although the 1.42Å peak is common to birnessite, todorokite and the disordered δ-MnO_2, the relative importance of this peak gives a measure of the abundance of the disordered δ-MnO_2 phase.

These data were combined with those compiled by Monget et al (12). The published analyses were filtered by removing all analyses of nodules recovered from less than 4000 meters (except for two coastal nodules at 33°S, 75°W under 3950 meters of water) and by removing all nodules with Al+Si percentages greater than 10%. The latter filter eliminates nodules with significant detrital core material. If more than one nodule from the same station have been analyzed, the compositional data were averaged together. The compositional data from the combined data set of 50 nodules at 40 stations were then plotted to produce Figures 1a-1f that show the regional distribution of Mn, Fe, Ni, Cu, Zn, and Co in ferromanganese nodules from the southeast Pacific Ocean.

REGIONAL COMPOSITION AND MINERALOGY OF FERROMANGANESE NODULES

The striking pattern of nodule compositions from the southeast Pacific suggest that Mn compositions of ferromanganese nodules are strongly related to the biological productivity in surface waters (compare Figure 1a to Figure 3). Productivity is the major control of sedimentary redox conditions in the pelagic realm, since the oxidation of organic matter within sediments can significantly lower the Eh of the sediments. Manganese is relatively immobile as Mn^{IV}, forming a variety of Mn oxides including the common marine minerals todorokite, birnessite, and δ-MnO_2. Although Mn^{IV} is the stable valence in seawater (Eh of 0.75V) and in surface sediments in contact with seawater, manganese can be reduced to the soluble Mn^{II} at a relatively high Eh of about 0.5V at a pH of 8 (14), permitting it to be remobilized and diffuse back to the more oxidizing sediment surface. Subsequent oxidation to Mn^{IV} will result in deposition on the manganese nodule growing at the sediment seawater interface, as has been suggested by Lynn and Bonatti (4) and Price and Calvert (3). As reducing conditions become more intense, cycling of the Mn becomes more intense, and more may accumulate in the nodule.

The relationship between productivity and sedimentary redox conditions can be explored by a simple yet powerful semiquantitative technique first employed by Lynn and Bonatti (4) to map the intensity of redox conditions. There is commonly a color change that can be observed in tops of cores from reducing environments which marks a redox boundary in the core. Fe^{III} reduction to Fe^{II} (15) probably

causes the sediment color to change from brown to gray-green, although Lynn and Bonatti give strong evidence that it marks the precipitation boundary of Mn and thus a much higher Eh (about 0.5V). The color change does mark the depth at which the diffusion of oxidants into the sediment from seawater can no longer buffer the Eh, causing it to drop rapidly. The depth to this boundary thus gives a measure of intensity of reducing conditions within the sediment.

Figure 4 is a map of the depth to this boundary measured in 161 cores taken by Oregon State University in the eastern Pacific and combined with Lynn and Bonatti's data set. Comparison with Figure 3 shows the strong relationship between sedimentary redox conditions and surface productivity. Secondary control of the redox conditions is from continental organic carbon added from the continental margins by rivers.

Reduction and remobilization of Mn may thus be a major control of the regional pattern of Mn enrichment in nodules. Nodules are also enriched in Mn at the edges of productivity regions, however, where thick oxidizing sequences of sediments preclude significant remobilization of manganese, (11), and a second mechanism is needed to enrich Mn in the nodules found in these regions, as suggested by Lyle et al (5). Mn and Fe are probably added to the sediment as an amorphous ferromanganese oxyhydroxide colloid or adsorbed on grains that fall through the water column (15). In the margins of productive regions, amorphous silica in the form of diatom and radiolarian tests are also added in significant quantities to the surface sediment. During

dissolution and reprecipitation of a more stable assemblage, the Fe is fractionated into an iron-rich smectite, while the manganese has no stable phase other than the oxide. This mechanism could produce relatively iron-free Mn oxides. This type of fractionation may also occur during diagenesis under more reducing conditions.

Fe and Co (Figures 1b and 1c) have antisymmetrical distributions to manganese. Their highest concentrations are found in the midst of the poorly productive central gyre region and drop rapidly as productivity increases. Although Fe^{III} can be reduced to Fe^{II} in reducing sediments, formation of authigenic clays, phosphates, and in some cases, sulfides, will limit its mobility (17). In all but the most oxidizing marine environments Co will remain as Co^{II}, and not be influenced by reduction or oxidation reactions. In central gyre nodules where low productivity leads to oxidizing conditions in the sediment, enrichment of Co in the δ-MnO_2 phase may be strongly influenced by Co^{II}-Co^{III} oxidation and replacement of Mn^{IV} in the mineral (18). The antisymmetric distribution of Fe and Co with manganese could result from dilution by manganese. If Fe and Co accumulate slowly in a nodule at a roughly constant rate, an additional flux of remobilized manganese to the nodule would reduce their concentrations in the nodule. This will be further discussed in the next section.

Cu, Ni, and Zn exhibit more complex behavior than Mn, Fe, or Co. Cu and Ni are most highly enriched at the margin of the productive region, while Zn is enriched at this margin and also within the highly productive region (Figures 1d, 1e, 1f). This behavior is similar to

that reported in the Central Equatorial Pacific (13). Nodules with the greatest abundance of the manganese mineral todorokite are also found at the margins of the productivity region (Figure 2). The enrichment of Cu, Ni, and Zn in these nodules could thus be caused by preferential uptake of these elements by todorokite over either δ-MnO_2 or birnessite. There are several lines of evidence, however, that suggest that this hypothesis is not completely true. Although there is data (5) and plausible argument (19) that the disordered δ-MnO_2 mineralogy will not incorporate as much Cu, Ni, Zn, or other divalent cations as todorokite, even when elemental availability to both minerals is similar, there is no evidence for birnessite-todorokite fractionation. Burns and Burns (19) indicated that Cu, Ni, and Zn replace Mn^{II} in both todorokite and birnessite. Studies of a hydrothermally formed suite of manganese oxides ranging from pure birnessite to nearly pure todorokite dredged from the Galapagos Rise (9) show no correlation between mineralogy and the concentration of Cu, Ni, or Zn. Admittedly these elements are present in the manganese oxides in very low abundances and may never reach a concentration where preferential uptake may be significant. Todorokite has been synthesized by treating a synthetic birnessite with a 10% solution of Cu, Ni, or Co (20), while Giovanoli et al (21) has demonstrated that Cu, Ni, and Zn stabilize the metal-rich buserite (equivalent to my usage of todorokite) over its Mg equivalent. The zone of high Cu, Ni, and Zn that coincides with the region of high todorokite may thus represent the stabilizing of the todorokite structure by these elements and not an enrichment of

Cu, Ni, and Zn in nodules by their preferential uptake in todorokite.

Biogenic vectors may be responsible for nodules enriched in Cu, Ni, and Zn (6). Trace metals are incorporated in the soft parts or tests of plankton, or perhaps are adsorbed to test surfaces. These sink to the bottom after the organism dies, where most dissolve and release their trace metal constituents. The trace metals can then be incorporated into the growing manganese nodule. Evidence for this type of mechanism comes from elemental analyses of phytoplankton (22) which show significant abundances of Cu, Ni, and Zn in both the organic fraction and tests. Additional support is provided by studies of variations of the water column composition of Cu, Ni, and Zn. Ni and Zn have a high deep water concentration that correlate with dissolved Si and suggest that dissolution of tests or the accompanying organic fractions releases these elements (23, 24). Cu distribution in the water column is not so simple, yet still looks like its primary control may be by scavenging onto particulates (25). Deep waters are also enriched in Cu indicating that it is released at the bottom.

The transport and concentration of Cu, Ni, and Zn at the sediments by plankton would most probably produce the highest accumulation rates of these elements in nodules underneath the regions of highest surface productivity. This may not be at all obvious from nodule concentration data, however. Manganese uptake by nodules, although also related to productivity, need not accumulate in a constant proportion to the minor elements. Although one might postulate a linear increase of Cu, Ni, or Zn accumulation rates with productivity, remobilization of Mn

would probably cause an additional flux of Mn to the nodules. Because Mn oxides are the major component of ferromanganese nodules, any additional flux of Mn would overwhelm the additional fluxes of other elements. Examination of concentration data would then show a high of Cu, Ni, and Zn at the margins of the productive zone because of Mn dilution in more highly producitve regions. To truly understand the processes of incorporation of these elements into manganese nodules, we must examine elemental fluxes into nodules and not elemental abundance data.

ESTIMATION OF ELEMENTAL ACCUMULATION RATES IN NODULES

Although the study of elemental accumulation rates provide unambiguous information about the uptake of elements in nodules, the difficulty in dating nodules has hindered progress in this field. Most commonly nodules have been dated by alpha counting of ^{230}Th. A known surface area is scraped and the scraped material weighed to calculate the depth of the sample interval. The decay of excess ^{230}Th in the depth intervals is then used to determine the age (26). The technique suffers because of the slow growth rates of the nodules -- all of the excess ^{230}Th commonly decays away in the upper few millimeters of the nodule. Extreme care is necessary to obtain good dates.

A simpler technique, total alpha counting, is fast becoming the standard method of nodule dating (27, 28, 29). The distribution of total alpha activity in a nodule slice is measured with plastic films. To date the nodule, it is assumed that the exponential decrease of

alpha tracks is due to the unsupported decay of ^{230}Th and its daughters. The assumption seems to be reasonable in most cases (29).

Other dating techniques have been occasionally applied to nodules, including ^{10}Be, K-Ar dating of nodule cores, and ^{234}U decay (26). These have been primarily applied to extend dating beyond the outer few millimeters of the nodule.

Despite the inherent difficulties in dating nodules, about 50 have now been dated (26, 30). Most have growth rates between 1 and 10 mm/10^6 yr, although recent data extends growth rates in pelagic nodules to greater than 50 mm/10^6 yr. The existing data suggest the slowest growing nodules form in regions of low productivity. Nodules with high growth rates come from areas of higher productivity, where addition of remobilized Mn to the nodule should increase its growth rate. This concept has been illustrated by Calvert (31) who shows that Mn/Fe ratios increase in nodules with higher growth rates. This implies that it could be possible to predict growth rate of nodules, and therefore elemental accumulation rates, from their chemical composition.

There are 20 dated nodules with reasonably complete chemical analyses performed on them (30, 32, 33). The elemental abundances of Mn, Fe, Ni, Cu, and Co from these nodules formed the basic data set for a multiple regression analysis to predict the growth rates of manganese nodules. These elements were chosen because their abundances are most commonly reported in the nodule literature and because they comprise the bulk of the oxide fraction of the nodule. Some elements,

for example Fe and Co, may accumulate in nodules primarily through direct precipitation from seawater. If so, the growth rate of the nodule should be inversely proportional to the concentrations of these elements (33). Accordingly, the inverse of all the elemental abundances were also included in the regression. The elemental abundances in the 20 nodules were first normalized to remove the effects of non-oxide diluents and the corrected abundances for these 5 elements as well as their inverses were entered into a stepwise multiple regression analysis.

An equation with 2 terms explained the majority of the variance in the data set:

$$\text{GROWTH RATE} = 6.30(1/\text{Fe}) + 42.02(\text{Fe}) - 31.20$$

where $\text{Fe} = \text{Fe}/\text{Fe} + \text{Mn} + \text{Ni} + \text{Cu} + \text{Co}$

The entire equation is significant at >99.9% confidence level. Of the two terms, 1/Fe explained 86% of the variance in the growth rate data set, while Fe explained an additional 3%. Standard error of the estimate is ± 5.8 mm/10^6 yr. A plot of estimated sedimentation rate against measured rates is shown in Figure 5.

Growth rates for the same data set used to produce Figure 1 were estimated by this equation. The data set suggest that nodule growth rates may be greater than 100 mm/10^6 yr in certain cases, approaching growth rates as have already been reported for shallow water and fresh water nodules (26). When combined with elemental abundance data, the growth rates produce the elemental accumulation rate patterns mapped in Figure 6.

The distribution of Fe accumulation (Figure 6a) shows some increase with productivity. Manganese (Figure 6b) has a much more intense increase when it enters the productive region, however. Where Fe accumulation rates are about 10x greater in the productive region than in the central gyre, manganese accumulates up to 200x faster. The huge difference in response to productivity between Mn and Fe produces their anticorrelated behavior.

Manganese shows the strongest reaction to the change in productivity, even though manganese is less biologically active than Fe. Its remobilization by minor changes in Eh conditions has probably the greatest effect on its distribution in nodules, as suggested by the concentration data.

Fe may respond to productivity in two possbile ways. Significant amounts of Fe are incorporated into phytoplankton (22), and thus high productivity and subsequent dissolution of biogenic remains may provide Fe to nodules. Alternatively Fe could adsorb to tests or other sinking particles and be carried in this fashion to the sediments and ultimately to nodules. Either process will probably not be as significant as diagenetic remobilization of Mn.

Cobalt (Figure 6c) shows no strong pattern, but does have some correlation with productivity. Because it shows no enrichment in phytoplankton (22), the enrichment in more productive regions is probably a response to adsorption and transport by particulates. Because plankton produce the majority of particles in the pelagic realm, there should be some relation to productivity.

Of major interest is the pattern of Cu, Ni, and Zn accumulation in the nodules (Figures 6d,e,f). Unlike the concentration data (Figures 1d,e,f) all these patterns show strong similarity. The accumulation rate patterns for all three elements also show a strong resemblance to primary productivity in the surface waters, and suggest that transport of Cu, Ni, and Zn to the sea floor by biologic activity delivers these transition elements to ferromanganese nodules. It is unlikely that these elements are enriched in surface sediments by reduction within the sediment column. Zn is not reduced, while Cu is fixed by more reducing conditions (14). Ni may be reduced and remobilized as the Eh drops below that of seawater, however. Since its distribution does not resemble Mn more closely, I argue that supply is a more important control on its distribution.

CONCLUSIONS

The data I have presented in this paper suggest a few relatively simple processes produce the regional variations in ferromanganese nodule compositions observed in the Southeast Pacific. First, to all nodules comes a low background flux of Fe, Mn, Co and other trace metals that directly precipitate from seawater. This seawater flux provides all of the transition metals to nodules from the central gyre and provides most, if not all, of the transition metals to ferromanganese coatings growing on hard substrate, even if they occur in more productive regions.

A strong input of biogenic debris to sediments enriches nodules

growing within the sediment in manganese, either by fractionation of Mn from Fe either through formation of iron-rich smectites, or through reduction and remobilization of Mn. The addition of Mn to the nodule allows the formation of more ordered manganese minerals, forming first todorokite at the margins of the equatorial productivity region, and then birnessite where surface productivity is higher.

Cu, Ni, and Zn are carried by the rain of biogenic debris to the sediments, where dissolution frees them to be incorporated within the nodules. High concentrations in the nodules (about 1% Cu and Ni) of these elements may stabilize the todorokite structure at the margins of productive regions.

The strong relationship between manganese concentration in nodules and redox conditions of sediments may explain the variation of Mn and Fe within nodule layers. High Mn layers would have grown during times of more intense reducing conditions (and hence higher productivity of surface waters), while high Fe, low Mn layers would have been produced when sediments were more oxidizing (lower productivity) or if the nodule were exhumed by strong bottom currents or benthic biological activity. In the latter case, the nodule has been isolated to some extent from diagenetic reactions within the sediment and its chemistry is more controlled by authigenic precipitation reactions from seawater. It may therefore be possible to use nodules to trace the productivity of surface waters through time, if one can eliminate exhumation effects.

ACKNOWLEDGEMENTS

I would like to thank E. Suess, J. Dymond, J. Corliss, and J. Dasch for their comments and criticism of this work. Support for the study was provided by an International Nickel Company fellowship and the NSF/IDOE Nazca Plate Project # . The study is part of the author's Ph.D. research at Oregon State University.

REFERENCES

(1) Bonatti, E, T. Kraemer, and H. Rydell, 1972. Classification and genesis of submarine iron-manganese deposits. In Horn, D. R. (ed.). Papers from a conference on Ferromanganese Deposits on the Ocean Floor. NSF/IDOE Publication, pp. 149-166.

(2) Calvert, S. E., and N. B. Price, 1977. Geochemical variation in ferromanganese nodules and associated sediments from the Pacific Ocean. 5,43-74.

(3) Price, N. B., and S. E. Calvert, 1970. Compositional variation in Pacific Ocean ferromanganese nodules and its relationship to sediment accumulation rates. Marine Geol. 9,145-171.

(4) Lynn, D. C., and E. Bonatti, 1965. Mobility of manganese in the diagenesis of deep-sea sediments. Marine Geol. 3,457-474.

(5) Lyle, M., J. Dymond, and G. R. Heath, 1977. Copper-nickel-enriched ferromanganese nodules and associated crusts from the Bauer Basin, Northwest Nazca Plate. Earth Plan. Sci. Lett. 35,55-64.

(6) Greenslate, J. L., J. Z. Frazer, and G. Arrhenius, 1973. Origin and deposition of selected transition elements in the seabed. In M. Morgenstein (ed.). Papers on the origin and distribution of manganese nodules in the Pacific and prospects for exploration. pp. 44-69. Honolulu, Hawaii.

(7) Scott, R. B., P. A. Rona, B. A. McGregor, and M. R. Scott, 1974. The TAG hydrothermal field. Nature. 251,301-302.

(8) Lalou, C., E. Brichet, T. L. Ku, and C. Jehanno, 1977. Radiochemical, scanning electron microscope (SEM) and x-ray dispersive energy (EDAX) studies of a FAMOUS hydrothermal deposit. Marine Geol. 24,245-258.

(9) Corliss, J. B., M. Lyle, J. Dymond, and K. Crane, 1978. The chemistry of hydrothermal sediment mound deposits near the Galapagos Rift. Earth Plan. Sci. Lett. In press.

(10) Cann, J. R., C. K. Winter, and R. G. Pritchard, 1977. A hydrothermal deposit from the floor of the Gulf of Aden. Mineral. Mag. 41,193-199.

(11) Boudreau, B. P., and M. R. Scott, 1978. A model for the diffusion-controlled growth of deep-sea manganese nodules. In preparation.

(12) Monget, J. M., J. W. Murray, and J. Mascle, 1976. A world-wide compilation of published, multicomponent/analyses of ferromanganese concretions. NSF-IDOE Manganese Nodule Porject Technical Rept. 12

(13) Piper, E. Z., and M. E. Williamson, 1977. Composition of Pacific Ocean ferromanganese nodules. Mar. Geol. 23,285-303.

(14) Lyle, M. The formation and growth of ferromanganese oxides on the Nazca Plate. Corvallis, Oregon State University Ph.D. Thesis. 170 pp.

(15) Pourbaix, M., 1974. Atlas of Electrochemical Equilibria in Aqueous Solutions, 1974. Nat. Ass. Corr. Eng., Houston. 644 pp.

(16) Hartmann, M., P. J. Muller, E. Suess, and C. H. van der Weijden, 1976. Chemistry of late quaternary sediments and their interstitial waters from the NW African continental margin. "Meteor" Forsch.-Ergebn. C. pp. 1-67.

(17) Dymond, J., J. B. Corliss, G. R. Heath, C. W. Field, E. J. Dasch, and H. H. Veeh, 1973. Origin of metalliferous sediments from the Pacific Ocean. Geol. Soc. Am. Bull. 84,3355-3372.

(18) Krauskopf, K. B., 1956. Separation of manganese from iron in sedimentary processes. Geochim. Cosmochim Acta. 12,61-84.

(19) Burns, R. G., 1976. The uptake of cobalt into ferromanganese nodules, soils, and synthetic manganese (IV) oxides. Geochim. Cosmochim. Acta. 40,95-102.

(20) Burns, R. G., and V. M. Burns, 1977. Mineralogy. In Glasby, G. P. (Ed.). Marine Manganese Deposits. Elsevier. pp. 185-249.

(21) McKenzie, R. M., 1971. The synthesis of Birnessite, cryptomelane, and some other oxides and hydroxides of manganese. Mineral. Mag. 38, 493-502.

(22) Giovanoli, R., P. Burki, M. Giuffredi, and W. Stumm, 1975. Layer structured manganese oxide hydroxides. IV: The Buserite group; structure stabilization by transition elements. Chimia. 29,517-520.

(23) Martin, J. H., and G. A. Knauer, 1973. The elemental composition of plankton. Geochim. Cosmochim. Acta. 37,1639-1653.

(24) Sclater, F. R., E. Boyle, and J. M. Edmond, 1976. On the marine geochemistry of nickel. Earth Plan. Sci. Lett. 31,119-128.

(25) Bruland, K. W., G. A. Knauer, and J. M. Martin, 1978. Zinc in northeast Pacific water. Nature. 271,741-743.

(26) Boyle, E. A., F. R. Sclater, and J. M. Edmond, 1977. The distribution of dissolved copper in the Pacific. Earth Plan. Sci. Lett. 37,38-54.

(27) Ku, T. L., 1977. Rates of accretion. In Glasby, G. P. (ed.). Marine Manganese Deposits. Elsevier, New York. pp. 249-269.

(28) Heye, D., 1975. Wachstumsverhaltnisse von manganknollen. Geolog. Jahrb. 122 pp.

(29) Fisher, D. E., 1977. Fission/alpha analysis of the U, Th families. Nature. 265,227-229.

(30) Anderson, M. E., and J. D. Macdougall, 1977. Accumulation rates of manganese nodules and sediments: an alpha track method. Geophys. Res. Lett. 4. pp. 351-353.

(31) Heye, D., and V. Marchig, 1977. Relationship between growth rate of manganese nodules from the central Pacific and their chemical constitution. Mar. Geol. 23,M19-M25.

(32) Calvert, S. E., 1977. Geochemistry of oceanic ferromanganese deposits. Phil. Trans. Roy. Soc. London, Series A.

(33) Somayajulu, B. L. K., G. R. Heath, T. C. Moore, and D. S. Cronan, 1971. Rates of accumulation of manganese nodules and associated sediment from the equatorial Pacific. Geochim. Cosmochim. Acta. 35,621-624.

(34) Krishnaswami, S., and D. Lal, 1972. Manganese nodules and budget of trace solubles in oceans. Proceedings Nobel Symp. 20, 307-320.

(35) Krishnaswami, S., 1976. Authigenic transition elements in Pacific pelagic clays. Geochim. Cosmochim. Acta. 40, 425-434.

(36) Love, C. M., and R. M. Allen (eds.), 1975. EASTROPAC Atlas, V. 10: Biological and nutrient chemistry data from principal participating ships third survey cruise, February-March 1968. Washington, D.C., U.S. Dept. Commerce.

(37) Lisitzin, A. P., 1970. Sedimentation and geochemical considerations. In Wooster, W. S. (ed.). Scientific Exploration of the South Pacific. Washington, D.C. Nat. Acad. Sci. 89-133.

TABLE I. Ferromanganese nodule analyses, this study

NAME	LAT (S)	LONG (W)	Mg	Al	Si	Mn	Fe	Co	Ni	Cu	Zn	TOD*	BIRN*	M*
Y71-9-86MGI	5 05	90 47	1.61	.624	2.39	44.5	1.48	.016	.549	.340	.163	30	37	33
C136	8 47	89 26	2.01	2.64	6.42	26.5	10.4	.185	1.38	.688	.129	43	4	52
C151	8 58	86 22	1.81	2.00	6.91	31.8	5.10	.035	.858	.693	.098	65	2	33
C165	13 29	83 40	1.55	2.26	6.40	34.4	5.23	.031	.907	.608	.097	31	30	39
Y73-3-20P	13 38	102 34	2.26	1.89	4.14	33.6	6.55	.041	1.45	.870	.177	32	18	50
C169	14 24	81 33	1.43	2.07	5.87	36.9	4.00	.021	.663	.442	.097	15	42	43
C141	14 55	87 43	1.98	2.61	6.48	27.5	8.24	.121	1.41	.860	.139	44	4	52
w7706-19	22 14	79 31	1.34	3.28	8.67	16.6	17.5	.292	.413	.241	.065	0	0	100
DM981	22 40	160 47	1.24	2.76	7.01	16.5	20.6	.540	.267	.116	.057	0	0	100
DM1006	38 08	125 21	1.58	3.25	8.55	21.5	13.3	.183	.759	.311	.083	19	0	81
DM994	48 19	96 28	1.39	4.21	12.9	15.8	12.2	.143	.480	.273	.059	12	15	73

*TOD = todorokite 9.6A peak area, BIRN = birnessite 3.6A peak area, M = MnO_2 1.42A peak area, all expressed as percent of combined peak areas.

Figure Captions

Figure 1: Regional distributions of Mn, Fe, Co, Ni, Cu, and Zn in the southeast Pacific. Data are from this study and (12).

Figure 2: Mineralogy of ferromanganese nodules in the southeast Pacific (this study). T = todorokite, B = birnessite.

Figure 3: Primary productivity of surface waters in the southeast Pacific based on EASTROPAC data (35). Inset shows the generalized productivity of the Pacific Ocean (36).

Figure 4: Thickness of the oxidized layer in cores from the southeast Pacific. Data from this study and (4). The most reduced sediments map surface productivity patterns and continental input of organic matter.

Figure 5: Ferromanganese nodule growth rates estimated from Fe content (see text) plotted against measured growth rates, for 20 nodules that have been both dated and chemically analyzed (30, 32, 33).

Figure 6: Estimated accumulation rates of Mn, Fe, Co, Ni, Cu, and Zn in southeast Pacific nodules. Note the difference between Cu, Ni, and Zn accumulation rates and their elemental abundances (Figure 1).

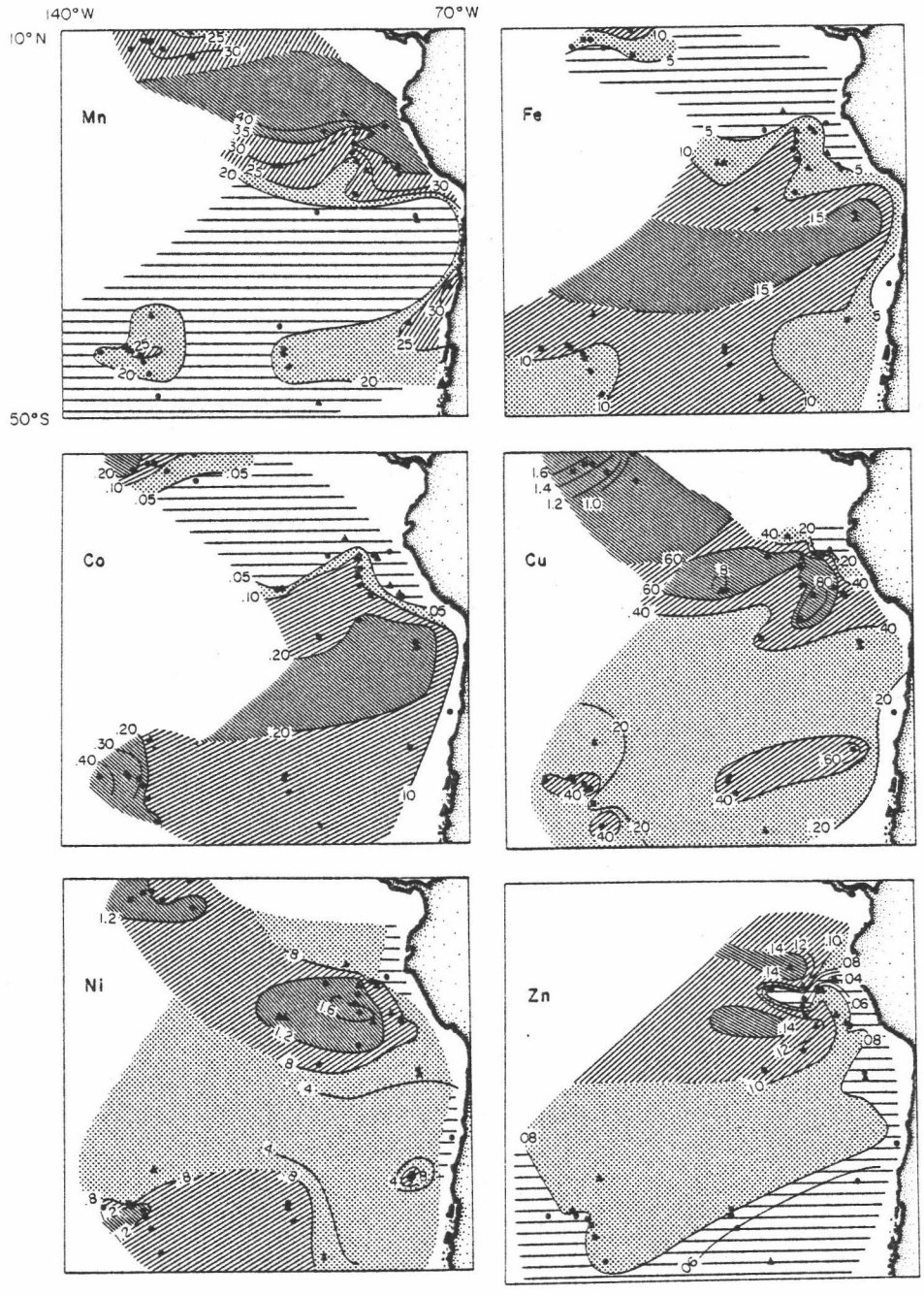

Figure 1

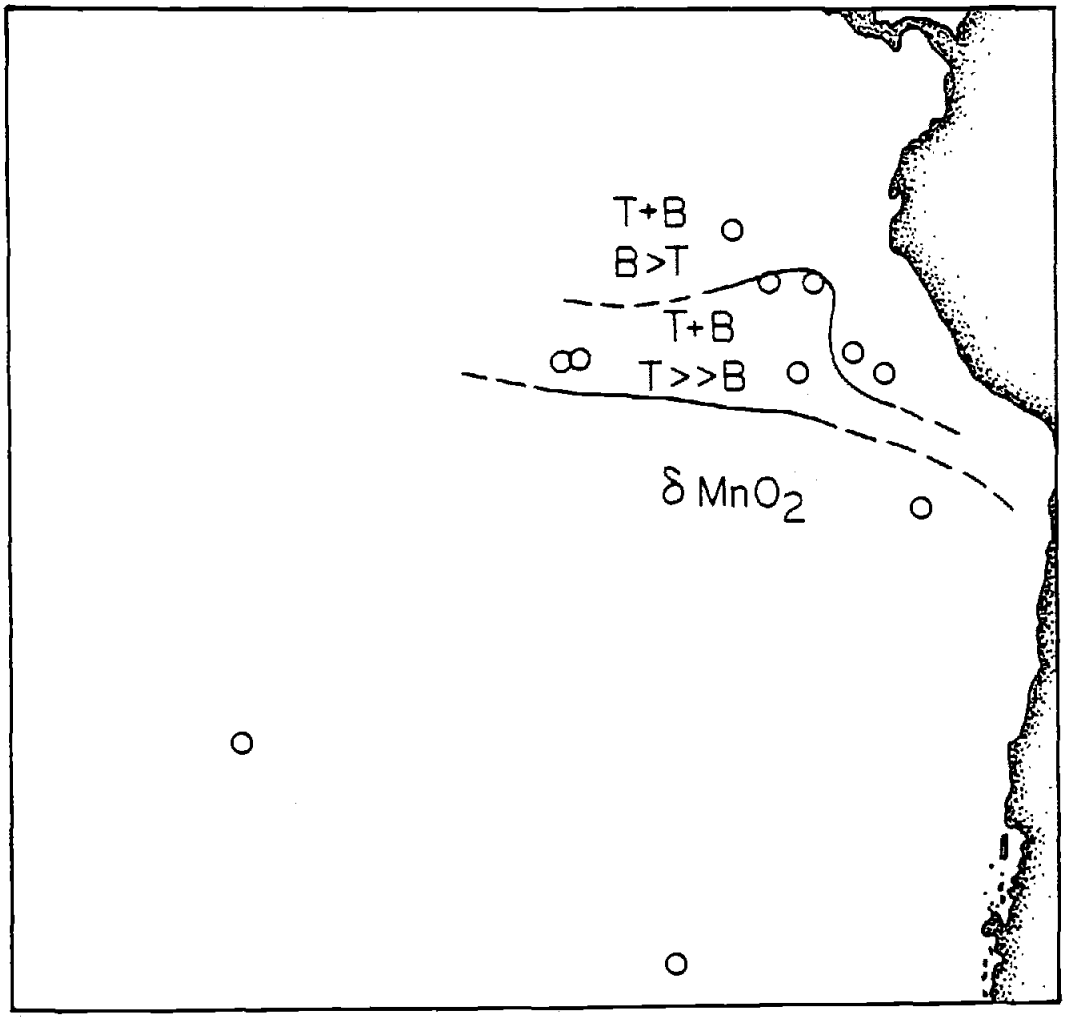

Figure 2

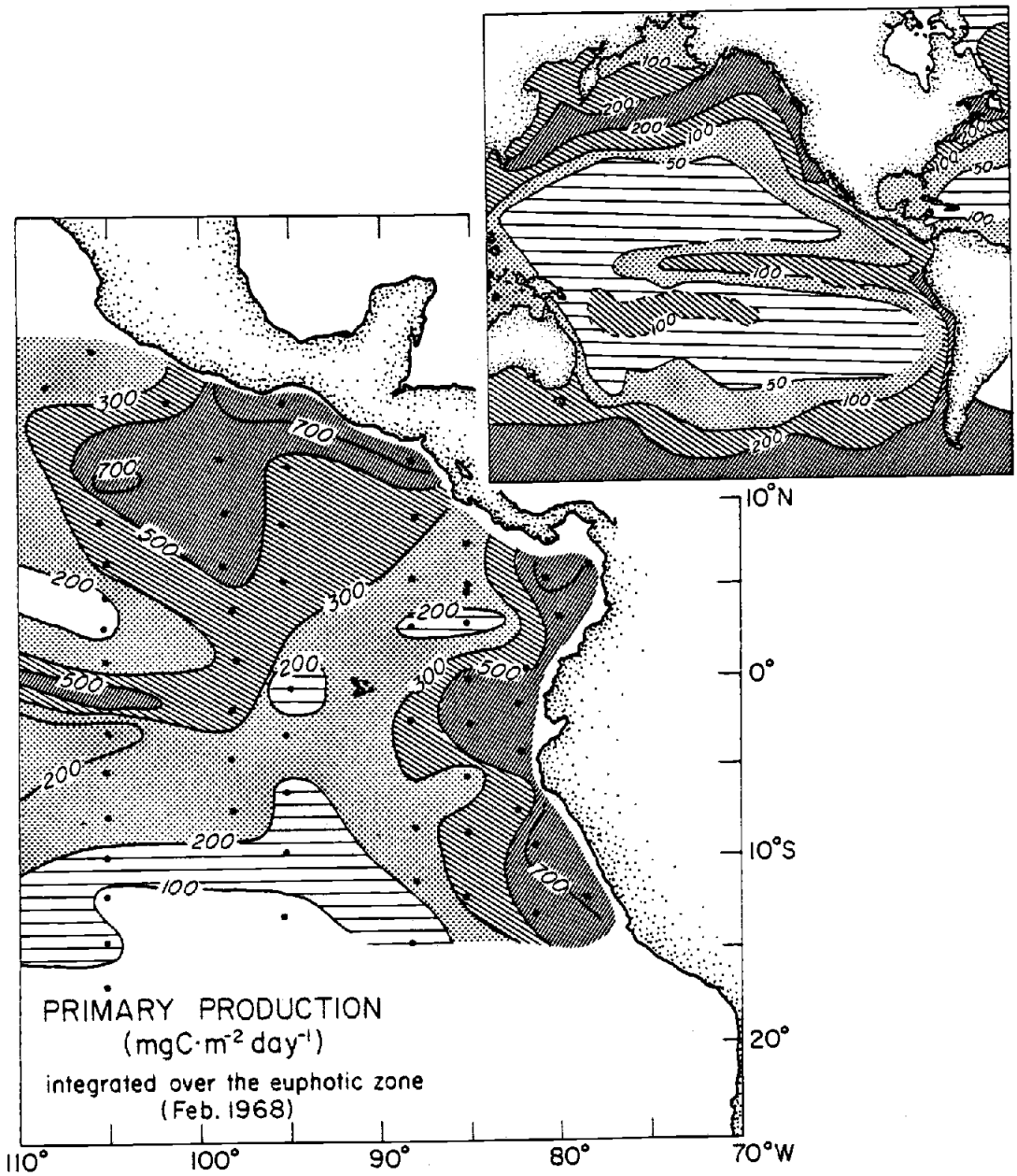
PRIMARY PRODUCTION
(mgC·m⁻² day⁻¹)
integrated over the euphotic zone
(Feb. 1968)
10°N
0°
10°S
20°
110°
100°
90°
80°
70°W

Figure 3

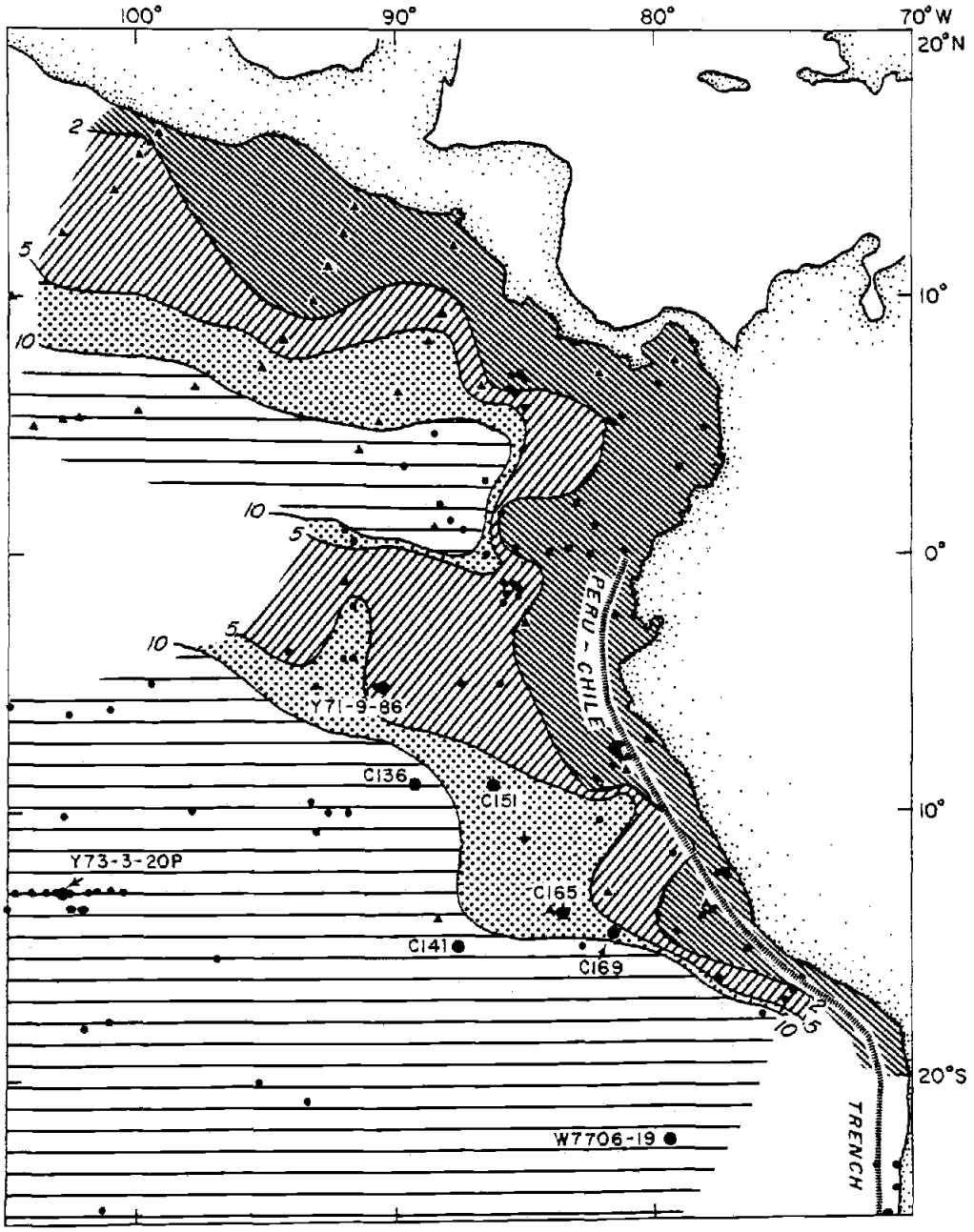
100°
90°
80°
70° W
20°N
10°
0°
10°
20°S
2
5
10
10
5
10
5
PERU - CHILE
TRENCH
Y71-9-86
C136
C151
Y73-3-20P
C165
C141
C169
W7706-19

Figure 4

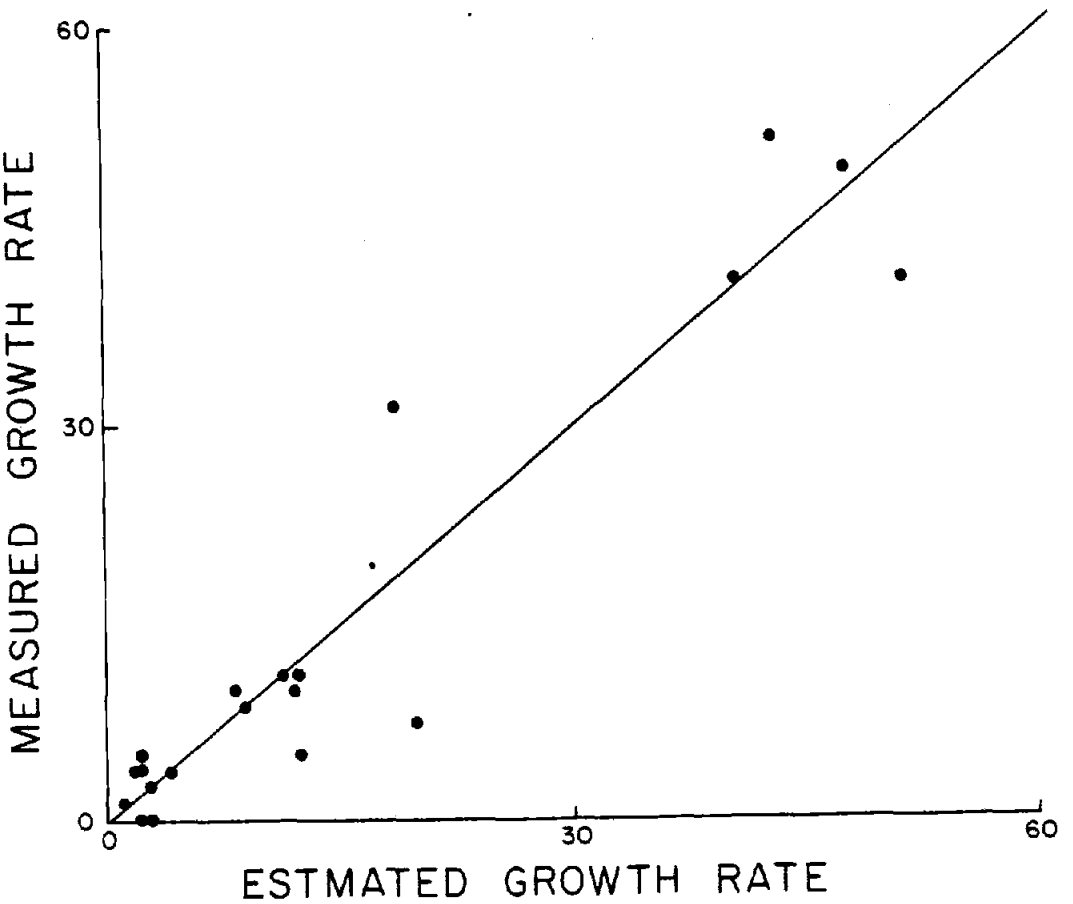

Figure 5

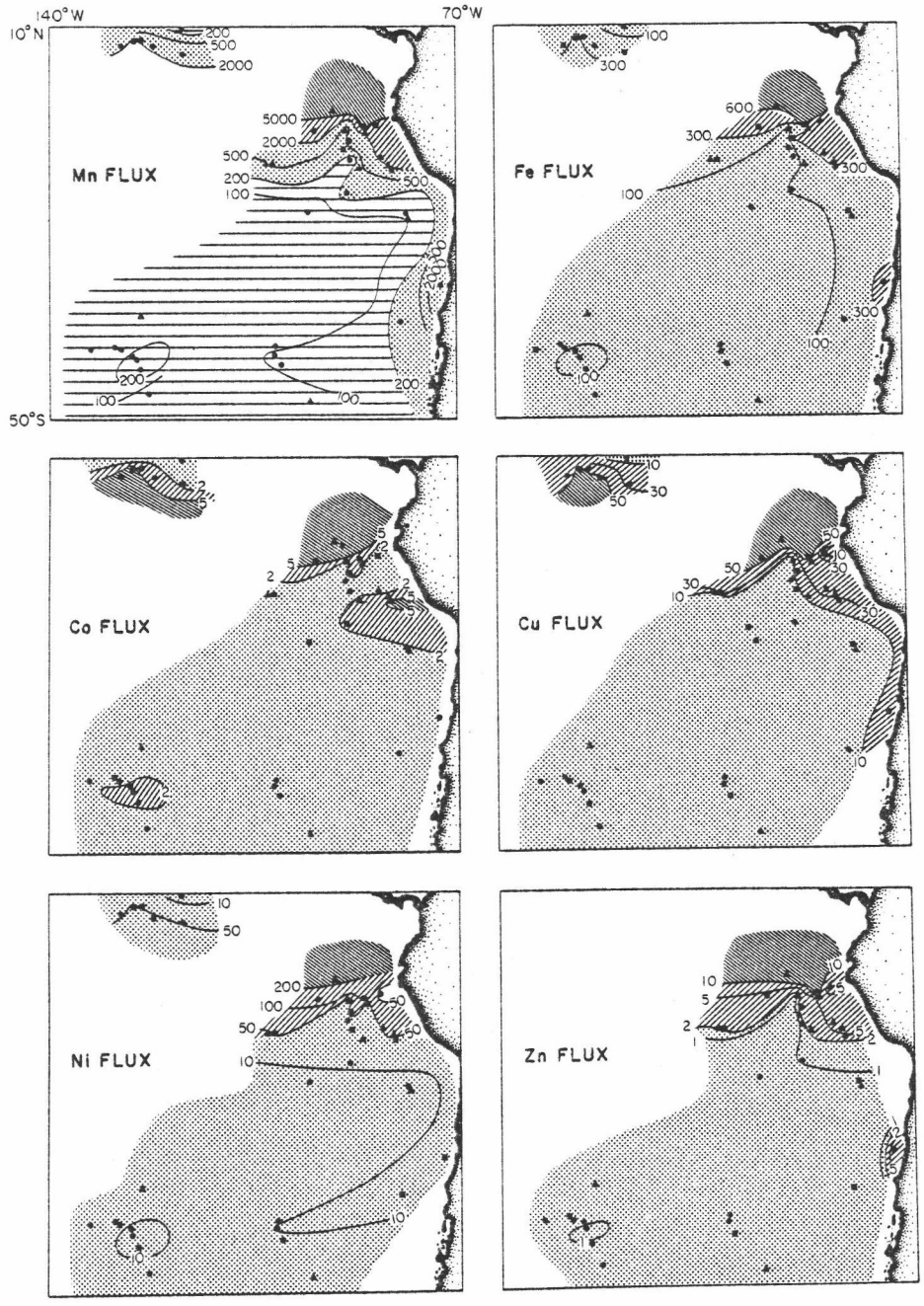

Figure 6

CHAPTER 4

THE FORMATION AND GROWTH OF FERROMANGANESE OXIDES ON THE NAZCA PLATE

by

Mitchell Lyle
School of Oceanography
Oregon State University
Corvallis, OR 97331

ABSTRACT

Marine ferromanganese oxides form four major ferromanganese deposits: hydrothermal crusts, ferromanganese coatings on basalt, ferromanganese nodules, and a mixture of micronodules and other dispersed hydroxyoxides within marine sediments.

Hydrothermal crusts grow only near active marine hydrothermal systems that cool newly emplaced basaltic crust. The crusts are characterized by rapid growth rates, extreme fractionation of Mn from Fe, low accessory element concentrations, and well crystallized manganese minerals.

Ferromanganese coatings on basalt can receive an Fe-rich component from a hydrothermal source but are mainly composed of ferromanganese oxides grown by direct precipitation from seawater (hydrogenous formation). They have δ-MnO_2 mineralogy, have almost equal Mn and Fe abundances, are relatively enriched in the rare earth elements, highly enriched in Ce and Co, and have relatively low Cu, Ni, and Zn abundances. Coatings with a large hydrothermal component are more enriched in Fe, and generally have lower trace element contents.

Nodule and micronodule compositional variations resulting from different sources of transition metals may be further modified by diagenetic reactions within the sediments. The most extreme of these is preferential reductive mobilization of manganese within the sediment column by oxidation of organic carbon and subsequent Mn diffusion to the seawater-sediment interface. Because supply of organic carbon to marine sediments comes primarily from biological productivity in the surface waters and to

a lesser extent from terrigenous sources, ferromanganese oxides formed or altered by this process lie beneath highly productive surface waters or near continents. They are characterized by relatively pure well-crystallized manganese oxides, generally the 7 Å mineral birnessite, and by rapid growth rates. Mn/Fe ratios are 5 or greater, and accessory element contents are low.

Ferromanganese deposits enriched in Mn relative to hydrogenous precipitates are also found in the Bauer Deep and other areas along the fringes of the most highly productive regions, where sediments are not reducing enough to remobilize Mn. Oxic diagenetic reactions, such Fe-smectite formation from biogenic opal, fractionate Fe from ferromanganese hydroxyoxides. The released Mn precipitates as nodules and micronodules.

Iron and manganese that form the ferromanganese deposits have only two ultimate sources: runoff from the continents and hydrothermal fluids that have interacted with cooling basalts formed on the mid-ocean ridges. Seawater acts as a reservoir and mixing chamber for these two sources as currents carry the introduced metals far from their input point. The relative magnitudes of terrigenous and hydrothermal input are roughly equal on the Nazca Plate, although terrigenous input may dominate worldwide.

INTRODUCTION

The ferromanganese oxides form four major types of marine deposits: nodules, coatings on rocks, hydrothermal crusts, and micronodules. Most spectacular are the huge deposits of ferromanganese nodules, found throughout the oceans in regions of slowly accumulating sediments (Mero, 1965). The nodules are generally at least 1 cm in diameter while some grow to be greater than 10 cm across. They have shapes that range from flat discs to almost spherical concretions and are primarily composed of Fe and Mn oxides, although they contain at least trace amounts of almost every naturally occurring element.

Ferromanganese oxides also occur as coatings on basalt or other hard substrate. Normally these coatings are on the order of 1 mm thick on fresh basalts, but may reach several centimeters in thickness on older rocks. Their chemistry to a certain extent resembles that of the nodules, although they tend to be more iron-rich and have systematic variations in the other transition metals (Lyle et al., 1977; Toth, 1977).

The most recently documented ferromanganese deposits occur near mid-ocean ridges and are associated with cooling of newly emplaced crust by seawater (Corliss et al., in press; Moore and Vogt, 1975; Cann et al., 1977; Lalou et al., 1977; Scott et al., 1974). They occur as crusts coating basalt or sediment and can be distinguished from other basalt coatings by the extreme purity of the constituent manganese oxides.

Hydrothermal deposits of essentially pure Fe-oxides or mixed Fe-oxides and Fe-smectites have also been reported (Toth, 1977).

The fourth type of ferromanganese oxides are micronodules and dis-

persed oxides within sediments. Micronodules are small concretions less than 1 mm in diameter that grow separately within the sediment or attached to other sedimentary grains. Much of the dispersed oxide fraction occurs as coatings on other sediment components though a significant fraction may also form separate particles in the extremely fine fraction of the sediment. The chemistry and mineralogy of micronodules has not undergone the extensive study that macro-nodules have. Reported compositions do resemble the larger concretions, however (Dymond and Eklund, 1978; Lopez, 1977; Friedrich, 1976).

Although the ferromanganese oxides occur in a diverse set of morphologies and have diverse mineralogies and elemental abundances, this diversity can be accounted for by relatively few processes. In Figure 1, I have illustrated the pathways through which ferromanganese oxides enter the oceans and then become redistributed. As I will show in later sections, the true source of Fe, Mn, and other elements in ferromanganese deposits can only rarely be distinguished. Hydrothermally influenced deposits can be recognized near the axis of the mid-ocean ridge; terrigenous deposits are generally so reorganized by diagenesis that only process and not source can be recognized. The majority of elements that eventually find their way into the various types of concretions have been relatively well mixed after being added to the oceans. Precipitation from the oceanic reservoir forms what others have called hydrogenous or authigenic deposits (Krishnaswami, 1976).

Diagenesis due to interactions between newly precipitated ferromanganese hydroxyoxides and other sedimentary components dominate the re-

gional geochemistry of the ferromanganese deposits. In regions of relatively low surface productivity or in deposits that grow only in contact with seawater, little or no diagenesis occurs. These deposits have elemental abundances and a mineralogy that can be considered hydrogenous (authigenic).

Interactions of ferromanganese oxides with biogenic silica occur where productivity of the surface waters is of intermediate value. Formation of Fe-rich smectites fractionates Fe from Mn; more manganese rich oxides are thus formed (Heath and Dymond, 1977; Lyle et al., 1977). Ni, Cu, and Zn absorbed or incorporated in the microfossil tests and released by dissolution can also be added to the growing concretions (Calvert and Price, 1977; Greenslate et al., 1973; Lyle, in prep.).

Under regions of high productivity, large amounts of organic carbon are added to the sediments. Reduction of Mn^{IV} to Mn^{II} coupled with the oxidation of organic matter remobilizes Mn within the sediment column and deposits it in an oxidized surface layer. Some of the remobilized Mn can be added to surface concretions, enriching them highly in Mn. Because Fe and other transition metals are not mobilized concurrently, relatively pure Mn oxides form.

The body of this paper will explore sources of Fe and Mn on the Nazca Plate and the effects that source and diagenesis have on the major ferromanganese oxide deposits. I will begin with estimates of the magnitude of Mn and Fe sources on the plate and suggest possible dispersal paths. I will then describe the various ferromanganese deposits, beginning with hydrothermal deposits, whose chemistry is strongly in-

fluenced by source, followed by ferromanganese coatings on basalt which can be influenced by hydrothermal input but also form from the more indiscriminate hydrogenous 'source'. The regional geochemistry of ferromanganese nodules, micronodules, and the leachable fraction of sediments will illustrate the diagenetic processes that control the geochemistry of ferromanganese oxides growing on or within sediments.

PROCEDURES

Ferromanganese Nodules and Ferromanganese Basalt Coatings

Either one half or one quarter of each ferromangan nodule in the study was coarsely ground (-30 mesh) in an agate mortar. In addition, portions were scraped from the tops and bottoms of each of three nodules (C141, C165, C169) which had distinguishable top and bottom features as described by Raab (1972) and subjected to separate analysis. A split was taken for X-ray diffraction analysis and ground fine (<325 mesh) under butanol in an autogrinder. Random powder mounts were X-rayed at 500 sec/deg 2θ with Cu-K α radiation from 5-70° 2θ. A second split was dissolved whole under heat and pressure in hydrofluoric acid and aqua regia and analyzed in replicate for Mg, Al, Si, Ca, Mn, Fe, Co, Ni, Cu, and Zn by atomic absorption spectrophotometry (see Dymond et al., 1973, for more complete description of the technique). The precision of analyses was better than 8% for Al, Si and Ca and better than 5% for the other elements.

Accuracy determined by in-house standards were of the same level. A third split was dissolved in oxalic acid buffered at pH 3 by ammonium oxalate (Heath and Dymond, 1977) to separate the oxide fraction of the nodule from silicate and other refractory components. The solution was filtered through prewashed, preweighed 0.45μ filters to determine the percent of non-oxide components within the nodule and to allow the calculation of the composition of the oxide fraction and of the residue. Residues collected on the filters were also subjected to X-ray diffraction analysis to determine their mineralogy. The leachate was analyzed by AA for Mg, Al, Si, Mn, Fe, Co, Ni, Cu, and Zn. Ca was not analyzed because it forms an insoluble oxalate precipitate. Precision of the analysis was determined by repeated leaching of an in-house Bauer Deep sediment standard. The analyses indicate a precision of better than 15% for Si, better than 10% for Co, and better than 5% for the others.

Two other splits of the ground nodule material were taken for instrumental neutron activation analysis (Gordon et al., 1968). One was irradiated untreated for the elements Sc, Co, Ag, As, Sb, Ba, La, Ce, Nd, Sm, Yb, Tb, Lu, Hf, Th, and U. The second was leached as described above. The residue was collected and weighed, and a portion irradiated to analyze for the elements listed above. The material scraped from the tops and bottoms of the nodules had too little sample for the residue study.

Ferromanganese coatings were treated similarly to the nodules except in sampling. One sample, FDR75, was thick enough that the sampling procedure was similar to the nodules. The others were scraped from their substrate of either fresh or altered basalt. Only FDR75 and

DM 1016 had enough sample to attempt the neutron activation residue study.

The data from these analyses are presented in Tables I and II. Also included in the table are four samples from other recent studies (Corliss et al., in press; Toth, 1977; Lyle et al., 1977) located on the Nazca Plate.

Micronodule and Sediment Analysis

Surface sediment samples were available from the same stations as all nodules in this study except Y73-3-22D, in the Bauer Deep. The samples were first split for micronodule analysis and a bulk sediment study. The split designated for bulk sediment analysis was further subdivided for bulk chemical analysis, leach chemical analysis, and for X-ray diffractometry. Bulk chemical analysis was accomplished by a combination of atomic absorption spectrophotometry and neutron activation analysis as had been done for the nodule study.

Leach chemical analysis was performed to separate the micronodule and dispersed oxide fraction from the other sediment components by the same technique as for the nodules. The oxalic acid leach solution was filtered through prewashed, preweighed 0.45 μ filters, and the leachate analyzed for Mg, Al, Si, Mn, Fe, Co, Cu, Ni, and Zn by AA.

A third part of the bulk sediment was examined by X-ray diffractometry. The subsample was first leached with acetic acid buffered at pH 5 with sodium acetate to remove any calcium carbonate. A preliminary study revealed that this treatment did not chemically attack micronodule

material to any significant extent. The acetic acid leached sample was ground fine (<325 mesh) under butanol in an autogrinder and random powder mounts of the material were X-rayed using Cu-Kα radiation at a scan rate of 500 sec/degree 2θ over a range of 5° to 70° 2θ.

Micronodules were separated from the second split of the sediment by a combined physico-chemical technique. The sediment samples were first wet sieved at 44 μ (325 mesh) to remove the clay fraction. Clay aggregates were dispersed and removed by gently rubbing the sample through the sieve under flowing water. Calcium carbonate debris was removed by leaching with acetic acid buffered at pH 5 with sodium acetate. This has the additional effect of probably removing any adsorbed or surface-coating ferromanganese oxides. The coarse fraction was examined both before and after leaching as a qualitative determination of minerals present in the sediment. Results are described in Appendix 3.

The final separation of micronodule material from the coarse fraction of the sediment was achieved by the buffered oxalic acid leach technique. The leach was filtered again at 0.45μ and the difference in weight between the residue and original sample was used to determine the weight of micronodules analyzed. Accuracy of the micronodule weight is to within 1-2 milligrams.

Atomic absorption analysis was performed for Mg, Al, Si, Mn, Fe, Co, Ni, Cu, and Zn. Precision determined by replicate analyses is better than 10% for all elements. Absolute composition seems good for samples where greater than 5 mg of micronodule material was leached. Relative abundances for those samples where less micronodule material was leached

still seem good except for Y71-9-86 MG1. There was so little micronodule material leached in this sample that the data was ignored. Sediment and micronodule analyses are reported in Tables III and IV.

SOURCES OF Mn AND Fe ON THE NAZCA PLATE AND THEIR DISPERSAL AGENTS

Ferromanganese

oceanic ferromanganese deposits. There are only two ultimate sources of manganese and iron in seawater and marine sediments - the continents and the mantle. Erosion strips sediments and dissolved constituents from the land and cycles them into the oceans. Emplacement of basaltic crust derived from the mantle and the high temperature interaction between seawater and rock will also leach Mn, Fe, and other constituents and deliver them to the oceans.

The relative proportions of Mn and Fe that enter the oceans at rise crests are probably best estimated from the composition of sedimentary deposits at the East Pacific Rise (Dymond et al., 1973; Heath and Dymond, 1977). Although hydrothermal solutions emanating from rise crests have now been collected (Corliss et al., in prep.) local conditions are important enough to produce major variations in solution chemistry (Stakes, 1978). The sediments most probably collect precipitates from large numbers of hydrothermal fields in all stages of development. They therefore remove the effects of local variations. The Fe/Mn ratio of East Pacific Rise sediments is relatively constant at 3.0 all along the Rise Crest (Heath and Dymond, 1977). I
will use this as the ratio of Fe to Mn from hydrothermally derived

material. Lyle (1976) (see Appendix 1) has estimated the hydrothermally derived manganese input to the oceans to be 9×10^{11} gm/yr. The estimate is based on accumulation rates of Mn in a rough transect across the EPR at 11-17°S. The worldwide estimate is based upon the assumption that manganese leached by crustal alteration is proportional to the amount of crust emplaced per year. The input of manganese to the oceans at the spreading margins of the Nazca Plate can be estimated through use of the same assumption. The production of 0.92 km^2 new crust per year (based upon Minster et al., 1974) around the Nazca Plate will produce 3×10^{11} gm Mn/yr to the oceans. From the hydrothermal ratio given above, approximately 9×10^{11} gm Fe/yr are released by the same process.

Terrigenous fluxes of Mn and Fe from South America are necessarily tentative because of the sparse amount of data available. Before I discuss the methods I used to estimate continental fluxes, I first wish to develop a qualitative model for the mechanism that controls continental loss of Mn and Fe.

Mn and Fe are removed from the continents through the erosion of highlands and transport of dissolved and particulate erosion products to the sea in rivers. Although Mn and Fe are dissolved components in river water, most Mn and Fe are associated with the particulate fraction carried by the river (Boyle et al., 1977; plus suspended sediment load of about 400 mg/l, Turekian, 1969). As the manganese and iron pass into the marine environment, the dissolved fraction converts to particulate form (Boyle et al., 1977; Graham et al., 1976) and either settles

out of the water column within the estuary or passes into the open ocean to deposit on the continental shelf with most of the suspended load of the river.

Because of the large percentage of organic debris carried by the rivers, these shelf sediments are mildly to strongly reducing throughout the entire sediment column. Any Mn^{IV} existing as oxide particulates or adsorbed to other grains could be remobilized and cycled back to the sea. Most of the dissolved load of Mn which had precipitated in the estuaries and a significant fraction of the particulate Mn should thus escape from the sediments. Fe not contained in silicate phases is also reduced, but I will assume that much of this Fe is fixed by formation of diagenetic minerals such as sulfides, clays, and phosphates (Krauskopf, 1956). The continentally derived Mn and Fe, now fractionated to be more Mn rich, is carried away by surface currents and mixed with normal ocean waters.

Continental Mn, Fe Input to the Nazca Plate

The continental Mn and Fe contribution from South America to the Nazca Plate could be estimated from runoff data for the Pacific Coast of South America. Since little runoff data for rivers on the western side of the continent are available, however, I have used maps of average rainfall for Chile and Colombia (Prohaska, 1976; Snow, 1976) and contoured the sparse data for the Pacific coast of Ecuador presented in Ferdon (1950) to estimate average rainfall to these countries. I assumed that for a maximum estimate, rainfall must equal runoff. By this

technique I estimated that 3×10^{14} l/yr flows from Colombia to the Pacific while 2×10^{14} l/yr and 1×10^{15} l/yr flow from Ecuador and Chile, respectively. Average total runoff from Peru is 4×10^{14} l/yr, primarily from the north coast (Zuta and Guillen, 1970). The total for the entire coast is about 2×10^{15} l/yr.

The total mass of Mn and Fe that reaches the shelf will be equivalent to the dissolved plus particulate load of the river, since I assume that all dissolved Mn and Fe will coagulate and precipitate. The amount of continental material added to the continental shelf can now be estimated by assuming that the particulate load of the river is proportional to runoff. On the Pacific Coast of South America, this does not seem to be a bad assumption; Scholl and others (1970) have demonstrated that the volume of Cenozoic sediments on the Chile margin are proportional to the rainfall on land. Their maximum denudation rate suggests that Chile supplies approximately 10^{14} gm/sed per year to the shelf, and implies an average suspended load of 100 mg/liter. Turekian (1969) has estimated average suspended load for the world's rivers to be 400 mg/liter, which I will use for a maximum suspended load. The rivers of South America thus supply a suspended sediment load of 2 to 8×10^{14} gm/yr to the shelf and slope of the continental margin.

The average sediment composition of 20 cores taken from the continental margin of Ecuador and Peru is about 400 ppm Mn and 4.7% Fe (Erwin Suess, personal communication). An estimate for remobilization for this shelf sediment can be made by comparing this average to either average igneous rock or average shale composition es-

timates (Broecker, 1974; Wedepohl, 1969a,b). The difference should represent the remobilized fraction. Estimates of Mn content in the average shale or igneous rock range from 600 to 950 ppm -- significantly higher than the Peru shelf sediments. Average Mn loss can be estimated to be 200 to 550 ppm from the continental shelf sediments of South America. Fe contents of Peru shelf sediments fall within the ranges quoted for average igneous rock or shale. I cannot therefore distinguish Fe loss from these sediments by this approach.

Approximately 4×10^{10} to 4.4×10^{11} gm of Mn would be remobilized from particulates each year on the continental shelf of South America. If the same type of argument is applied to the suspended load discharged by the world's rivers, continental Mn flux should be $1\text{-}7 \times 10^{12}$ gm/yr. Elderfield (1976) calculated that precipitation of Mn in deep-sea sediments required $1\text{-}7 \times 10^{12}$ gm of Mn in excess of the dissolved stream supply. Elderfield's value is for all other sources including hydrothermal sources; nonetheless, the similarity of the numbers provides support for my model. Total Mn removed from the continent will also include the dissolved Mn, which will have a flux of 1×10^{10} gm/yr (based upon 7 ppb Mn in average river water; Turekian, 1969). The total Mn flux from South America should be about 5×10^{10} to 4.5×10^{11} gm/yr. Table V lists the fluxes of Mn and Fe from terrigenous and hydrothermal sources around the Nazca Plate.

DISTRIBUTION OF TERRIGENOUS AND HYDROTHERMAL Fe AND Mn

Iron and manganese entering oceans at mid-ocean ridges will be dispersed in a much different fashion than that derived from the South

American continent. Hydrothermal Mn and Fe is injected in dissolved form into the bottom waters, so bottom flow will govern the hydrothermal distribution. Terrigenous Mn and Fe will be added to near-surface waters passing over the continental shelf, so that surface currents or midwater flow will govern the dispersal in this case. Reducing abyssal sediments near the continents may also cause remobilization of terrigeneous Mn and addition into bottom waters, however,

Figure 2 illustrates the generalized surface circulation for the Nazca Plate and shows where maximum river runoff occurs. As this figure demonstrates, most continentally derived elements will travel along the coast and be carried offshore between 15°S and the equator.

As terrigenous Mn and Fe are being carried by the near-surface currents, they will be continually stripped from the waters by adsorption onto biogenic tests or by incorporation into the planktonic organisms. The highest productivity occurs along the continental margin (Zuta and Guillen, '970); Mn and Fe may thus cycle many times between waters and sediments before escaping the margin. The surface waters of the Eastern equatorial Pacific are also highly productive (Love and Allen, 1975) so the cycling of continental Mn and Fe to the sediments near the equator should be very effective.

Circulation of abyssal waters that controls the distribution of hydrothermal Mn and Fe is more poorly understood than surface circulation. Lonsdale (1976) has developed general circulation patterns for the southeast Pacific, however. Flow over the East Pacific Rise most probably passes through fracture zones in the north and is forced

south by topographic confinement of the Fossil Galapagos Rise (Figure 3). Hydrothermal components for this highly active section of the mid-ocean ridge are thus largely confined in the Bauer Deep. A second flow of abyssal waters enters through fracture zones on the southern boundary of the Nazca Plate. There is much less crustal production on this segment of the mid ocean ridge, however, so hydrothermal influence is probably not as great as in the northwest corner of the plate.

Most manganese and iron from either hydrothermal or terrigenous sources gets stripped from seawater near where they enter the oceans. Biological vectors remove much of the terrigenous Fe and Mn along the margin and in the northeast corner of the plate. Hydrothermal Fe and Mn precipitate rapidly to the sediment as indicated by accumulation rates (Dymond and Veeh, 1975) and modeling studies (Weiss, 1977). The remains mix together to form the hydrogenous 'source'.

As will be seen in the next two sections, effects of the hydrothermal source can be distinguished near the East Pacific Rise Crest. Extensive diagenesis of terrigenous source material masks its distinctive characteristics, however. Diagenetic processes will control the geochemistry of deposits near the continental margins.

HYDROTHERMAL FERROMANGANESE DEPOSITS ON THE NAZCA PLATE

Hydrothermal ferromanganese deposits are one of the few marine ferromanganese deposits where source can have demonstrable effect on the geochemistry of the deposit. Marine hydrothermal systems debouch

fluids relatively rich in both manganese and iron, but carry only trace amounts of the other common elements in ferromanganese deposits. High concentrations of H_2S, such as found in the Galapagos hydrothermal fluids (Corliss and others, in press), suggest Fe and other trace metals are precipitated in the rocks as sulfides. The huge influx of Fe and Mn causes the deposits to grow quite rapidly, as has been reported by Scott and others (1974), Moore and Vogt (1975), and has been inferred by Corliss and others (in press).

The rapid growth rate precludes incorporation of large abundances of trace metals from seawater (Toth, 1977; Corliss and others, in press), and also prevents large scale preferential enrichment of elements such as Ce and Co from seawater as may be seen in more normal deposits.

Fractionation of Fe from Mn is common in hydrothermal-type deposits due to precipitation of Fe as sulfides before the hydrothermal fluid leaves the vent (Corliss and others, in press), as silicates (Stakes, 1978), or through preferential precipitation of Fe over Mn from seawater (Bonatti and others, 1972). Relatively pure Mn oxides and Fe-silicates, sulfides, or oxides instead of mixed phases are thus normally found.

Documented hydrothermal deposits are all local features near hydrothermal vents (Lalou and others, 1977; Scott and others, 1974; Cann and others, 1977; Corliss and others, 1978). The influence of hydrothermal activity extends further, however, as is indicated by metalliferous sediments near active spreading centers (Bostrom and Peterson, 1969; Dymond and others, 1973), and by compositions of ferromanganese coatings

as was discussed by Toth (1977) and as will be discussed in the next section.

FERROMANGANESE COATINGS ON BASALT

Toth (1977) has suggested that ferromanganese coatings on basalt are formed by hydrogenous precipitation of ferromanganese oxides and associated elements from seawater, diluted near the Rise crest by hydrothermal Fe and Si. Findings in this study agree with his conclusions.

Hydrogenous formation of ferromanganese oxides is assumed to occur because seawater is oversaturated in Fe and Mn due to continual addition from terrigenous and hydrothermal sources. The excess will precipitate to sediments, nodules, and basalt as well as coprecipitate other elements from seawater. Calvert and Price (1977) have established criteria that describes hydrogenous ferromanganese deposits. They assumed that ferromanganese nodules that have the same Mn/Fe ratio as the oxide fraction of the associated sediment have not been diagenetically altered (calculated from Al contents and compositions of the aluminosilicate fraction of the sediment). Mineralogy and elemental abundances in these nodules can be considered to represent hydrogenous ferromanganese oxides. By use of this criterion they suggest that hydrogenous ferromanganese oxides are distinguished by having a δ-MnO_2 mineralogy, a Mn/ Fe ratio near unity, relatively high concentrations of Ce, Co, Pb, and Ti, and relatively low concentrations of Cu, Ni, Zn and Mo.

On the other hand, hydrothermal precipitates are distinguished by

very low trace element concentrations and by rare earth element abundance patterns similar to seawater (Toth, 1977; Corliss and others, in press). The Ce content is low in these precipitates, presumably because of the low trace element content of the hydrothermal fluid and the relatively rapid growth which precludes large-scale cerium adsorption from seawater. Toth (1977) also suggests that hydrothermal precipitates incorporated into ferromanganese coatings will be Fe-rich.

Figure 4 illustrates the regional distribution of Mn, Fe, Ce, and Co in ferromanganese coatings from this study. Although Fe is not always most highly enriched in coatings recovered near the Rise Crest, trace element contents, illustrated by Co and Ce, are lowest there as would be expected if ferromanganese coatings growing near the rise crest have a hydrothermal component. It is unlikely that the Ce high near the continent is caused by terrigenous input since enrichments as high or higher are seen in hydrogenous ferromanganese nodules in this study recovered far from the continents (e.g. nodule DM 981, Ce = 1770 ppm, versus Coating FDR 75, Ce = 769 ppm).

Additional support for a hydrothermal component in Rise Crest ferromanganese coatings is illustrated by Figures 5 and 6. Rare earth abundance patterns of ferromanganese coatings (Figure 5) show that Rise Crest coatings typically have lower absolute abundances of the rare earths and patterns more similar to seawater than coatings from off the Rise Crest. Figure 6 demonstrates that the La/Ce ratio of coatings from the Rise Crest are similar to seawater, while coatings from off the Rise Crest are much more highly enriched in Ce.

FERROMANGANESE NODULES

Calvert and Price (1977a) and Lyle (in preparation) have demonstrated that diagenesis related to surface productivity in equatorial Pacific waters produces profound modifications of ferromanganese nodule mineralogy and chemistry. Nodules under regions of low productivity seem to be products of hydrogenous precipitation from seawater alone. Where productivity is high, the high flux of organic carbon and its oxidation produce reducing conditions within the sediment column. Mn^{IV} in oxides becomes reduced to the more soluble Mn^{II} and diffuses back to the surface. Lyle (in preparation) estimates extremely high growth rates for nodules from this region, due to the high Mn flux. Concentrations of other elements in these nodules are low for the same reason -- the remobilization of Mn and its precipitation on nodules dilutes the concentrations of other elements.

In the borderlands between high productivity and low productivity, sedimentation rates are low enough that much of the organic carbon is oxidized at the surface of the sediment column. There is little evidence that the sediments become reducing or that Mn is remobilized. Ferromanganese nodules from this region still exhibit enrichment in manganese when compared with hydrogenous nodules, however. Heath and Dymond (1977) and Lyle et al. (1977) have suggested that reaction of poorly crystalline ferromanganese hydroxyoxides precipitated from seawater

with biogenic opal forms an Fe-rich smectite while the manganese released will form micronodules or precipitate on nodules.

Productivity in the surface water, besides controlling manganese concentration in nodules, provides transport for bioactive trace metals to the ocean floor. Cu, Ni, and Zn may thus be enriched in nodules in regions underneath moderate to highly productive surface waters (Piper and Williamson, 1977).

In this section I will present a more detailed analysis of this proposed diagenetic scheme.

Hydrogenous Nodules

Nodules from low productivity regions (DM981, DM994, DM1006, and W7706-19, in this study) appear to be little modified from hydrogenous type deposits discussed in the last section. They have a δ-MnO_2 mineralogy, low Mn/Fe ratios, high Ce and Co contents, and relatively low Cu, Ni, and Zn abundances. The nodules from this study also exhibit high rare earth element, Sc, As, Th, and U abundances (Table I). Nodules considered hydrogenous by Calvert and Price (1977A) and those from low productivity regions in this study show little compositional difference between the oxide fraction of the sediments and that of the nodule at the same station (the oxide fraction in this study is defined as the fraction leachable by oxalic acid).

Hydrogenous precipitation most probably adds Mn, Fe, and co-precipitated trace elements in relatively constant proportions, and will continue to add elements even to nodules highly modified by diagenesis.

Good correlations should thus exist for all elements whose prime source is from hydrogenous precipitation alone. Good correlations are found between Fe, As, and rare earths, Hf, Th, and Sc in all the nodules of this study, as illustrated by scatterplots of Fe against As, La, Sc, and Hf (Figure 7). Fe-hydroxides are used to strip rare earths from seawater for analysis (Hogdahl and others, 1968) and to strip Th and U from solution during separation for isotope studies (Ku, 1966). Fe-hydroxides are also known to quantitatively coprecipitate As (Onishi, 1969).

These elements should thus coprecipitate with Fe if it precipitated from seawater and thus support the postulate that they are hydrogenous.

Evidence that hydrogenous precipitation continues to occur even in areas where diagenesis reorganizes the ferromanganese oxide can be demonstrated by nodule top and bottom studies. Raab (1972) discovered that nodules from the central Equatorial Pacific with morphologically distinguishable tops and bottoms resemble hydrogenous deposits on the upper surface, but are enriched in Mn, Ni, Cu, Zn, and Mo on the lower surface. Calvert and Price (1977) interpret this to demonstrate a higher amount of hydrogenous enrichment on the upper surface versus a larger diagenetic component in the lower one. Three nodules in this study (C141, C165, and C169) also have morphologically distinct tops and bottoms. C141 from a region of moderate productivity, has an Mn/Fe

ratio of 1.9 for its top versus 10.5 for the bottom. The upper surface also has a δ-MnO_2 mineralogy typical of hydrogenous deposits, while the lower surface is primarily birnessite. C165 and C169, both within the more highly reducing productive region, show no strong difference in the Mn/Fe ratio from top to bottom. Birnessite is the only manganese mineral to occur on either surface of either nodule. Diagenetic processes and the concomitant higher accumulation rates for Mn presumably more important at these sites probably overwhelm the small flux from hydrogenous precipitation.

Nodules from low productivity regions can be strongly enriched in Ce with respect to other rare earths (Figure 8), but this may be due to oxidation to Ce^{IV} in highly oxidizing marine environments (Piper, 1974). Co also can be oxidized from Co^{II} to Co^{III} at about the same Eh (Figure 9). Both are most highly enriched in nodules from what appear to be the most oxidizing environments, and each is enriched in constant proportion to the other (Figure 8b). Enrichment of Ce and Co by oxidation and preferential uptake can also be considered hydrogenous precipitation.

Diagenesis and its Effects on Ferromanganese Oxide Geochemistry

Nodules highly enriched in manganese in lakes, estuaries, and continental shelves (Calvert and Price, 1977b) can be explained best by diagenetic remobilization of Mn and its precipitation in more oxidizing environments. Similar patterns in pelagic environments (high Mn/Fe ratios in nodules from organic carbon-rich equatorial Pacific sediments) led

Price and Calvert (1970) to propose the same type of mechanism for pelagic nodules. Because Fe in ferromanganese oxides disorders the manganese structure and probably reduces the available sites for Cu, Ni, Zn and other trace metals (Burns and Burns, 1977) diagenetic separation of Mn and Fe can have profound effects on the geochemistry of the ferromanganese oxide. In addition, the added flux of Mn -- one of the major components of the oxide -- should produce major increases in the growth rate of the nodule.

Krauskopf (1956) best describes the separation of manganese from iron by redox reactions, and demonstrates theoretically that the lower solubility of Fe^{II} silicates, carbonates, and sulfides would enhance the fractionation of the two elements. Figure 9 illustrates redox reactions that would occur in the marine environment for oxides and hydroxides (Pourbaix, 1974) at pH 8. Because of the relative constancy of marine pH conditions, a pH range need not be considered. It shows that redox governed Fe and Mn precipitation/dissolution are separated by ∿800 mV when the elements are present in concentrations reported in seawater (Brewer, 1975), and are still separated by greater than 700 mV when at concentration levels measured in pore waters (Hartmann and Muller, in press). Manganese would thus be the first to be mobilized as the sediment becomes more reducing than oxygenated seawater and would thus be easily separated from coexisting Fe hydroxides.

The only other element that may be enriched by reducing diagenetic reactions is Ni. The concentration of Ni in seawater is at the level

that would be expected if it were in redox equilibrium with oxygenated seawater. Any lowering of Eh conditions within the sediment should remobilize precipitated Ni oxides, unless the Ni became fixed in other minerals (e.g., Mn oxides or silicates). M. Bender (personal communication) notes a strong correlation between dissolved Ni and dissolved Mn in pore water, suggesting that its distribution is governed by solid solution with or adsorption onto the manganese oxides, and not by the thermodynamic stability of Ni oxides.

Redox conditions in marine sediments are controlled by the oxidation of organic carbon. Organic carbon provides by far the largest reservoir of electrons (Stumm and Morgan, 1970) and biogenic catalysis of its oxidation is quite common. On the Nazca Plate, organic carbon is added to the sediments from the continents and from biological activity in the surface waters. The combined flux is most important in the northeast corner of the plate following the same arguments as presented earlier in this paper for terrigenous dispersal. Redox conditions determined by mapping the thickness of the oxidized tops of cores taken from the Nazca Plate demonstrate the response of the sediments to this flux.

There is commonly a color change that can be observed in the tops of cores from reducing environments which marks an oxidation boundary. Fe^{III} reduction to Fe^{II} probably causes the sediment color to change from brown to gray-green (Hartmann et al., 1976) although Lynn and Bonatti (1965) give good evidence that it marks the precipitation boundary of Mn and thus a much higher Eh (about 400-500 mV). In either

case the color change marks the depth at which the diffusion of oxidants into the sediment from seawater can no longer buffer the Eh, which consequently plummets. The depth to this boundary thus gives a measure of intensity of reducing conditions within the sediment. Figure 10 maps the depth of this boundary measured in 161 cores taken by Oregon State University in the eastern Pacific and combined with the data set of Lynn and Bonatti (1965). The color change generally cannot be distinguished when the oxidized zone becomes thicker than about 20-30 cm.

Nodules in this study that were recovered from within the region of reducing sediments at depth (Y71-9-86, C151, C165, C169) all have distinctive chemical compositions and mineralogy.

Birnessite is generally the dominant manganese mineral present, although one sample (C151) was composed of a well crystallized todorokite. Mn/Fe ratios are extremely high, in all cases greater than 5 for the bulk nodule compositions (see Table I). Other transition metal trace element contents are relatively low. For example, all samples contain less than 1% Ni, and the rare earth concentrations are about 10% of hydrogenous nodules (e.g., DM 981 or W7706-19).

Sb and Ag are both enriched in the nodules formed by reducing diagenesis (RD nodules). The good correlation between Sb and Mn (Figure 11) at higher Mn contents, and the similarity between Mn^{IV} and Sb^{V} ionic radii (Whittaker and Mantus, 1970) suggest that it may replace Mn^{IV} in the manganese lattice. Ag is very actively sorbed by manganese oxides (Anderson et al., 1973). Any available silver, perhaps from

the continents, may enter these nodules.

Lyle (in preparation) has estimated accumulation rates for nodules and can demonstrate that although concentrations of most accessory elements are low, their accumulation rates in RD nodules are as high or higher than accumulation rates in hydrogenous nodules. Cu, Ni, and Zn fluxes are more than 10 times higher in RD nodules than fluxes to hydrogenous nodules, for example.

Cu, Ni, and Zn do not become remobilized by redox reactions within the sediments (see Figure 9); the high accumulation rates of these elements in RD nodules must be due to another process. High productivity occurs over the areas where RD nodules occur, and the remains of plankton falling to the sea floor may transport significant quantities of transition metals and other elements to the sediments (Murray and Brewer, 1977). Most of the planktonic debris redissolves (Heath, 1974; Hurd, 1973), much of it at the sea floor (Edmond, 1974), where part of the trace metal load may become incorporated in nodules. Because planktonic debris supplies the bulk of organic carbon to pelagic sediments and because the oxidation or organic carbon controls the redox condition of the sediments, highest accumulation rates will occur in nodules in regions of reducing diagenesis.

Oxic Diagenetic Reactions

There is little evidence that sediment on the borders of regions of biogenic sedimentation become reducing enough to remobilize manganese.

There is no color change in the surface sediment, and only rarely is there a surface maximum of manganese abundance in sediment cores, a feature characteristic of Mn remobilization (Lynn and Bonatti, 1965). Yet within this region nodules are commonly recovered with Mn/Fe ratios of 2 or greater. Nodules recovered only a few degrees further south have Mn/Fe ratios of approximately 1 (compare W7706-19 with C141) while ferromanganese coatings presumably growing in seawater recovered at the same site as nodules grown in sediment have a significantly lower Mn/Fe ratio (Lyle et al., 1977). These data suggest that precipitation of ferromanganese oxides from bottom waters enriched in Mn cannot explain the relative enrichment of Mn in these nodules.

Dissolution of the more sparse biogenic remains that settle to the bottom here and incorporation of the released elements into nodules could not enrich nodules in Mn either. Mn/Fe ratios in the hard parts of phytoplankton are less than 1, while Fe is approximately an order of magnitude more abundant than Mn in the organic fraction (Martin and Knauer, 1973).

A mechanism is needed to fractionate iron from manganese in an oxic environment. One possible mechanism was suggested by Lyle et al. (1977) and Heath and Dymond (1977). Fe-rich smectite formation could occur by the dissolution of opaline silica tests and recombination with Fe from FeMn hydroxyoxides. The Mn released would form manganese minerals in nodules and micronodules.

The general reaction can be written as follows:

$$SiO_2 \text{ (opal)} + FeMnOOH \rightarrow Fe_4(Fe,Al,Si)_8\ O_{20}(OH)_4 \cdot nH_2O \text{ (Fe-smectite)} + MnO_{1-x} \text{(todorokite, birnessite)}$$

This reaction cannot be evaluated by the thermodynamics of the solids alone, however, because of the microcrystalline nature of the reactants and products. A free energy of formation can be estimated for the smectite (Nriagu, 1975; Tardy and Garrels, 1974), and has been measured for a typical birnessite (Bricker, 1965). One may be justified in approximating the free energy of formation of ferromanganese oxyhydroxides as being greater than that of goethite, and could assume the free energy of opal to be similar to amorphous silica (Robie and Waldbaum, 1972). With these assumptions and using the average Fe-smectite composition reported in Dymond and Eklund (1978) and free energies for aqueous Al, Mg, Ca, Na, and K as reported in Tardy and Garrels (1974), the free energy for the reaction can be calculated to be about -122 kcal/mole.

The additional free energy contributed by the formation of a surface may reverse the stability of the reaction, however. For example, goethite has an enthalpy of formation for its surface of 1250 ergs/cm^2 at 70°C (Langmuir and Whittemore, 1971). If this is approximately equal to the free energy of the surface, approximately 4000 kcal/mole will be added to the free energy of formation of 10 Å crystallites by the surface free energy. Approximately the same

magnitude of energy is probably needed to form smectite surfaces, too. The stability of either the dispersed hydroxyoxides or a smectite, MnO_2 assemblage most probably depends on the ability of the smectite to nucleate and grow. Nucleation sites may actually be provided by the opaline biogenic remains -- Hurd (1973) provides evidence that authigenic mineral formation may occur on opaline tests. If this be true, the lack of opaline tests in regions of poor productivity (e.g., the central portion of the Nazca Plate) may prevent smectite formation and the resulting fractionation of Fe and Mn in two ways -- by limiting the available silica to make smectites and by limiting the available nucleation sites for clay formation.

Nodules from oxic diagenetic (OD) regions (C136, C141, Y73-3-22D, Y73-3-20P in this study) have Mn/Fe ratios of 2 or greater. They are also characterized by high Ni and Cu contents, moderate to high rare earth and other 'hydrogenous' elements, and a mineralogy dominated by todorokite. Lyle (in preparation) suggests that the high values of Cu, Ni, and Zn occur in this region because of the lower Mn flux than to nodules there. Because Mn is a major component of nodules, a high flux of Mn due to remobilization will dilute the other transition metal concentrations.

Composition and Mineralogy of the Nonleachable Fraction of Ferromanganese Nodules

In addition to the ferromanganese oxide fraction, which is soluble in oxalic acid, nodules contain up to 30% by weight of insoluble residue.

Table VI lists the mineralogy of each of the nodule residues along with the mineralogy of the bulk sediment in each station. Examination of this table reveals that the mineralogy of the nodule residue is similar to sediment mineralogy, with a few important exceptions. Smectite 001 peaks are generally much weaker in the nodule residue, but this could be an artifact of the leach procedure. The oxalic acid leach can attack smectite to some extent, even though it is a mild leach (Dudas and Harward, 1971). Barite is present in sediments from some of the reducing diagenetic nodules though it is not seen in the module residue. In addition, the oxic diagenetic nodule residues and some of the hydrogenous nodules have a reversal of the relative intensity of the plagioclase and quartz peaks. Invariably, the quartz peak is more intense in the sediment while the reverse is true in the nodule residue. Hydrogenous nodules have goethite in the nodule residue that can not be detected in the sediment, although some of the sediments do have peaks similar to FeOOH polymers as listed in Burns and Burns (1977). These data suggest that at least some of the residue minerals within the nodule grow authigenically. Quartz and goethite may be forming within OD and hydrogenous nodules.

Chemical data show no consistent differences between residue and sediment except in the rare earth elements (Table 1, see also Figure 12). Nodule residues commonly have 3 to 10 times higher abundances of these elements than the sediments they were recovered with. This

could be an artifact of the leaching procedure, however, since oxalates precipitate rare earths effectively. Because of the small size of the samples being leached, at no time was the solubility product of the rare earth oxalates reached. Calcium oxalate is detected in all of the nodule residues, however, and during its precipitation a significant percentage of the rare earths leached from the oxide fraction could have coprecipitated. The relatively constant ratio of the abundance of rare earths in the residue to the abundances in the sediment (Figure 12) even at very low absolute rare earth concentrations suggest that coprecipitation did not occur, however.

MICRONODULES AND THE DISPERSED OXIDE FRACTION OF THE SEDIMENT

Micronodules and the dispersed oxide fraction of sediments are probably the most poorly understood of the ferromanganese deposits. Mineralogical data is available for only a few micronodule deposits. Glover (1977) reports either birnessite or a birnessite-todorokite mixture in micronodules from a Caribbean core, while Dymond and Eklund (in press) reports todorokite in micronodules from the Bauer Deep. Somewhat more chemical composition data is available, however. Glover (1977) reported compositions that are essentially manganese oxides with low abundances of the other transition metals, while Dymond and Eklund (in press) reported compositions similar to nodules, although lower in Ni and Cu. Friedrich (1976) reports micronodule compositions similar to nodules recovered from the same location in the central Pacific.

Micronodules in this study also have similar compositions to nodules at the same station (see Table 4). Absolute elemental abundances for the micronodule analyses in this study may not be highly accurate, though, since the weight of micronodules analyzed was determined by the difference between original sample weight and residue collected on a 0.45 μ filter.

Although I estimate the weight of the micronodule sample determined by this technique to be accurate to within 1 milligram, micronodule samples at stations C141, C136, C169, and C151 were less than 5 mg in size. Significant errors in absolute abundance for these stations could therefore occur. In order to eliminate the weighing error, I will compare the chemical compositions of these elements on a ternary diagram of Fe, Mn, and (Ni + Cu + Co x 10), as in Bonatti (1972) (see Figure 13).

Nodule and Fe-Mn coating data for the oxide fraction only (fraction leachable with oxalic acid) and including top and bottom data from the nodule are also included in the figure to enable comparison with the micronodule data. Also included in the figure are an approximate field for hydrogenous precipitates, assumed to be similar to the most hydrogenous nodules and ferromanganese coatings. Finally, the effects of dilution with a hydrothermal source and the effects of diagenetic changes on the ferromanganese oxides are indicated by arrows. Oxic diagenesis will not only add Mn, but will add transition metals from biogenic debris. The addition of remobilized manganese

during reducing diagenesis will dilute Fe and trace metal contents.

Micronodule compositions and nodule compositions map similar fields on this diagram. Micronodule compositions seem to be more uniform, however. All are relatively enriched in Cu, Ni, and Co, and except for Dm 981, the station from the central Pacific, all are more enriched in Mn than a hydrogenous 'source' material.

The composition of the sediment fraction leachable by oxalic acid is also given in Figure 13. This fraction is composed of both micronodules and the dispersed oxide fraction of the sediment. The composition of this fraction is similar to the hypothesized hydrogenous precipitate except for the sample C169, which is enriched in Ni, Cu, and Co, and Y71-9-86, the station furthest north, which is depleted in Mn. Because Y71-9-86 probably experiences the most severe reducing diagenesis, I speculate that the Mn depletion represents actual loss of Mn from the sediment either to seawater or to the nodule at the surface of the core. The enrichment of C169 in trace metals may also demonstrate diagenesis of the sedimentary oxides to a less severe degree.

Figure 14, which shows the distribution of the Mn/Fe ratio in the leachable fraction of the sediment, demonstrates that there are systematic variations in its composition. Except for Y71-9-86, which may have lost Mn from the sediment, the Mn/Fe distribution maps the redox intensity shown in Figure 10, and confirms that a component of Mn is added to the surface sediments by remobilization.

The variations of the nodule, micronodule and leachable component of the sediment suggest the following scenario for their formation and diagenesis. Hydrogenous precipitation provides ferromanganese hydroxyoxide to sediments and nodules. Within the sediment the ferromanganese hydroxyoxides reform to make more manganese-rich micronodules and a more Fe-rich residue of dispersed oxides or cryptocrystalline smectite. In regions of oxic diagenesis, a portion of the freed Mn is added to the nodule to make it relatively Mn-rich. Dissolution of biogenic silica (which also drives the oxic diagenesis) will release Cu, Ni, and Zn to be also incorporated in nodules and the sediment fraction.

In regions of reducing diagenesis, more dramatic effects occur. An additional component of manganese cycles back to the surface sediments from below, and is added both to nodules and to micronodules, though there may be preferential uptake by the nodules.

Nodules continue to grow and micronodules do not for a simple reason. Micronodules stay in their stratigraphic position in sediment. After a period of time, all available ferromanganese hydroxyoxides have diagenetically altered or all readily soluble biogenic opal has been used and the small-scale diagenesis stops. Growth rates of nodules demand that they be continually moving to the benthic boundary layer, either by benthos pushing them upward or by another mechanism. They are thus continually surrounded by reactive components and claim their share of newly formed ferromanganese oxides.

CONCLUSIONS

The geochemistry of ferromanganese oxides is governed by source and by diagenetic processes, as is listed in Figure 1. Ferromanganese deposits near mid-ocean ridges can be demonstrably influenced by a hydrothermal source; deposits near the continents are so diagenetically altered that source cannot truly be distinguished, however. Most of the ferromanganese deposits appear to have received ferromanganese hydroxyoxides from a well-mixed reservoir of terrigenous and hydrothermal source material that is commonly known as the hydrogenous or authigenic 'source'.

Hydrothermal and terrigenous sources add approximately equal quantities of Mn around the rim of the Nazca Plate. Because a large fraction of the oceanic crust is produced at the edge of the Nazca Plate and because river input to the plate is low, the terrigenous source for Mn dominates worldwide. Total input for Mn worldwide is about 2 to 8 x 10^{12}gm/yr. This estimate is two orders of magnitude higher than that based upon the dissolved load of rivers alone. The residence time of Mn in the oceans is therefore much more similar to that of iron (40-160 yr).

Diagenesis can profoundly modify the chemical composition and mineralogy of the ferromanganese oxides. Both oxic and reducing diagenesis are most probably strongly influenced by surface productivity. Dissolution of biogenic silica and formation of authigenic smectites is a possible fractionation

process that fixes iron from mixed Fe-Mn-hydroxyoxides. The freed Mn can precipitate as oxides and coprecipitate Cu, Ni, and Zn also released by the dissolution of biogenic silica.

High productivity regions receive a large organic carbon flux along with high fluxes of other biogenic remains. Oxidation of the organic carbon lowers redox conditions sufficiently for both Fe and Mn to be reduced. Lower solubilities of Fe minerals binds Fe in the solid phase. Mn, however, will diffuse back to the surface sediments to precipitate to micronodules and to the larger concretions. The added component of Mn that fluxes from below causes these nodules to grow at a fast rate, forming nodules of relatively pure Mn oxides lower in Cu, Ni, and Zn than oxic diagenetic nodules.

Because surface productivity controls the type and intensity of diagenesis, regional distributions of ferromanganese oxide compositions and mineralogy will map surface productivity. Hydrogenous-type nodules will be found in the central gyres of the oceans, while nodules enriched in Ni, Cu, and Zn will occur at the edges of high productivity regions, as is reported by Piper and Williamson (1977). Highest Mn concentrations will be found underneath the most productive regions. Ferromanganese oxides grown only in contact with seawater will have hydrogenous compositions, however, no matter where they are found; they are not influenced by diagenetic reactions in the sediments.

Anderson, B. J., Jenne, E. A., and Chao, T. T., 1973, The sorption of silver by poorly crystalline manganese oxides: Geochim. Cosmochim. Acta, v. 37, p. 611-622.

Bonatti, E., Honnorez, J., Joensuu, O., and Rydell, H., 1972, Submarine iron deposits from the Mediterranean Sea, in Stanley, D. S.,ed., The Mediterranean, p. 701-709.

Bostrom, K., and Peterson, M. N. A., 1969, The origin of aluminum-poor ferromanganoan sediments in areas of high heat flow on the East Pacific Rise: Mar. Geol., v. 7, p. 427-447.

Boyle, E. A., Edmond, J. M., and Sholkovitz, E. R., 1977, The mechanism of iron removal in estuaries: Geochim. Cosmochim. Acta, v. 41, p. 1313-1324.

Brewer, P. G., 1975, Minor elements in sea water, in Riley, J. P., and Skirrow, G., eds.,Chemical Oceanography , 2nd ed., v. 1, p. 415-497.

Bricker, O., 1965. Some stability relations in the system $Mn-O_2-H_2O$ at 25° and one atmosphere pressure: Am. Mineral. v.50 p 1296-1354.

Broecker,W.S.,1974. Chemical Oceanography. Harcourt Brace Jovanovich 214 p.

Burns,R.G., and Burns, V.M., 1977. Mineralogy: in Glasby, G.P., ed. Marine Manganese Deposits. Amsterdam, Elsevier p.185-249.

Calvert, S.E., and Price, N.B., 1977. Geochemical variation in ferro-manganese nodules and associated sediments from the Pacific Ocean: Mar. Chem. v.5 p.43-74.

Calvert, S.E., and Price, N.B.,1977b. Shallow water,continental margin and lacustrine nodules: distribution and geochemistry: in Glasby, G.P., ed. Marine Manganese Deposits. Amsterdam, Elsevier p. 45-87.

Cann, J.R., Winter, C.K., and Pritchard, R.G., 1977. A hydrothermal deposit from the floor of the Gulf of Aden: Mineral. Mag. p. 193-199.

Corliss, J.B., Lyle, M., Dymond, J., and Crane, K., 1978. The chemistry of hydrothermal sediment mound deposits near the Galapagos Rift: Earth Plan. Sci. Lett., in press.

Corliss, J., Dymond, J., Gordon, L., von Herzen, R., Ballard, R., Green, K., Edmond, J., Williams, D., Bainbridge, A., Crane, K., and van Andel, Tj., in preparation. Exploration of submarine thermal springs on the Galapagos Rift: submitted to Science.

Dudas, M.J., and Harward, M.E., 1971. Effect of dissolution treatment on standard and soil clays: Soil Sci. Am. Proceedings v. 35 p. 134-140.

Dymond, J., and Veeh, H.H., 1975. Metal accumulation rates in the southeast Pacific and the origin of metalliferous sediments: Earth Plan. Sci. Lett. v. 28 p. 13-22.

Dymond, J., Corliss, J.B., Heath, G.R., Field, C.W., Dasch, and Veeh, H.H., 1973. Origin of metalliferous sediments from the Pacific Ocean: Geol. Soc. Am. Bull. v. 84 p. 3355-3372.

Dymond, J., and Eklund, W., 1978. A microprobe study of metalliferous sediment components: Earth Plan. Sci. Lett., in press.

Edmond, J., 1974. On the dissolution of carbonate and silicate in the deep ocean. Deep Sea Res. v. 21 p. 455-480.

Elderfield, H., 1976. Manganese fluxes to the oceans: Marine Chem. v. 4 p. 103-132.

Ferdon, E.N., Jr., 1950. Studies in Ecuadorian Geography: School of Amer. Res. Monograph 15 86 p.

Friedrich, G.H., 1976. Manganese micronodules and their relation to manganese nodule fields: In Glasby, G.P. and Katz, H.R., eds., United Nations Economic and Social Commission for Asia and the Pacific CCOP/SOPAC Technical Bull. no. 2 p. 39-53.

Glover, E.D., 1977. Characterization of a marine birnessite: Am. Mineral. v. 62 p. 278-285.

Gordon, G.E., Rundle, K., Goles, G.G., Corliss, J.B., Benson, M.H., and Oxley, S.S., 1968. Instrumental neutron activation analysis of standard rocks with high resolution γ-ray detectors. Geochim. Cosmochim. Acta v. 32 p. 369-396.

Graham, W.F., Bender, M.L., and Klinkhammer, G.P., 1976. Manganese in Narragansett Bay. Limn. Oc. v. 21 p. 665-673.

Greenslate, J.L., Frazer, J.Z., and Arrhenius, G., 1973. Origin and deposition of selected transition elements in the seabed: In Morgenstein, M., ed., Papers on the origin and distribution of manganese nodules in the Pacific and prospects for exploration. Hawaii Inst. Geophys. p. 45-70.

Hartmann, M., Muller, P.J., Suess, E., and van der Weijden, C.H., 1976. Chemistry of late quaternary sediments and their interstitial waters from the NW African continental margin: "Meteor" Forsch.-Ergebn. C. 67 p.

Hartmann, M., and Muller, P.J., in press. Trace metals in interstitial waters from Central Pacific Ocean Sediments. in Manheim, F., and Fanning, K., eds. Proceedings of the Joint Oceanographic Assembly, Edinburgh, 1976.

Heath, G.R.,1974. Dissolved silica and deep sea sediments: in Hay, W.W., ed. Studies in Paleo-oceanography. Soc. Econ. Pal. Min. Spec. Pub 20, p. 77-93.

Heath, G.R., and Dymond, J., 1977. Genesis and transformation of metalliferous sediments from the East Pacific Rise, Bauer Deep, and Central Basin, northwest Nazca Plate: Geol. Soc. Amer. Bull. v.88 p. 723-733.

Hogdahl, O.T., Melsom, S., and Bowen, V.T., 1968. Neutron activation analysis of lanthanide elements in sea water: Adv. in Chem. no. 73 p. 308-325.

Hurd, D.C., 1973. Interactions of biogenic opal, sediment, and seawater in the Central Equatorial Pacific. Geochim. Cosmochim. Acta v.37 p. 2257-2282.

Krauskopf, K.B., 1956. Separation of manganese from iron in sedimentary processes: Geochim. Cosmochim. Acta v.12 p. 61-84.

Krishnaswami, S., 1976. Authigenic transition elements in Pacific pelagic clays: Geochim Cosmochim. Acta v.40 p. 425-434.

Ku, T.L., 1966. Uranium series disequilibrium in deep sea sediments (PhD. thesis) Columbia University, 157 p.

Lalou, C., Brichet, E., Ku, T.L., and Jehanno, C., 1977. Radiochemical scanning electron microscope (SEM) and x-ray dispersive energy (EDAX) studies of a FAMOUS hydrothermal deposit: Mar. Geol. v.24 p. 245-258.

Langmuir, D., and Whittemore, D.O., 1971. Variations in the stability of precipitated ferric oxyhydroxides. In Advances in Chemistry No. 106, Nonequilibrium Systems in Natural Water Chemistry, Amer. Chem. Soc.

Lisitzin, A.P., 1970. Sedimentation and geochemical considerations: In Wooster, W.S., ed. Scientific Exploration of the South Pacific. Washington D.C., Nat. Acad. Sci. p. 89-133.

Lonsdale, P. 1976. Abyssal circulation of the southeastern Pacific and some geological implications. J. Geophys. Res. v. 81 p. 1163-1176.

Lopez, C., 1978. Elemental distributions in the components of metalliferous sediments from the Bauer and Roggeveen Basins--Nazca Plate (MS thesis) Corvallis, Oregon State University, 153 p.

Love, C.M., and Allen, R.M., eds., 1975. EASTROPAC Atlas v. 10: Biological and nutrient chemistry data from principal participating ships third survey cruise, February-March 1968: Washington D.C., U.S. Dept. Commerce.

Lyle, M. 1976. Estimation of hydrothermal manganese input to the oceans: Geology, v.4 p. 733-736.

Lyle, M., Dymond, J., and Heath, G.R., 1977. Copper-nickel-enriched ferromanganese nodules and associated crusts from the Bauer Basin, Northwest Nazca Plate: Earth Plan. Sci. Lett. v.35 p. 55-64.

Lyle, M., in preparation. Processes that incorporate transition metals into ferromanganese: evidence from the southeast Pacific Ocean.

Lynn, D.C., and Bonatti, E., 1965. Mobility of manganese in the diagenesis of deep-sea sediments. Mar. Geol. v.3 p. 457-474.

Martin, J.H., and Knauer, G.A., 1973. The elemental composition of plankton. Geochim. Cosmochim. Acta v.37 p.1639-1653.

Mero, J.L., 1965. The Mineral Resources of the Sea: Amsterdam, Elsevier 312p.

Minster, J.B., Jordan, T.H., Molnar, P., and Haines, E., 1974. Numerical modeling of instantaneous plate tectonics: Geophys. J. R. Ast. Soc. v.36 p. 541-576.

Molina-Cruz, A., 1978. Late quaternary oceanic circulation along the Pacific coast of South America (PhD. thesis) Corvallis, Oregon State University 246p.

Moore, W.S., and Vogt, P.R., 1976. Hydrothermal manganese crusts from two sites near the Galapagos Spreading Axis: Earth Plan. Sci. Lett. v.29 p.349-356.

Murray, J.W., and Brewer, P., 1977. Mechanisms of removal of manganese iron, and other trace metals from seawater. In Glasby, G.P., ed. Marine Manganese Deposits. Amsterdam, Elsevier p. 291-325.

Nriagu, J.O., 1975. Thermochemical approximations for clay minerals. Am. Mineral. v. 60 p. 834-839.

Onishi, H. 1969. Arsenic. In Wedepohl, K.H., ed., Handbook of Geochemistry v. II. Berlin, Springer-Verlag.

Piper, D.Z., 1974. Rare earth elements in ferromanganese nodules and other marine phases. Geochim. Cosmochim. Acta. v. 38, p. 1007-1022.

Piper, D.Z. and Williamson, M.E., 1977. Composition of Pacific Ocean ferromanganese nodules. Mar. Geol. v. 23, pp. 285-303.

Pourbaix, M., 1974. Atlas of Electrochemical Equilibria in Aqueous Solutions, Houston, Nat. Ass. Corr. Eng. 644 p.

Prohaska, F., 1976. The climate of Argentina, Paraguay, and Uruguay: In Schwerdtfeger, W., ed. World Survey of Climatology v. 12--Climates of Central and South America. Amsterdam, Elsevier p. 13-113.

Raab, W., 1972. Physical and chemical features of Pacific deep sea manganese nodules and their implications to the genesis of nodules: In Horn, D.R., ed. Papers from a conference of ferromanganese deposits on the ocean floor. Washington, D.C., NSF/IDOE publication p. 31-50.

Robie, R.A., and Waldbaum, D.R., 1968. Thermodynamic properties of minerals and related substances at 298.15°K (25°C) and one atmosphere (1.013 bars) pressure and at higher temperatures. U.S. Geol. Surv. Bull. 1259, 256 pp.

Scholl, D.W., Christiansen, M.N., von Huene, R., and Marlow, M.S., 1970. Peru-Chile Trench sediments and sea floor spreading: Geol. Soc. Amer. Bull. v. 81 p. 1339-1360.

Scott, R.B., Rona, P.A., McGregor, B.A., and Scott, M.R., 1974. The TAG hydrothermal field: Nature v. 251 p. 301-302.

Snow, J.W., 1976. The climate of Northern South America: In Schwerdtfeger, W., ed. World Survey of Climatology v. 12--climates of Central and South America. Amsterdam, Elsevier p. 295-405.

Stakes, D.S., 1978. Submarine Hydrothermal Systems: Variations in mineralogy, chemistry, temperature, and the alteration of oceanic layer II (PhD thesis) Corvallis, Oregon State University.

Stumm, W., and Morgan, J.J., 1970. Aquatic Chemistry. New York, Wiley-Interscience 583 p.

Tardy, Y., and Garrels, R.M., 1974. A method for estimating the Gibbs energies of formation of layer silicates: Geochim. Cosmochim. Acta v. 38 p. 1101-1116.

Toth, J.R., 1977. Deposition of submarine hydrothermal manganese and iron, and evidence for hydrothermal input of volatile elements to the ocean: (MS thesis) Corvallis, Oregon State University 79 p.

Turekian, K.K., 1969. The oceans, streams, and atmosphere: In Wedepohl, K.H., ed. Handbook of Geochemistry V. 1. Berlin, Springer-Verlag p. 297-324.

Wedepohl, K.H., 1969a. Composition and abundance of common igneous rocks: In Wedepohl, K.H., ed. Handbook of Geochemistry V. 1. Berlin, Springer-Verlag p. 227-249.

Weiss, R.F., 1977. Hydrothermal manganese in the deep sea: scavenging residence time, and $Mn/^{3}He$ relationships: Earth Plan. Sci. Lett. v. 37 p. 257-262.

Whittaker, E.J.W., and Muntus. Ionic radii for use in geochemistry: Geochim. Cosmochim. Acta v. 34 p. 945-956.

Zuta, S., and Guillen, O., 1970. Oceanografia de las aguas costeras del Peru: Instituto del Mar del Peru Boletin v. 2 p. 161-323.

TABLE 1.
NODULE COMPOSITION DATA
(ALL VALUES IN PPM.)

BULK COMPOSITION

NAME	LAT(S)	LON(W)	%RES[1]	10D[2]	BIRN[2]	M[2]	MG	AL	SI	CA	SC	MN	FE	CO	NI
V71-86	5°05'	90°47'	15.4	30	37	33	16100.	6240.	23900.	14400.	3.50	445000.	14400.	164.	5490.
C136	8°47'	89°26'	25.0	43	4	52	20100.	26400.	64200.	21100.	7.21	265000.	104000.	1450.	13800.
C151	8°56'	86°22'	24.8	65	2	33	16100.	20000.	69100.	12300.	8.47	118300.	51000.	352.	6560.
73-220	13°40'	102°08'	19.8	78	0	22	0.	13500.	38700.	11300.	4.17	138000.	42600.	655.	13600.
V73-20	13°38'	102°34'	20.2	32	18	50	22610.	18900.	41400.	17130.	7.76	195300.	65400.	407.	14500.
C141	14°55'	87°43'	25.2	44	4	52	19363.	26100.	66800.	19330.	8.73	275000.	82400.	1270.	14100.
141TOP							13700.	17300.	59100.	20420.	10.40	260000.	138000.	1650.	9760.
141BOT							18400.	27700.	67500.	18300.	8.45	336000.	32400.	399.	15700.
C165	13°29'	83°40'	23.3	31	30	39	15600.	22600.	64000.	13930.	7.12	344000.	52300.	309.	9070.
165TOP							12400.	21800.	66500.	12200.	6.43	379000.	19600.	104.	3520.
165BOT							17000.	13400.	44700.	14500.	5.00	384300.	30100.	197.	14000.
C169	14°24'	81°33'	22.7	15	42	43	14300.	20700.	58700.	14280.	5.91	369300.	48000.	283.	6630.
169TOP							12400.	16100.	36000.	11700.	4.33	396000.	22900.	103.	7750.
169BOT							16200.	14300.	57200.	13700.	5.38	384000.	30400.	172.	12900.
770619	22°14'	79°31'	29.1	0	0	100	13400.	32800.	46700.	19500.	14.20	166000.	175000.	2920.	4130.
D4934	40°19'	96°28'	37.2	12	15	73	11300.	42100.	129000.	18600.	15.70	156000.	122000.	1430.	4800.
D41036	38°08'	125°21'	31.8	19	0	81	15400.	32500.	85500.	20200.	15.50	215100.	133000.	1930.	7590.
DM981	22°40'	160°47'	27.4	0	0	100	12403.	27600.	76100.	18300.	15.40	165000.	206000.	5400.	2670.

OXIDE COMPOSITION
(LEACHABLE WITH OXALIC ACID)

V71-86							16300.	2610.	5216.		2.70	491000.	10400.	191.	5730.
C136							25100.	12700.	18200.		6.50	352000.	118000.	2390.	13300.
C151							19700.	7440.	5910.		4.40	430000.	55400.	435.	11800.
73-220							20660.	10300.	8710.		2.50	411000.	65300.	791.	15700.
V73-20							27302.	11900.	7540.		6.10	419000.	58400.	442.	17100.
C141							25400.	13000.	14900.		6.40	381000.	91500.	1660.	19000.
141TOP							15300.	7830.	31100.			326000.	161000.	2130.	12700.
141BOT							21500.	8420.	6080.			464300.	26700.	484.	22000.
C165							16600.	8010.	8010.		4.10	460000.	44400.	418.	9970.
165TOP							13100.	6810.	9000.			528000.	14700.	199.	5850.
165BOT							18900.	6210.	5840.			481000.	29900.	247.	10100.
C169							15600.	5510.	9010.		3.60	469000.	38000.	267.	8030.
169TOP							12900.	4270.	4296.			506000.	21100.	133.	10200.
169BOT							14200.	5950.	6740.			476000.	31100.	259.	16700.
770619							17000.	14700.	33800.		14.40	234000.	211000.	4020.	5470.
D4934							17400.	24000.	35800.		27.00	258000.	169000.	2190.	7760.
D41006							21100.	17700.	174000.		14.40	328000.	166000.	2570.	11600.
DM981							13660.	17100.	32800.		15.10	226000.	229000.	7060.	3820.

RESIDUE COMPOSITION

V71-86							13400.	5420.	167000.			0.	44900.	76.	1460.
C136							4300.	61400.	208000.			0.	59000.	303.	505.
C151							12200.	61300.	258000.			0.	36900.	136.	2040.
V73-20							527.	46100.	183000.			0.	93300.	88.	2030.
C141							5720.	62000.	201000.			0.	57400.	51.	550.
141TOP							7100.	43400.	154000.			0.	62400.	27.	0.
141BOT							12400.	76200.	225000.			0.	47300.	182.	0.
C165							13100.	71100.	250000.			0.	74100.	22.	414.
165TOP							12400.	66600.	240000.			0.	33200.	0.	0.
165BOT							6750.	59900.	202000.			0.	314000.	0.	5510.
C169							11500.	74000.	233000.			0.	47300.	33.	502.
169TOP							16000.	61800.	129000.			0.	29800.	0.	0.
169BOT							10400.	63100.	216000.			0.	28300.	0.	650.
770619							5290.	62100.	206000.			0.	94800.	30.	175.
D4934							8260.	73300.	274000.			0.	49700.	34.	100.
D41006							5500.	60800.	215000.			0.	70100.	19.	216.
DM981							9540.	52900.	161000.			0.	150000.	72.	1600.

[1]percentage of material left after oxalic acid-ammonium oxalate leach

[2]10D=9.6Å peak area, BIRN=birnessite 7.1Å peak area, M= MnO_2 1.42Å peak area, all expressed as per cent of combined peak areas

TABLE 1. (CONTINUED)

BULK COMPOSITION

	CU	ZN	AS	AG	SB	BA	LA	CE	ND	SM	EU	TB	YB	LU	HF	TH	U
Y71-86	1400.	1630.	27.1	65.40	134.0	3770.	29.6	35.2	21.4	6.49	1.58	1.03	5.04	.66	1.53	2.46	5.73
C136	6880.	1290.	129.0	13.40	39.9	1690.	147.0	334.0	112.0	23.60	7.34	4.81	17.60	2.33	3.53	16.00	6.76
C151	6930.	644.	76.2	4.27	58.0	4050.	61.7	102.0	40.7	14.60	3.12	2.27	8.53	1.11	4.57	10.90	5.29
73-22D	9810.	4790.	130.0	.11	53.1	5790.	72.6		68.5	14.30	4.12	2.97	11.10	1.77	4.13		3.55
Y73-20	9700.	1770.	72.2	4.25	45.9	3140.	90.3	53.5	53.7	14.20	3.74	2.35	12.00	1.83	2.96	2.67	4.31
C141	8600.	1390.	86.6	3.34	35.0	2860.	102.0	250.0	79.9	21.10	5.62	3.80	14.20	2.20	6.34	14.20	5.06
141TOP	3560.	1090.	195.0		22.3	2740.	172.0	466.0	147.0	34.40	8.23	5.70	22.70	3.01	7.43	22.40	8.48
141BOT	7320.	3740.	41.4	12.40	60.9	1560.	52.6	101.0	48.9	12.40	3.20	2.29	8.61	1.35	2.09	7.00	2.50
C165	6090.	974.	59.4	10.30	63.6	2560.	50.0	131.0	66.6	11.80	2.66	1.82	7.23	1.03	2.79	9.32	6.14
165TOP	2750.	940.	23.4	3.25	84.0	1530.	20.0	47.4	16.3	4.30	.89	.95	7.92	.56	1.38	4.31	11.50
165BOT	9220.	1660.	47.1	34.10	66.5	1840.	38.4	81.2	46.6	9.93	2.28	1.71	6.47	1.05	1.62	6.75	3.86
C169	4420.	977.	40.9	29.60	68.7	2270.	35.7	71.4	34.7	9.11	1.98	1.53	5.98	.73	2.64	7.60	5.46
169TOP	6040.	2300.	32.9	53.20	50.1	930.	24.3	46.9	24.5	5.57	1.49	.93	4.27	.56	1.33	4.64	4.55
169BOT	8140.	2520.	52.3	93.20	51.5		35.4	71.2	27.7	9.43	2.27	0.09	6.44	1.12	1.85	7.19	4.55
770619	2410.	646.	177.0	3.76	32.3	1750.	202.0	950.0	170.0	34.70	7.89	5.24	21.10	3.36	11.60	40.70	9.25
DM994	2730.	593.	196.0	154.00	33.6	1930.	141.0	556.0	144.0	37.90	8.39	4.64	15.30	2.10	14.00	31.00	5.44
DM1006	3110.	829.	159.0	0.00	25.3	1970.	241.0	992.0	173.0	45.50	10.70	6.39	20.40	3.29	13.50	24.60	6.98
DM981	1160.	570.	233.0	0.00	40.6	1690.	246.0	1773.0	195.0	50.10	11.50	7.53	22.50	3.35	15.30	90.60	11.50

OXIDE COMPOSITION

Y71-86	4070.	1770.	35.0	82.00	135.0	4450.	10.5	16.0		2.20	.50	.50	4.40	.53	1.80	2.80	7.20
C136	4250.	1710.	166.0	15.00	41.0	1960.	51.0	326.0		14.00	4.20	3.80	17.10	2.10	6.50	20.00	8.70
C151	5470.	1360.	105.0	6.00	76.0	4700.	28.0	67.0		7.10	1.10	1.90	7.90	.90	5.40	12.70	6.90
73-22D	9690.	5090.	138.0		64.0	5580.	16.7			2.30	1.40	1.20	7.40	1.20	4.70	0.00	4.30
Y73-20	11000.	2250.	77.0	4.00	61.0	3680.	3.1	33.0		.40	.70	.30	7.10	1.00	3.30	2.90	5.40
C141	12600.	1670.	104.0	3.71	45.0	2860.	44.0	194.0	47.0	47.00	2.40	2.30	12.00	2.00	7.10	16.40	6.10
141TOP	4110.	1420.															
141BOT	12400.	4290.															
C165	7640.	1170.	74.0	12.40	82.0	2990.	20.0	62.0	16.0	4.20	.90	1.10	6.30	.90	2.70	10.10	7.30
165TOP	4460.	1240.															
165BOT	10800.	1960.															
C169	5650.	1130.	60.0	38.00	89.0	2620.	11.0	44.0		3.80	.50	1.10	5.30	.50	2.40	7.80	6.40
169TOP	5540.	2830.															
169BOT	9710.	3170.															
770619	3440.	956.	222.0	6.00	43.0	2060.	139.0	989.0	172.0	21.70	5.20	4.80	21.00	3.43	15.00	54.00	12.00
DM994	4490.	944.	154.0	145.00	52.0	2706.	93.0	595.0		24.00	5.10	2.90	15.30	2.43	13.00	45.00	7.30
DM1006	4730.	1164.	199.0	0.00	34.0	2560.	125.0	1100.0		26.00	6.30	4.90	19.00	3.40	12.00	34.00	10.00
DM981	1420.	671.	257.0	0.00	52.0	1540.	137.0	1710.0	76.0	27.00	6.70	5.80	21.00	3.00	15.00	113.00	14.00

RESIDUE COMPOSITION

Y71-86	0.	540.	0.0	9.81	2.3	1560.	31.5	96.6	145.0	20.40	4.95	2.75	6.84	.93	.57	1.48	.72
C136	0.	0.	19.5	2.25	2.6	512.	340.0	593.0	436.0	71.70	16.30	7.53	19.10	2.73	2.47	4.90	1.00
C151	1970.	0.	0.0	0.00	4.0	2360.	130.0	193.0	191.0	34.20	9.33	3.42	10.10	1.54	2.48	6.25	1.07
Y73-20	0.	0.	52.1	5.97	3.0	8100.	149.0	162.0	313.0	65.30	15.50	9.81	33.10	4.33	1.96	1.90	0.00
C141	0.	66.	32.4	3.92	3.2	3050.	299.0	731.0	499.0	63.30	15.50	8.73	22.60	2.92	3.69	7.09	1.37
141TOP	1790.	0.															
141BOT	0.	795.															
C165	1040.	337.	9.7	3.35	3.2	1100.	132.0	234.0	241.0	37.20	8.34	4.14	10.20	1.54	3.00	6.70	1.30
165TOP	0.	116.															
165BOT	0.	1360.															
C169	126.	454.	4.5	4.15	4.1	1110.	118.0	182.0	204.0	27.50	6.66	3.17	7.89	1.33	3.33	6.91	2.35
169TOP	7970.	257.															
169BOT	3000.	4760.															
770619	84.	0.	59.0	6.00	3.4	911.	331.0	847.0	350.0	61.30	15.10	8.50	21.10	3.25	5.25	7.39	0.00
DM994	20.	48.	17.7	28.36	1.8	526.	236.0	484.0	403.0	62.50	14.40	7.67	13.80	1.97	4.07	4.91	.96
DM1006	26.	171.	60.8	8.52	3.4	972.	397.0	969.0	749.0	93.10	21.40	10.30	21.50	3.13	4.25	4.21	0.00
DM981	525.	422.	196.0	8.19	8.4	1150.	535.0	1453.0	575.0	124.00	26.60	12.60	36.20	4.03	6.26	21.50	0.00

TABLE II. *Ferromanganese coating compositions*
(ALL VALUES IN PPM.)

BULK COMPOSITION

NAME	LAT(S)	LON(W)	%RESID[1]	TOD[2]	BIRN[2]	M[2]	MG	AL	SI	CA	SC	MN	FE	CO	NI
DM1	00°36'N	86°10'	----	0	0	100	0.	13300.	51700.	24600.	11.50	226000.	173000.	503.	7770.
DM2	00°36'N	86°10'	----	0	0	100	8800.	13200.	175000.	21000.	7.10	15100.	102000.	247.	4540.
732206	13°40'	102°08'	----	0	0	100	0.	14900.	54600.	0.	0.00	178000.	239000.	1420.	3790.
FOR 75	17°09'	75°15'	32.5	0	0	100	10300.	22600.	87000.	14400.	15.80	119000.	260000.	1450.	1020.
DM1029	21°07'	80°50'	26.9	0	0	100	15600.	21300.	73400.	24000.	10.73	156000.	179000.	2000.	3080.
DM1016	25°24'	98°47'	30.5	0	0	100	13400.	19700.	56700.	23200.	16.40	155000.	241000.	2450.	3010.
DM1011	33°00'	109°30'	28.2	0	0	100	14800.	19700.	95200.	24800.	15.30	96700.	278000.	663.	755.
KK7233	23°02'	113°56'	40.8	0	0	100	10100.	12700.	50900.	80200.	13.30	101000.	246000.	656.	1200.

OXIDE COMPOSITION

FOR 75							11000.	13200.	49200.		16.60	173000.	292000.	1920.	1430.
DM1029							16500.	14200.	26600.			206000.	227000.	2720.	4040.
DM1016							14900.	14100.	36200.		17.20	213000.	247000.	3270.	4060.
DM1011							12800.	11700.	41500.			134000.	333000.	1030.	995.
KK7233							12000.	12300.	46900.		15.10	162000.	324000.	925.	1790.

RESIDUE COMPOSITION

FOR 75							8940.	42000.	166000.		13.40	0.	192000.	16.	169.
DM1029							12960.	40600.	200000.			0.	58900.	968.	460.
DM1016							10300.	32500.	111000.		14.20	0.	230000.	43.	607.
DM1011							20100.	40200.	197000.			0.	137000.	0.	142.
KK7233							7380.	13200.	65200.		7.79	0.	133000.	25.	338.

[1]percentage of material left after oxalic acid-ammonium oxalate leach

[2]TOD=todorokite 9.6Å peak area; BIRN=birnessite 3.6Å peak area;
M= MnO_2 1.42Å peak area. All peak areas are expressed as per cent of combined peak areas.

TABLE II. (CONTINUED)

BULK COMPOSITION	CU	ZN	AS	AG	SB	BA	LA	CE	ND	SM	EU	TB	YB	LU	HF	TH	U
DM1	409.	774.	180.0	0.00	23.0	1440.	175.0	287.0	0.0	26.90	9.60	5.40	27.60	4.19	11.00	13.00	0.00
DM2	380.	524.	120.0	0.00	13.0	760.	92.0	111.0	73.0	15.50	4.30	2.70	14.90	2.43	7.20	7.70	0.00
7322DC	1740.	632.	344.0	0.00	40.7	1670.	246.0	182.0	0.0	43.60	10.40	7.40	22.90	4.39	0.00	0.00	0.00
FDR 75	1350.	582.	294.0	0.00	30.0	1610.	221.0	770.0	195.0	41.80	10.60	7.20	22.50	3.30	14.40	70.60	8.86
DM1028	1670.	684.	214.0	13.00	18.2	2560.	187.0	675.0	130.0	36.30	8.28	5.31	20.10	2.94	10.60	23.30	9.56
DM1016	1050.	695.	272.0	7.83	52.5	1250.	223.0	335.0	151.0	30.20	8.78	6.36	26.20	3.82	12.10	8.64	9.50
DM1011	701.	602.	299.0	6.09	14.4	1270.	159.0	243.0	157.3	31.00	7.49	5.43	17.80	2.54	12.20	7.89	8.36
KK7233	924.	666.	270.0	4.43	25.8	1690.	188.9	141.0	150.0	29.10	7.64	4.71	20.50	2.82	12.70	3.02	7.44
OXIDE COMPOSITION																	
FDR 75	1540.	689.	325.0	0.00	38.0	2040.	145.0	740.0	106.0	27.00	7.50	6.30	22.00	3.10	19.60	90.00	12.00
DM1028	2090.	870.															
DM1016	1080.	721.	257.0	11.00	67.0	1290.	99.0			10.00	1.70	2.10	20.10	2.90	13.60	10.90	12.00
DM1011	802.	694.															
KK7233	1100.	978.	343.0	3.00	35.0	2660.	42.0	53.0	44.0	7.50	2.20	1.80	16.00	2.00	15.00	4.00	10.00
RESIDUE COMPOSITION																	
FDR 75	948.	360.	159.0	5.20	6.0	987.	454.0	863.0	468.0	88.00	20.30	9.80	24.70	3.78	3.94	12.20	0.00
DM1028	523.	178.															
DM1016	988.	505.	315.0	0.00	9.3	1180.	617.0		690.0	113.00	29.10	18.90	43.30	6.53	7.21	1.76	0.00
DM1011	444.	366.															
KK7233	674.	370.	99.9	5.62	3.2	866.	503.0	347.0	398.0	80.30	20.20	11.50	31.60	4.70	2.95	.58	0.00

TABLE III. Sediment Compositions
(ALL VALUES IN PPM.)

BULK SEDIMENT

NAME	LAT(S)	LON(W)	$CaCO_3$%	H_2O%	ρ_{tot}[1]	MG	AL	SI	CA	S	MN	FE	CO	NI	CU	ZN
Y71-36	5°05'	90°47'	55.5	61.7	1.31	6530.	13500.	119400.	226000.	1.20	1340.	13600.	18.	141.	145.	196.
C136	8°47'	89°26'	3.0	---	---	18700.	74630.	236300.	13400.	23.10	12200.	63500.	132.	358.	349.	179.
C151	8°58'	86°22'	0.	---	---	16160.	69400.	271000.	5390.	22.40	6210.	46600.	33.	366.	475.	349.
Y73-20	13°38'	102°34'	16.7	79.5	1.17	13300.	25033.	121300.	73500.	24.20	43100.	116000.	220.	962.	957.	321.
C141	14°55'	87°43'	27.1	---	---	13310.	50800.	147000.	114000.	20.60	15500.	92900.	153.	354.	713.	265.
C165	13°29'	83°40'	0.6	---	---	16700.	83700.	272000.	10100.	21.90	10500.	51700.	67.	332.	470.	227.
C169	14°24'	81°33'	0.5	---	---	16200.	77300.	263000.	9600.	19.71	11400.	47100.	54.	336.	421.	218.
770613	22°14'	79°31'	0.	40.0	1.29	15700.	74800.	242000.	13100.	19.70	12400.	69500.	150.	399.	475.	196.
D4394	48°19'	96°28'	58.6	45.3	1.37	6870.	20400.	70200.	238000.	7.42	3630.	15600.	31.	46.	79.	68.
D41036	38°08'	125°21'	3.5	65.6	1.28	14500.	67100.	192000.	21700.	24.30	32700.	97300.	260.	1110.	831.	278.
D4381	22°40'	160°47'	8.5	68.3	1.21	19671.	78100.	204300.	41200.	24.91	18400.	74800.	325.	269.	353.	179.

LEACHABLE FRACTION
OF SEDIMENT*

Y71-46						2310.	1450.	0.			340.	1300.	17.	27.	100.	37.
C136						4280.	3110.	2960.			11400.	11100.	116.	331.	204.	55.
C151						4610.	3570.	0.			4700.	2340.	33.	171.	231.	70.
Y73-20						9360.	6120.	13700.			40100.	55300.	200.	912.	652.	245.
C141						5570.	2950.	4090.			13300.	17800.	150.	328.	339.	94.
C165						5750.	4240.	4110.			10300.	12200.	54.	279.	312.	68.
C169						5580.	3600.	0.			10300.	7620.	60.	293.	341.	33.
770613						4200.	5480.	0.			11300.	13400.	149.	392.	292.	71.
D4394						2220.	4650.	2460.			3020.	4480.	38.	42.	63.	28.
D41036						5760.	4040.	4400.			31300.	22400.	257.	1070.	533.	161.
D4381						5360.	6110.	5720.			15100.	21200.	205.	222.	203.	92.

TABLE III. (CONTINUED)

	AS	AG	SB	BA	LA	CE	ND	SM	EU	TB	YB	LU	HF	TH	U
BULK SEDIMENT															
Y71-86	0.0	44.70	.8	4760.	12.2	11.9	15.5	2.70	.64	.40	2.50	.33	.45	1.75	.40
C136	35.4	14.10	1.7	7430.	76.3	197.1	116.0	18.50	4.53	2.67	10.60	1.75	4.63	16.40	2.99
C151	4.0	19.50	2.6	5410.	26.7	41.7	43.7	5.36	1.26	.97	4.37	.62	1.15	9.01	2.47
Y73-20	26.1	3.55	9.3	16700.	151.0	73.6	169.9	29.20	7.19	5.41	26.20	3.47	4.69	6.41	2.14
C141	59.0	16.90	6.6	4810.	134.0	74.0	116.9	19.40	5.12	3.09	16.00	2.46	4.17	10.46	2.36
C165	17.3	34.40	3.6	3780.	34.0	61.0	34.9	7.64	1.72	1.21	4.74	.73	4.52	13.70	2.34
C169	18.2	14.30	3.8	3270.	34.4	54.1	33.0	6.63	1.56	.98	4.60	.64	3.43	11.90	2.76
770619	24.2	11.30	4.9	73.0.	93.2	109.0	73.8	12.30	2.47	2.01	6.99	1.05	5.27	15.50	1.86
D4994	3.1	24.20	.5	2280.	14.9	31.2	30.2	3.51	.83	.54	1.52	.21	1.54	4.32	.55
D41006	111.0	19.50	6.1	3120.	154.0	211.0	260.0	47.11	11.40	7.04	21.40	3.11	6.59	19.30	1.72
D4381	26.4	3.30	3.1	1414.	83.3	174.6	143.8	28.73	6.49	3.39	12.30	1.97	5.20	21.00	2.33

*Reported in mg of element leached/kg of total original sample
[1]Wet bulk density (gm/cm^3)

TABLE IV. Micronodule compositions.
(ALL VALUES IN PPM.)

NAME	LEACH[1]	MG	AL	SI	MN	FE	CO	NI	CU	ZN
C136	2.0	16600.	194000.	33200.	342000.	165000.	1480.	15500.	6140.	8600.
C151	2.8*	5500.	51100.	15900.	361000.	15900.	0.	9460.	7930.	2130.
Y73-20	37.8	10400.	26100.	25700.	378000.	239000.	1090.	12700.	6960.	1860.
C141	1.2	31610.	247000.	136000.	617000.	263000.	4710.	22800.	15300.	5300.
C165	31.3	13700.	20200.	14400.	392000.	114000.	292.	17900.	14000.	8740.
C169	3.5	2150.	33600.	7380.	85300.	21200.	61.	1560.	2030.	62.
770613	11.5	5480.	50900.	19000.	273000.	138000.	2720.	13000.	4900.	1510.
DM994	15.0*	33000.	171000.	67700.	63900.		942.	1590.	702.	686.
DM1006	29.0*	11200.	30200.	9710.	370000.	131000.	3020.	19000.	6130.	1580.
DM981	8.0	7240.	105000.	58200.	150000.	397000.	3840.	3470.	2330.	1330.

[1]Total micronodule sample leached from coarse fraction (in mg.).
Absolute elemental abundances are accurate for samples where greater than 5 mg were leached or when replicate analyses could be performed.

*Has replicate analysis

TABLE V. Mn and Fe Fluxes to the Nazca Plate ($\times 10^{11}$ gm/yr)

	Fe	Mn
Nazca Plate		
Terrigenous		
Dissolved	?	0.1
Remobilized from particulates	?	0.4-4.4
TOTAL	?	0.5-4.5
Hydrothermal	9	3
TOTAL FOR NAZCA PLATE	>9	3.5-7.5
World Ocean		
Terrigenous	?	10-70
Hydrothermal	27	9

TABLE VI. Mineralogy of Fe-Mn Coating and Nodule Residues*

STATION	Plag	Qtz	Phil	Bar	Mica	Smec	Goet	FeOOH
Fe-Mn COATINGS								
Rise Crest								
DM1011	M-S	W-M	--	--	?	--	--	?
KK7233	W-M	W	--	--	--	--	?	--
Off Crest								
DM1016	W-M	W	W	--	--	--	M	--
DM1028	W-M	W-M	W	--	VW	--	--	--
FDR75	W-M	S	VW	--	VW	--	--	--
NODULES								
Reducing Diagenetic								
Y71-86	M	M	W	--	W	W	--	--
sediment	S	S	W	M-S	W	M	--	--
C151	VS	VS	W-M	--	M	W	--	--
sediment	S	VS	M	M	M	M	--	--
C165	VS	VS	W-M	--	M	M	--	--
sediment	S	VS	M	--	M	M	--	--
C169	VS	VS	W-M	--	M	W	--	--
sediment	S	VS	M-S	--	M	M	--	--
Oxic Diagenetic								
C136	VS	VS	M	--	W	--	--	--
sediment	S	VS	M-S	--	W	W-M	--	--
C141	VS	VS	M	--	W-M	W-M	--	--
sediment	S	VS	M	--	W-M	W	--	--
Y73-20P	S	M	S	--	--	--	W	--
sediment	M	M	W-M	M-S	--	W	--	--
Y73-22D	S	S	S	--	--	--	M	--

*Plag=plagioclase, Qtz=quartz, Phil=phillipsite, Bar=barite, Mica=mica, Smec=smectite, Goet=goethite, FeOOH=hydrated polymer;

TABLE VI. (Continued)

STATION	Plag	Qtz	Phil	Bar	Mica	Smec	Goet	FeOOH
Hydrogenous								
770619	VS	VS	S	--	M	--	M	--
sediment	M-S	M-S	M-S	--	M	W	W-M	--
DM994	VS	VS	VS	--	W	--	M+	--
sediment	S	VS	M	--	M-S	W	--	--
DM1006	VS	VS	S	--	W	--	M	--
sediment	VS	S	S	--	W	--	--	S
DM981	S	M	M	--	W-M	--	W-M	--
sediment	S	VS	S	--	M+	W	--	?

FIGURE CAPTIONS

Figure 1: Pathways by which Mn and Fe enter the oceans and are subsequently reorganized

Figure 2: Generalized surface circulation of the Eastern Pacific Ocean after Molina-Cruz, 1978.

Figure 3: Abyssal circulation in the Eastern Pacific Ocean, after Lonsdale, 1976.

Figure 4: Regional distribution of Mn, Fe, Co, and Ce in ferromanganese coatings, this study.

Figure 5: Rare earth abundance patterns for ferromanganese coatings normalized to chondrites

Figure 6: La plotted against Ce for ferromanganese coatings. The line represents the La/Ce ratio in seawater. Solid circles are coatings from the Rise Crest.

Figure 7: Scatterplots of Fe against Sc, As, La, and Hf to demonstrate the coherent behavior of these elements.

Figure 8: Scatterplots of La against Ce and Ce against Co. They show that Ce can be highly enriched with respect to the other rare earths, but covaries with Co.

Figure 9: Redox equilibria at pH 8 for elemental concentrations as in seawater (Brewer, 1975) and in pore waters (Hartmann and Muller, in press). Lines go to the baseline at the Eh that elemental oxide precipitates (data from Pourbaix, 1974).

Figure 10: Thickness of oxidized layer in sediments of the Eastern Pacific. The figure combines data of Lynn and Bonatti (1965) (triangles) with that from Oregon State University (circles).

Figure 11: Scattergram of Mn against Sb. Note the good correlation in nodules with greater than 20% Mn.

Figure 12: La in ferromanganese nodule residues plotted against La in sediments. Note enrichments in nodule residues.

Figure 13: Composition of micronodule and leachable fraction of sediments plotted with ferromanganese nodule and Fe-Mn coating oxide fraction on a ternary diagram of Mn, Fe, and (Ni + Cu + Co) x 10. Stars indicate nodules for which micronodule compositions are reported.

Figure 14: Distribution of Mn/Fe ratios in the leachable fraction of the sediment from the Nazca Plate.

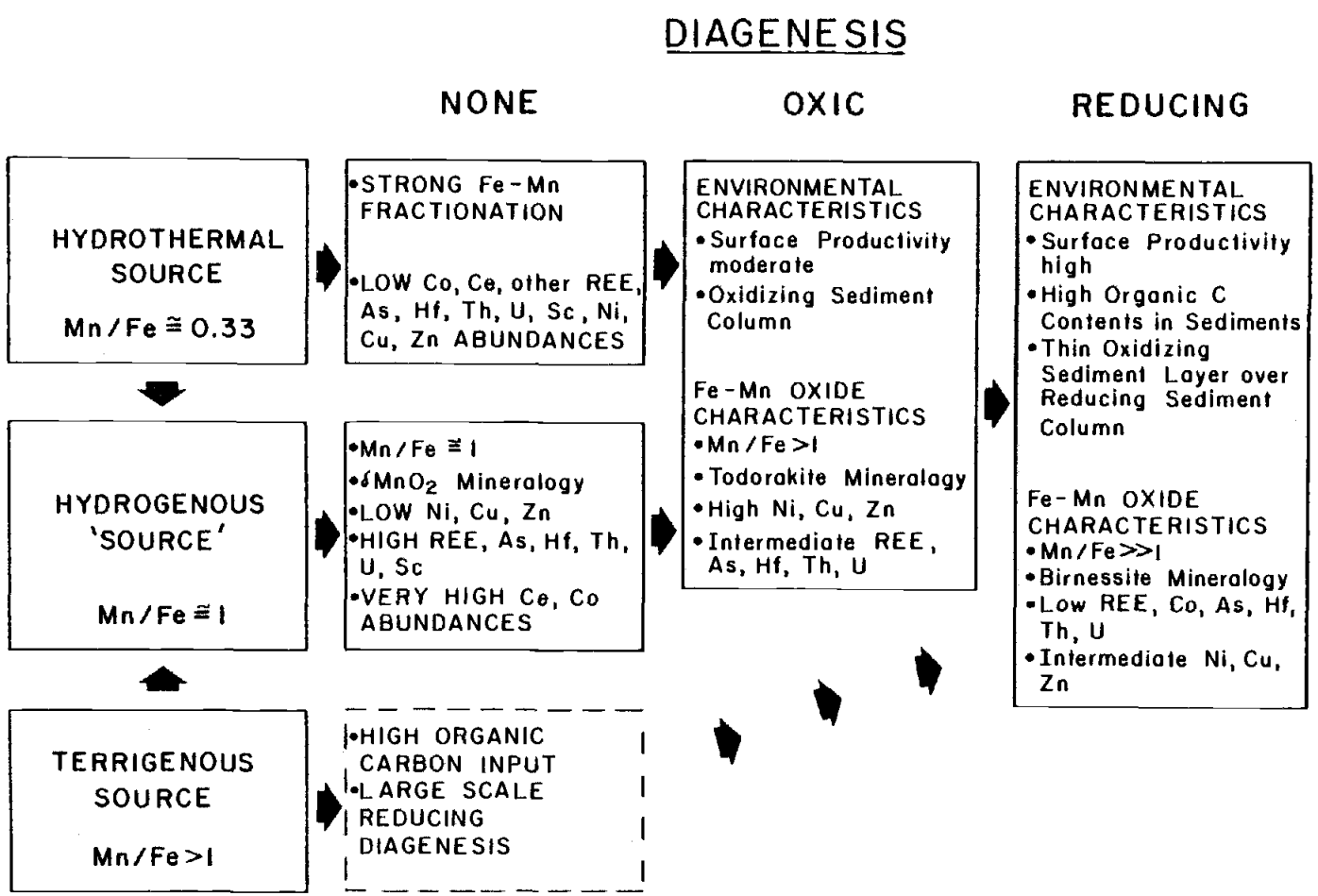
DIAGENESIS
NONE
OXIC
REDUCING
HYDROTHERMAL SOURCE
Mn/Fe ≅ 0.33
•STRONG Fe-Mn FRACTIONATION
•LOW Co, Ce, other REE, As, Hf, Th, U, Sc, Ni, Cu, Zn ABUNDANCES
ENVIRONMENTAL CHARACTERISTICS
• Surface Productivity moderate
• Oxidizing Sediment Column
Fe-Mn OXIDE CHARACTERISTICS
• Mn/Fe >1
• Todorokite Mineralogy
• High Ni, Cu, Zn
• Intermediate REE, As, Hf, Th, U
ENVIRONMENTAL CHARACTERISTICS
• Surface Productivity high
• High Organic C Contents in Sediments
• Thin Oxidizing Sediment Layer over Reducing Sediment Column
Fe-Mn OXIDE CHARACTERISTICS
• Mn/Fe >>1
• Birnessite Mineralogy
• Low REE, Co, As, Hf, Th, U
• Intermediate Ni, Cu, Zn
HYDROGENOUS 'SOURCE'
Mn/Fe ≅ 1
•Mn/Fe ≅ 1
•δMnO2 Mineralogy
•LOW Ni, Cu, Zn
•HIGH REE, As, Hf, Th, U, Sc
•VERY HIGH Ce, Co ABUNDANCES
TERRIGENOUS SOURCE
Mn/Fe >1
•HIGH ORGANIC CARBON INPUT
•LARGE SCALE REDUCING DIAGENESIS

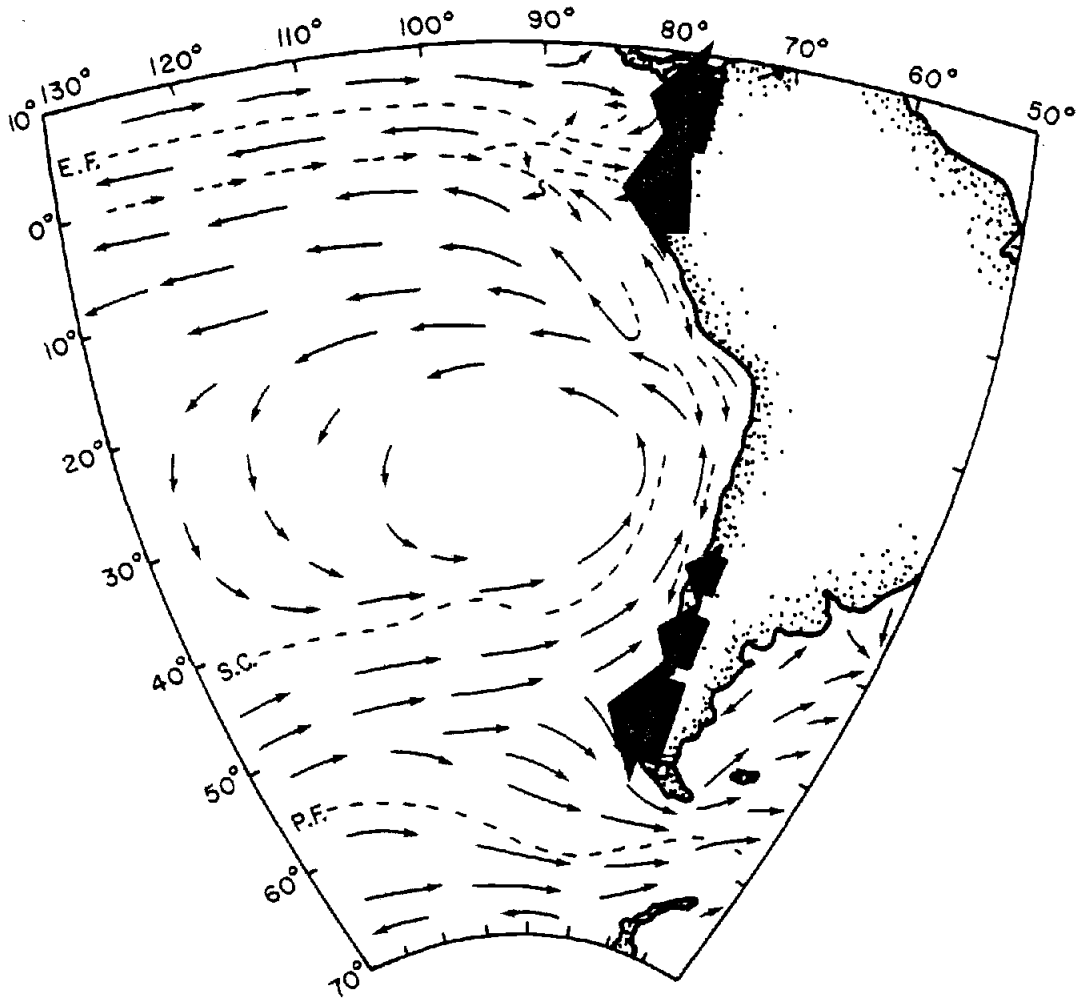
130°
120°
110°
100°
90°
80°
70°
60°
50°
10°
E.F.
0°
10°
20°
30°
40°
S.C.
50°
P.F.
60°
70°

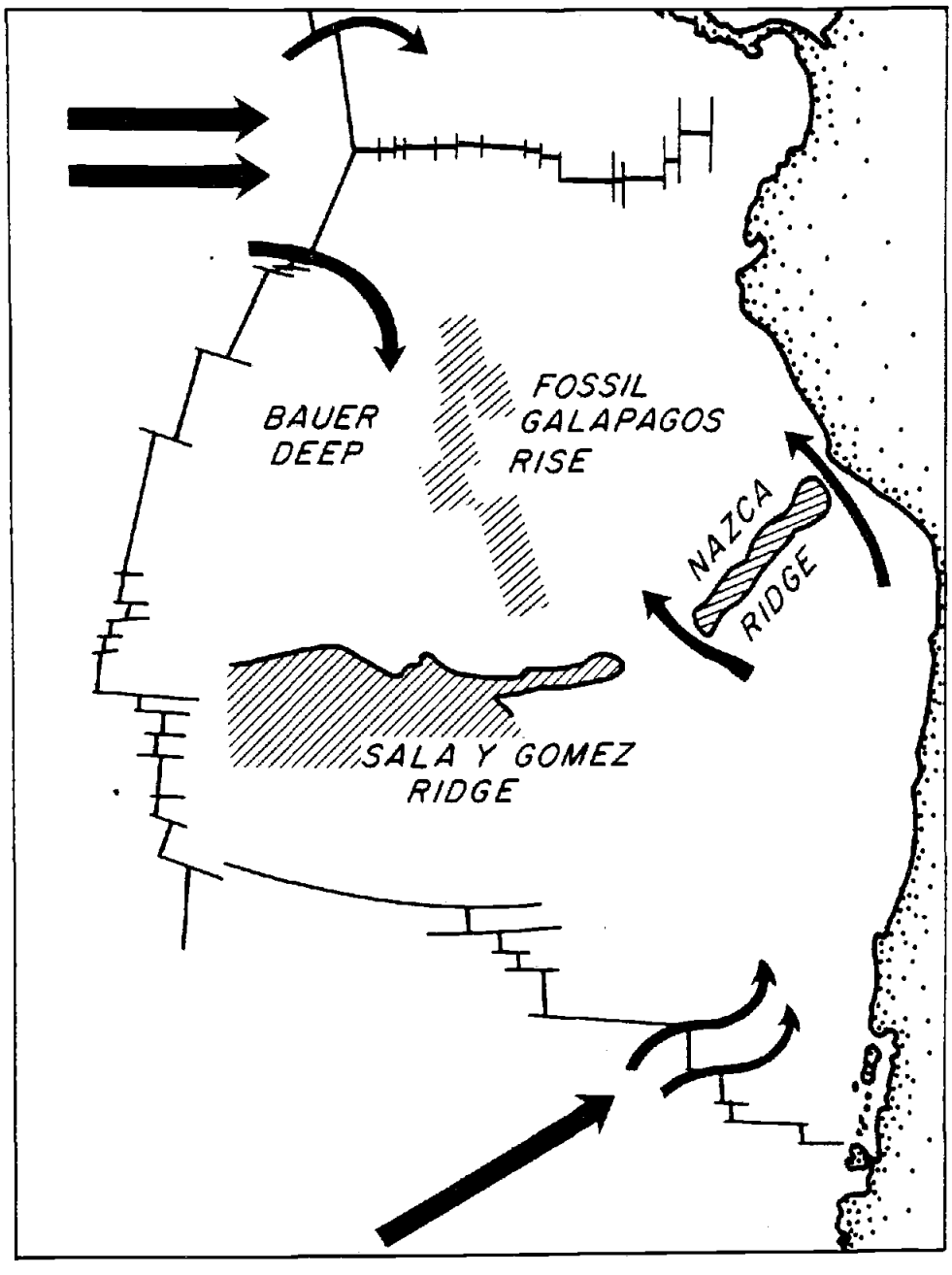
BAUER
DEEP
FOSSIL
GALAPAGOS
RISE
NAZCA
RIDGE
SALA Y GOMEZ
RIDGE

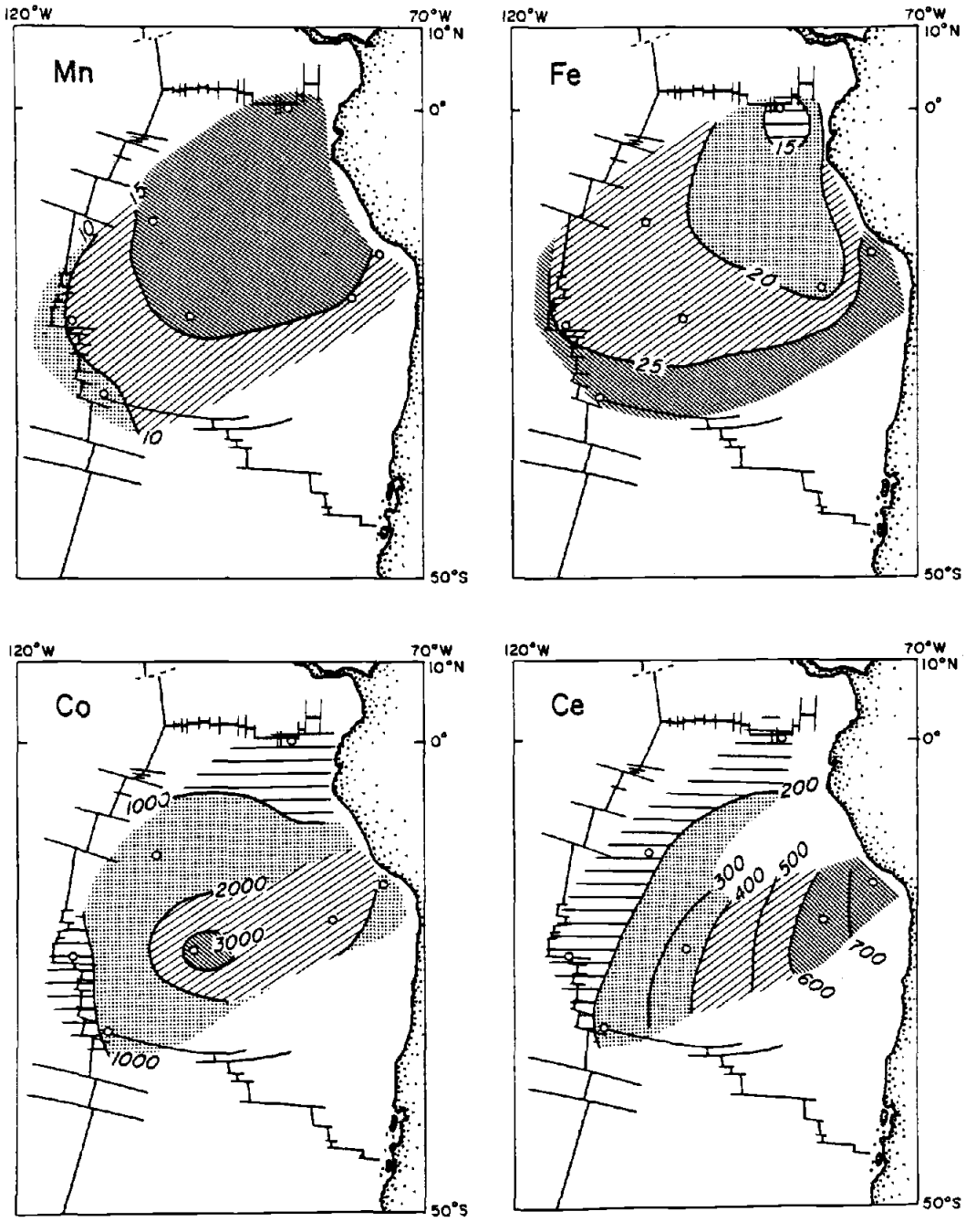
120°W
70°W
10°N
0°
50°S
Mn
5
10
10
Fe
15
20
25
Co
1000
2000
3000
1000
Ce
200
300
400
500
700
600

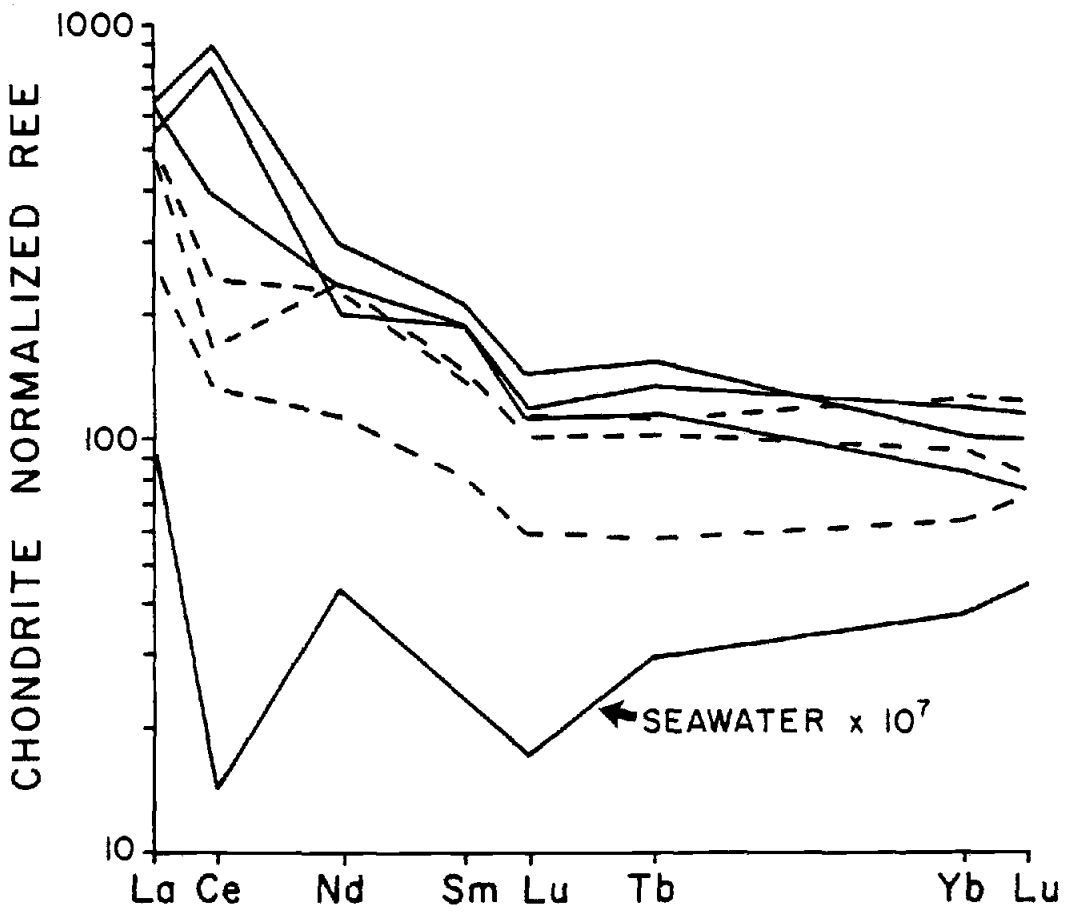
1000
100
10
CHONDRITE NORMALIZED REE
SEAWATER x 10⁷
La Ce Nd Sm Lu Tb Yb Lu

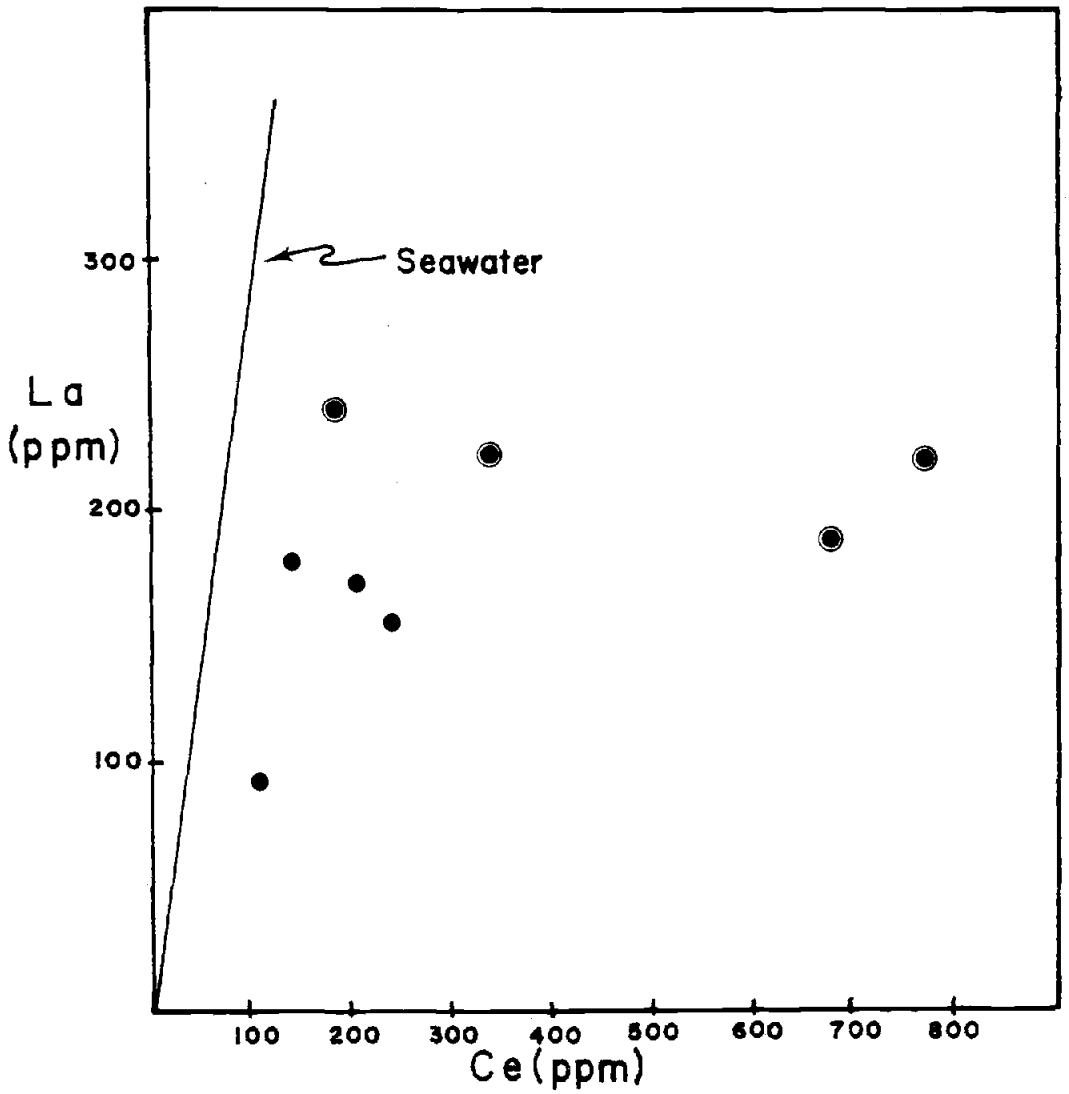
Seawater
La (ppm)
300
200
100
100
200
300
400
500
600
700
800
Ce (ppm)

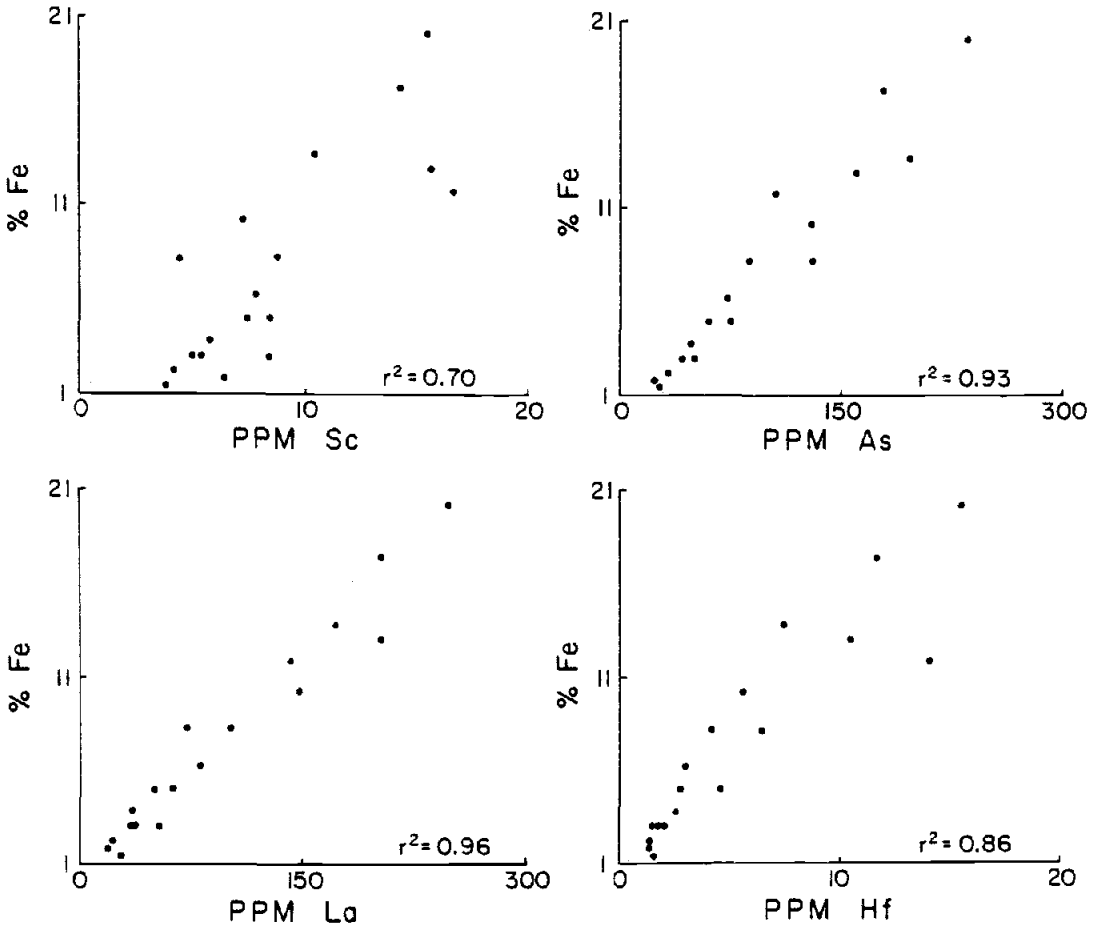
21
11
1
% Fe
0
10
20
PPM Sc
r² = 0.70
21
11
1
% Fe
0
150
300
PPM As
r² = 0.93
21
11
1
% Fe
0
150
300
PPM La
r² = 0.96
21
11
1
% Fe
0
10
20
PPM Hf
r² = 0.86

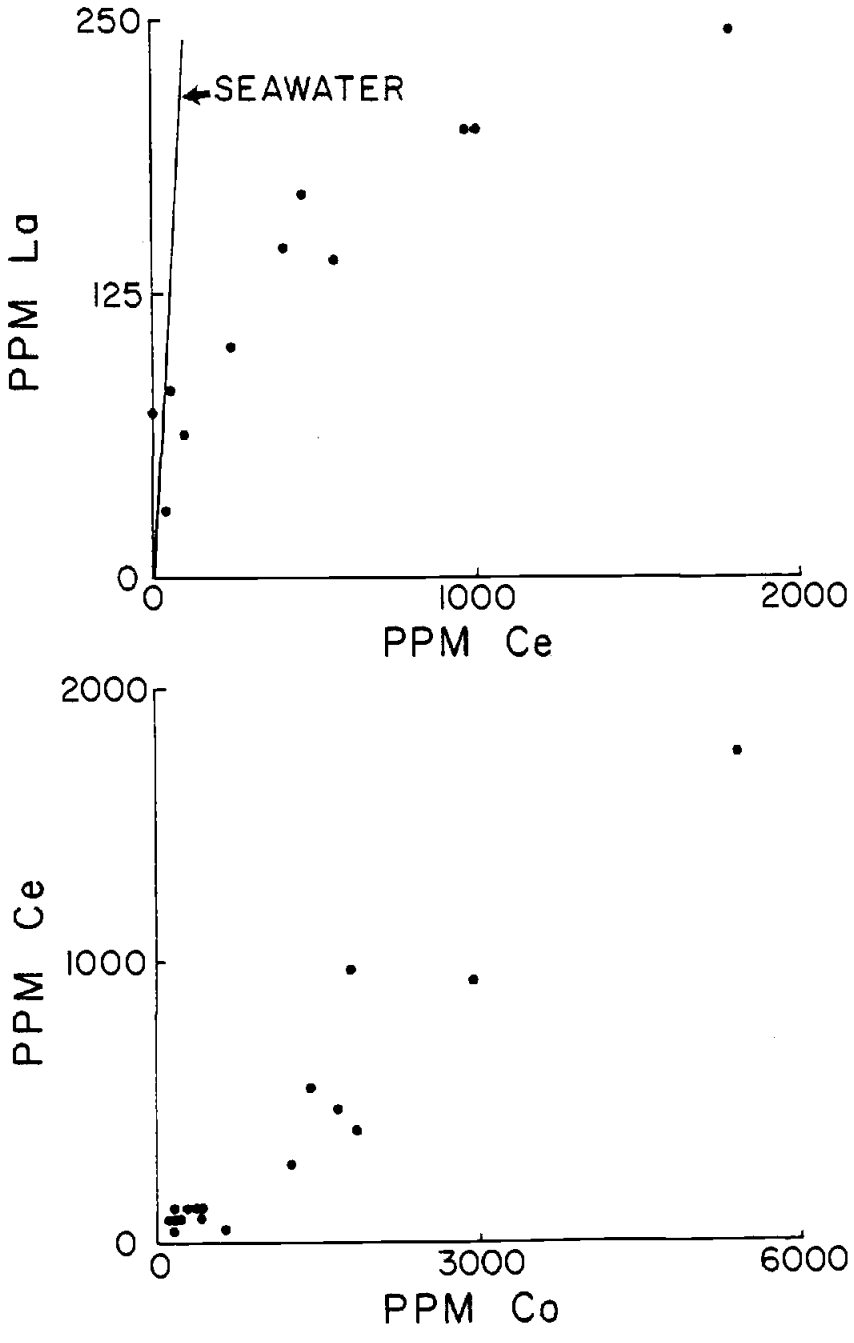
250
125
0
PPM La
SEAWATER
0
1000
2000
PPM Ce
2000
1000
0
PPM Ce
0
3000
6000
PPM Co

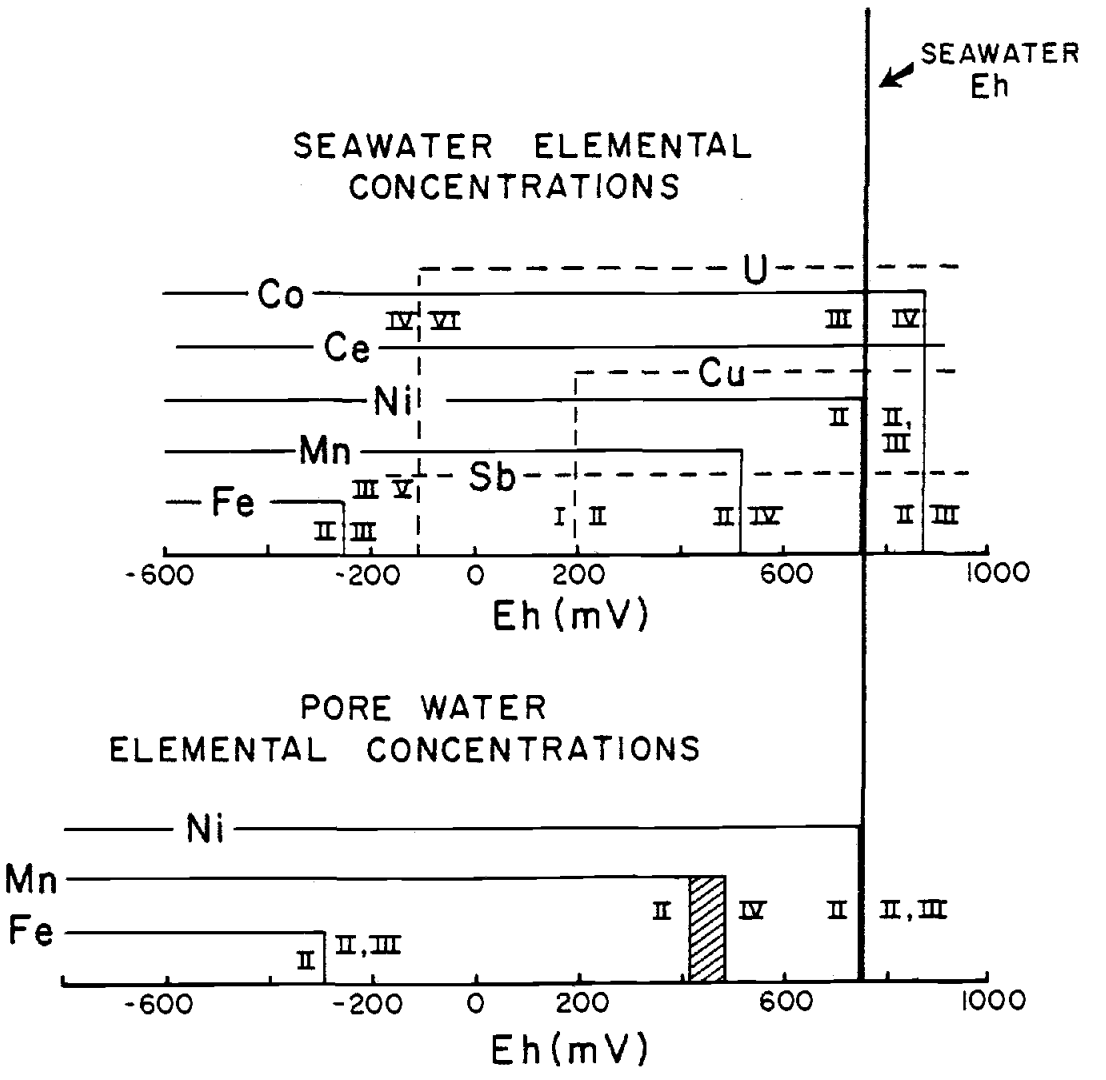
SEAWATER
Eh
SEAWATER ELEMENTAL
CONCENTRATIONS
U
Co
Ce
Cu
Ni
Mn
Sb
Fe
-600
-200
0
200
600
1000
Eh (mV)
PORE WATER
ELEMENTAL CONCENTRATIONS
Ni
Mn
Fe
-600
-200
0
200
600
1000
Eh (mV)

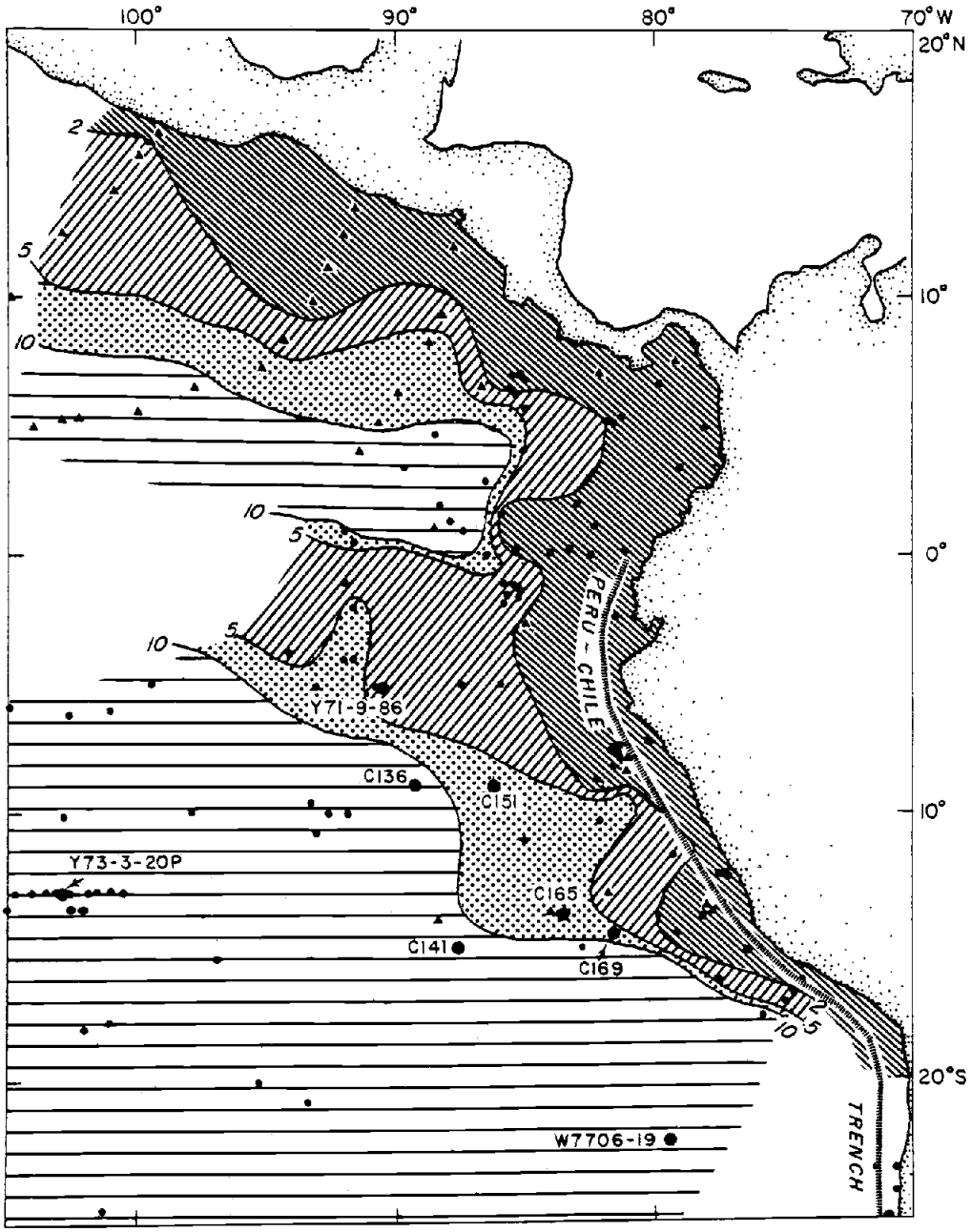
100°
90°
80°
70°W
20°N
10°
0°
10°
20°S
2
5
10
10
5
10
5
PERU - CHILE
TRENCH
Y71-9-86
C136
C151
Y73-3-20P
C165
C141
C169
W7706-19

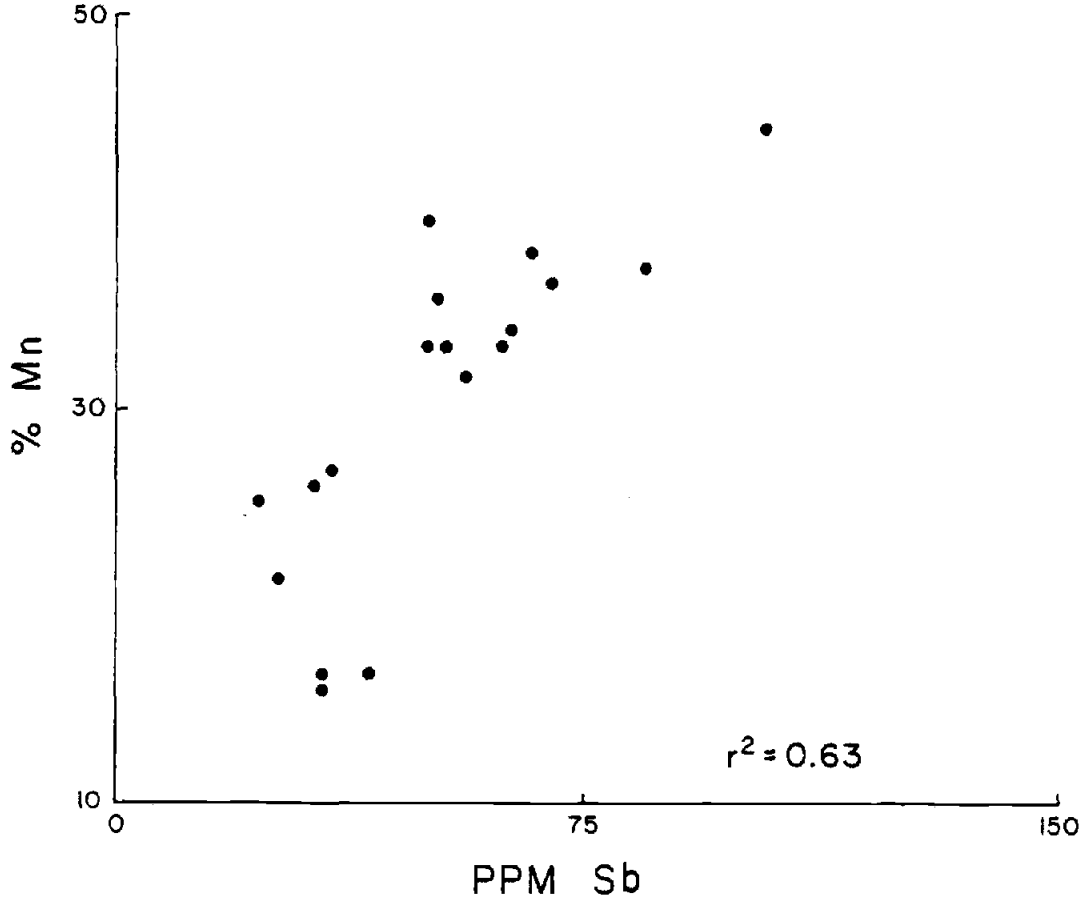
50
30
10
% Mn
0
75
150
PPM Sb
$r^2 = 0.63$

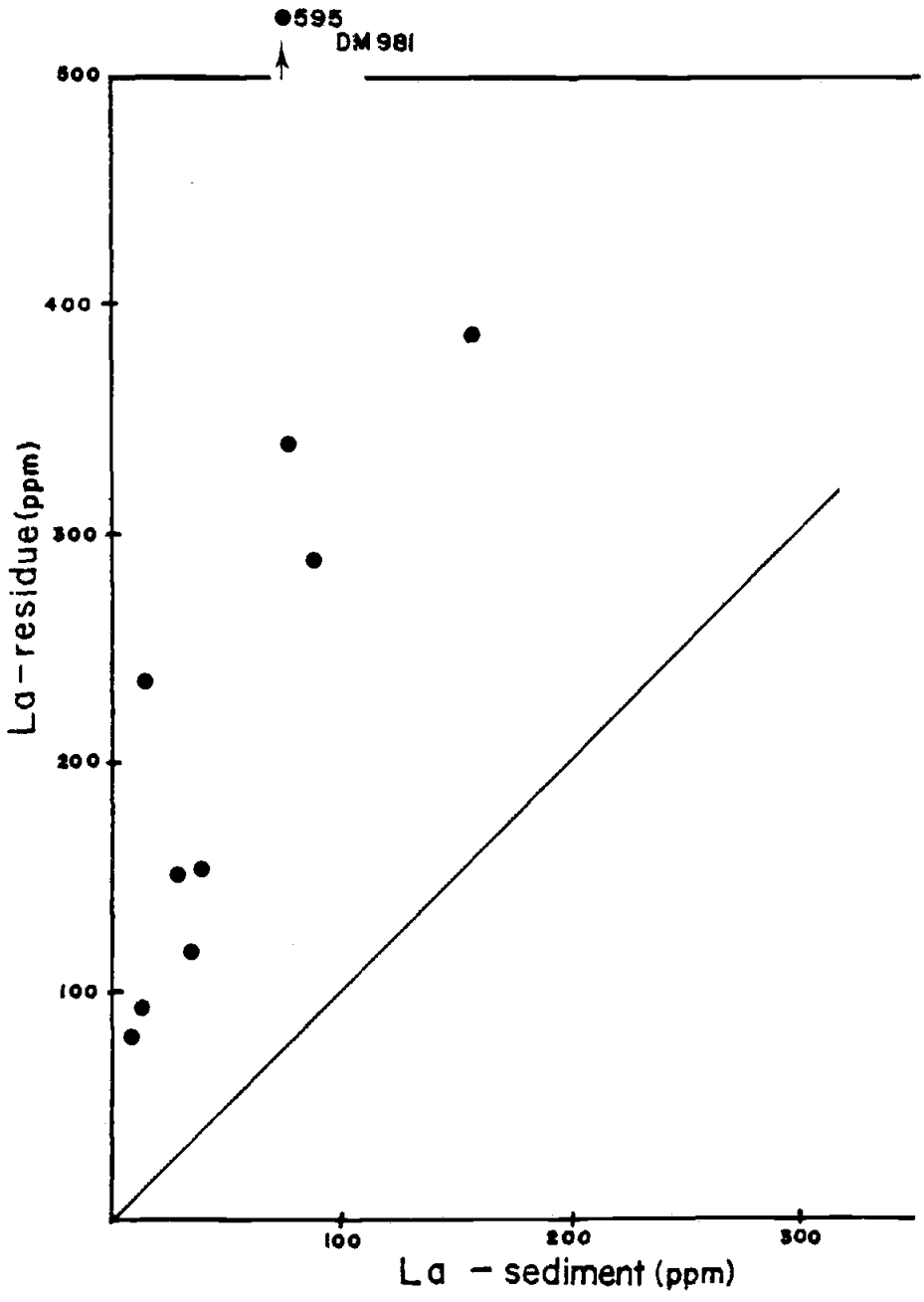
595
DM 98I
500
400
300
200
100
La - residue (ppm)
100
200
300
La - sediment (ppm)

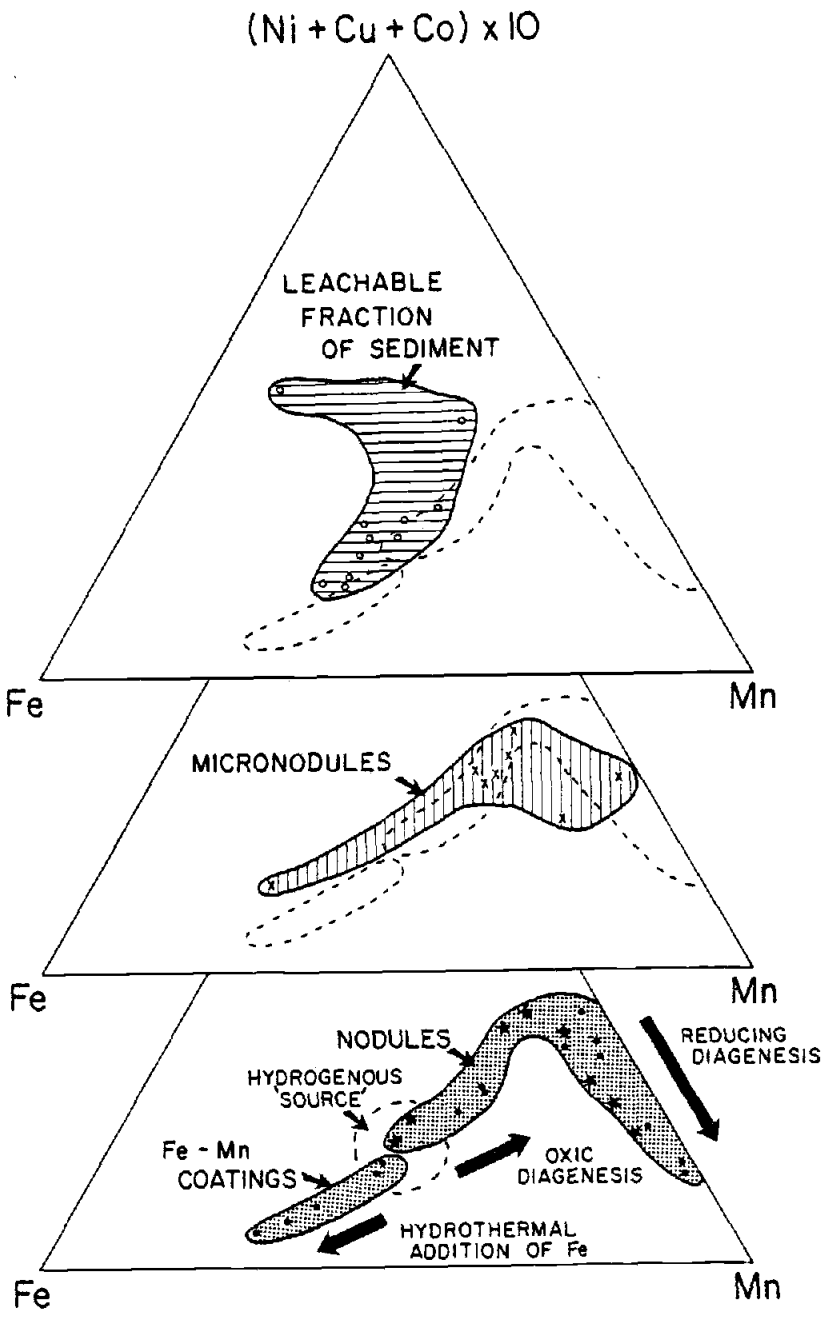
(Ni + Cu + Co) x 10
LEACHABLE
FRACTION
OF SEDIMENT
Fe
Mn
MICRONODULES
Fe
Mn
NODULES
HYDROGENOUS
SOURCE
Fe - Mn
COATINGS
REDUCING
DIAGENESIS
OXIC
DIAGENESIS
HYDROTHERMAL
ADDITION OF Fe
Fe
Mn

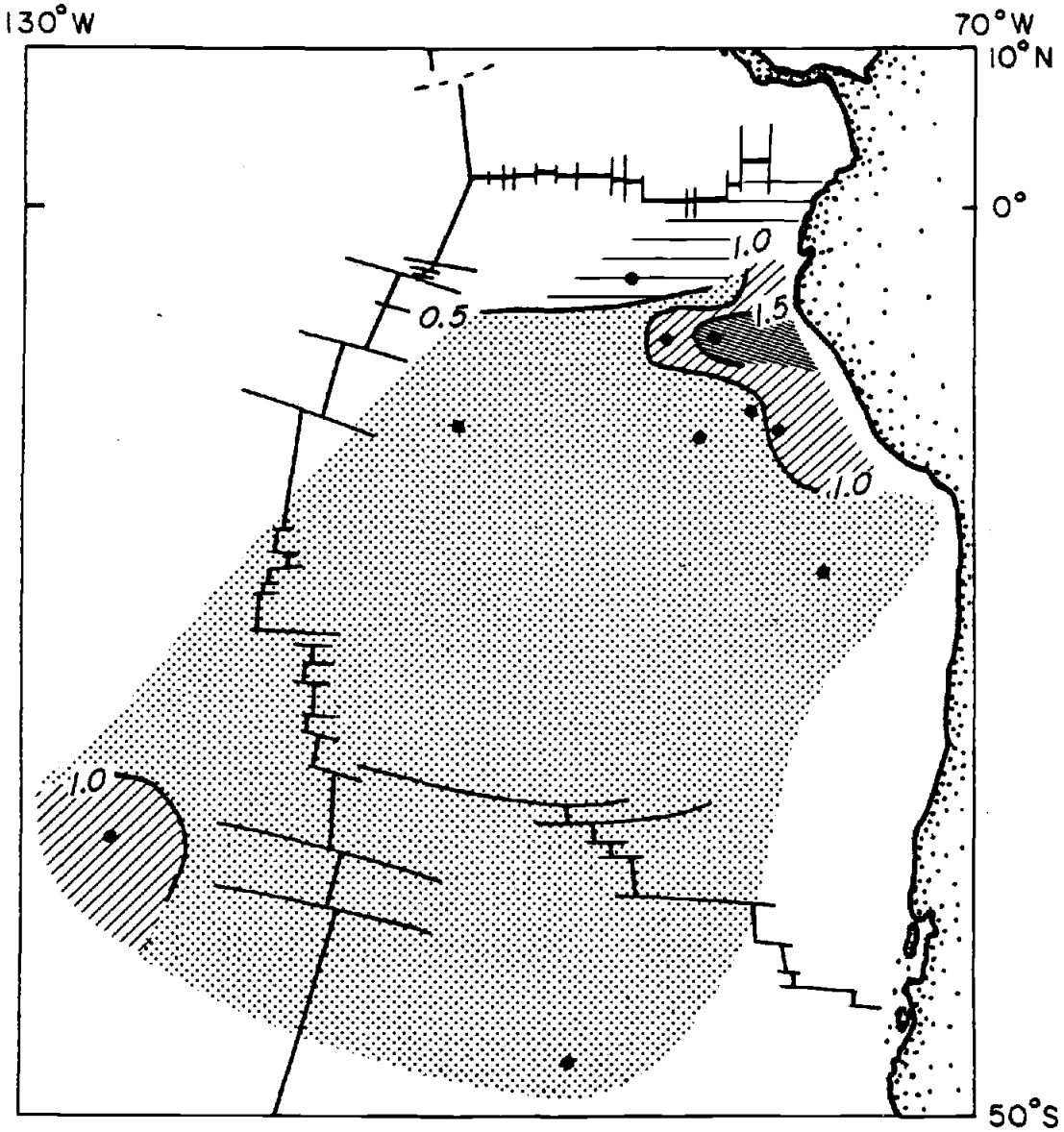
130°W
70°W
10°N
0°
50°S
0.5
1.0
1.5
1.0
1.0

APPENDIX 1

Estimation of Hydrothermal Manganese Input to the Oceans

Estimation of hydrothermal manganese input to the oceans

Mitchell Lyle
School of Oceanography
Oregon State University
Corvallis, Oregon 97331

ABSTRACT

Accumulation of manganese along the East Pacific Rise is much too rapid to be explained by simple authigenic precipitation. Since the rise crest sediments are oxidizing throughout the entire, though short, sedimentary column, it is unlikely that the high manganese accumulation rates represent upward flux of manganese during diagenesis. The most probable source of this excess manganese is hydrothermal activity. By assuming that the accumulation rate of hydrothermal manganese along mid-ocean ridge crests is proportional to the area of new crust formed per year, it is possible to estimate that 9×10^{11} g/yr of manganese is produced by hydrothermal activity at spreading centers. Data on manganese loss from basalt due to hydrothermal leaching and on manganese concentrations in hydrothermal solutions support this estimate. Hydrothermal manganese flux to the oceans is about three times higher than the dissolved load of manganese carried by rivers (2.5×10^{11} g/yr). Thus, hydrothermal manganese introduced at oceanic spreading centers should be considered one of the major sources of manganese input to the oceans.

INTRODUCTION

Studies of metalliferous sediments from the East Pacific Rise (Bostrom and Peterson, 1969; Bender and others, 1971; Dymond and others, 1973) call upon local introduction of mantle manganese, either from leaching of newly emplaced basalt by sea water during convective cooling (Corliss, 1971), or from the debouching of juvenile emanations that accompany rise crest magmatism (Bostrom and Peterson, 1966). A growing body of geophysical and geochemical evidence suggests that convective circulation of sea water through basalt is a major means of cooling new crust at spreading centers. Heat-flow studies (Talwani and others, 1971; Lister, 1972; Williams and others, 1974; Wolery and Sleep, 1976) strongly support the idea of convective cooling of new crust, while oxygen isotope data on submarine greenstones (Muehlenbachs and Clayton, 1972) and observations of an active marine hydrothermal system (Zelenov, 1964) indicate that sea water is the hydrotherma fluid. Juvenile emanations, if they exist, must be a minor component of this fluid.

Even though the removal of manganese from its mantle source is the subject of some controversy, it now seems clear that there is addition of manganese to the oceans from this source. Because hydrothermal circulation at spreading centers seems to be an important process, mid-ocean ridge crests could supply a significant amount of manganese to the oceans.

Mobilization and upward diffusion of manganese have been suggested as an alternative mechanism for producing high accumulation rates of manganese in surficial sediments. Mn^{IV} can be reduced to Mn^{II} in reducing sediments at depth, diffuse upward, and reprecipitate in an oxidizing zone neat the surface. This ptocess could account for high manganese concentrations in areas of high productivity (Li and others, 1969; Lynn and Bonatti, 1965) where the oxidized zone is relatively thin. Bender (1971), however, has demonstrated that such diffusion will not account for true "excess" manganese in most of the Pacific Ocean. In the relatively thick sequences of oxidized sediments on the East Pacific Rise (Sayles and Bischoff, 1973), upward mobilization of manganese supplies an insignificant amount of excess manganese to the surface sediments.

As a result of recent studies of metal accumulation rates across the East Pacific Rise (Dymond and Veeh, 1975; McMurtry and Burnett, 1975), sufficient data exist to place a lower limit on the flux of hydrothermal manganese at oceanic spreading centers. This estimate can be compared to continental input of manganese to assess the significance of rise crest hydrothermal activity as a source of manganese to the oceans.

ESTIMATION OF RIDGE CREST HYDROTHERMAL INPUT OF MANGANESE

The estimate of hydrothermal input used here is based upon accumulation rates of manganese in cores that form a rough transect extending 1,200 km to either side of the East Pacific Rise between lat 10° and 17°S (Table 1; Fig. 1). In addition to a "normal" rise crest sedimentation regime, this span also includes a catchment basin, the Bauer Deep, to the east of the East Pacific Rise crest. The relatively high accumulation rates that occur 800 to 1,200 km east of the rise

crest are most probably caused by the trapping of hydrothermal sediments wafted from the spreading center or from local hydrothermal sources (Dymond and Veeh, 1975). Because the higher accumulation rate of manganese in the Bauer Deep has hydrothermal origins, I extended the span of the transect to include this region.

Because manganese is essentially insoluble in oxygenated sea water (Krauskopf, 1956), almost all manganese introduced by hydrothermal activity should precipitate to the sediments near the East Pacific Rise crest. Accordingly, almost all hydrothermal manganese should reach the sediments within the transect. From a graphic integration of Figure 1, I obtained the average total manganese accumulation rate for this span, 2.3 mg/cm²/1,000 yr. If the influence of hydrothermal manganese extends farther than the bounds I chose for the transect, it will only make my final estimate of the hydrothermal input a lower limit.

The average total accumulation rate of manganese across the East Pacific Rise includes the manganese added by detrital and hydrogenous sources in addition to hydrothermal manganese. Both detrital and hydrogenous sources in addition to continentally derived material: the hydrogenous component represents manganese supplied by rivers in a soluble form, and the detrital component represents that carried in particulate form.

The continental influence must be removed to determine a true hydrothermal manganese input. Since most detrital sedimentation is blocked from the East Pacific Rise by the Peru-Chile Trench and the fossil Galápagos Rise (Bischoff and Sayles, 1972), sediments in the transect contain very little detrital material. Heath and Dymond (1977), using a form of normative analysis, have estimated the detrital manganese component in East Pacific Rise sediments to be approximately 3 percent of the total manganese. The accumulation rate of hydrogenous and hydrothermal manganese is, therefore, about 2.2 mg/cm²/1,000 yr.

Hydrogenous manganese can be estimated from the flux of dissolved manganese river water to the oceans. According to Turekian (1969), the average concentration of dissolved manganese in river water is 7 ppb. If the average yearly river output is 3.6×10^{16} l of water (Turekian, 1969), the average input of dissolved manganese to the oceans is 2.5×10^{11} g/yr. This is equivalent to an average accumulation rate of 0.07 mg/cm²/1,000 yr. Here, I shall assume that hydrogenous manganese is accumulating at a rate of about 0.1 mg/cm²/1,000 yr. The average hydro-

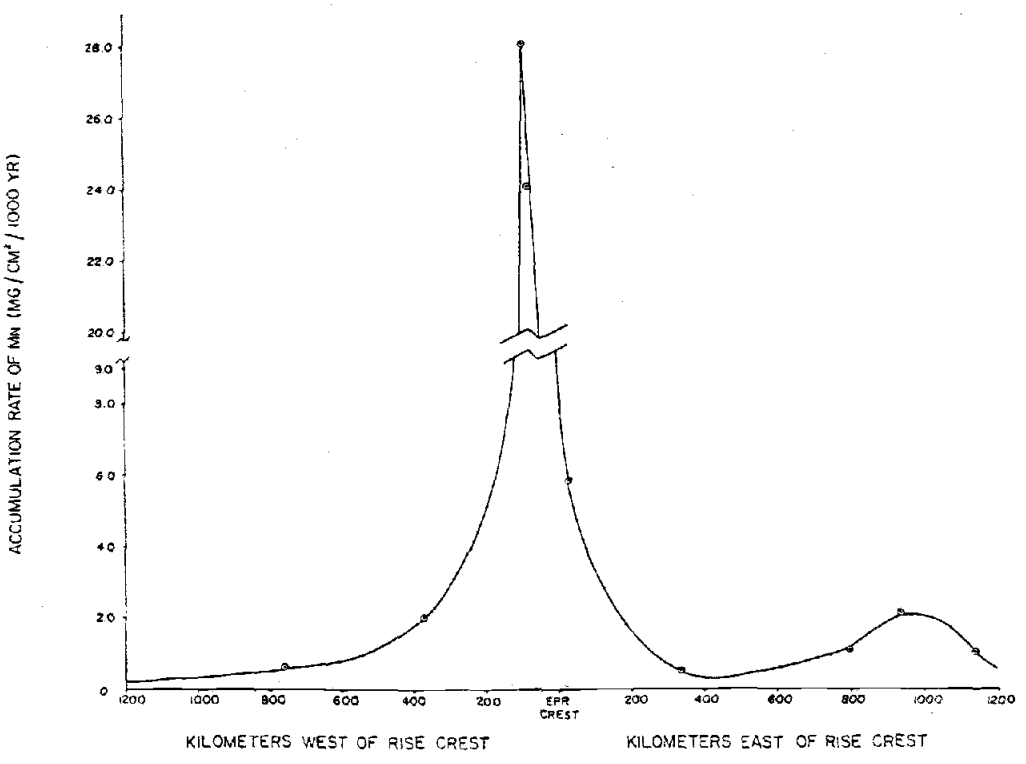

Figure 1. Profile of manganese accumulation rates across East Pacific Rise between lat 10° and 17°S.

thermal manganese accumulation rate within 1,200 km of the East Pacific Rise is, therefore, about 2.1 mg/cm²/1,000 yr. This is equivalent to an annual production of 5.0×10^7 g of hydrothermal manganese for every kilometre of the rise crest. This estimate is insensitive to the boundary conditions used. Changes in the length of the transect, in the hydrogenous manganese component, and in the detrital component will not significantly change the mass of hydrothermal manganese produced per year. Increasing the length of the transect will lower the average accumulation rate of manganese, but because of the increased area over which the manganese accumulates, the mass of manganese remains approximately constant. For instance, if the transect were extended 500 km farther to either side of the rise crest, the average manganese accumulation rate would drop to 1.6 mg/cm²/1,000 yr. After removing the continental influence and multiplying by the new area, the new estimate of hydrothermal manganese production is 4.9×10^7 g/yr for every kilometre of the rise crest.

Although the estimate is more sensitive to changes in detrital and hydrogenous manganese accumulation, major misestimations of these still have little effect. Increasing both detrital and hydrogenous accumulation rates by a factor of 3 reduces the hydrothermal production by only 16 percent, to 4.0×10^7 g/yr per kilometre of East Pacific Rise crest, while reducing them by a factor of 3 increases the hydrothermal production 6 percent, to 5.3×10^7 g/yr.

With an estimate of East Pacific Rise production of manganese, it should now be possible to estimate the world-wide manganese production by marine hydrothermal systems, if the heat from cooling basalt drives the convective circulation in these systems and if the manganese leached is a direct function of the amount of basalt produced. As a first approximation, it can be assumed that manganese of hydrothermal origin should be proportional to crustal production at spreading centers. For the East Pacific Rise, the production of 1.6×10^{-4} km² of new crust by a 1-km section of rise crest (from a half-spreading rate of 8 cm/yr; Rea and others, 1973) forms 5.0×10^7 g/yr of hydrothermal manganese. World crustal production of 2.94 km²/yr of new crust (Williams and Von Herzen, 1974) would therefore produce about 9×10^{11} g of hydrothermal manganese.

Errors may result from extrapolation of manganese production at fast-spreading ridge crests, such as the East Pacific Rise, to slow-spreading ones, such as the Mid-Atlantic Ridge. There may be significant differences in crustal structure (for example, crack spacing and fault placement) or in other fundamentals (such as size and location of the heat source) that could make hydrothermal processes different at the two types of spreading center. The sparse sedimentary data concerning manganese accumulation rates in the Atlantic do not show rates as high as would be expected from extrapolation of East Pacific Rise data (Bender and others, 1970). Accumulation rates of manganese in manganese crusts from the Trans-Atlantic Geotraverse geothermal area, however, are significantly higher—13 to 24 mg/cm²/1,000 yr (Scott and others, 1974)—than the maximum expected of about 5 mg/cm²/1,000 yr. It is impossible to say from the data available whether the extrapolation is valid.

It is still possible to put bounds on the error this assumption may lead to, however. The Mid-Atlantic Ridge, which accounts for 30 percent of the total length of the mid-ocean ridge system, produces only about 18 percent of the new crust formed every year. Faulty extrapolation could lower the hydrothermal manganese estimate by only about 20 percent, or 1.8×10^{11} g/yr. It is improbable that it would produce errors toward greater hydrothermal manganese production.

Other, more serious errors may result from assuming that hydrothermal manganese production is directly proportional to crustal production. No data are currently available to evaluate directly the worth of this assumption. Two indirect tests described in the next section indicate that the model presented in this paper is at least reasonable, however.

TESTS OF HYDROTHERMAL MANGANESE PRODUCTION ESTIMATE

Available data allow two independent tests of my estimate for hydrothermal manganese production. Data on manganese loss from basalts as well as on hydrothermal solution compositions can show whether a hydrothermal manganese production of 9×10^{11} g/yr is reasonable.

Corliss (1971), by comparing elemental abundances in rapidly quenched pillows to those in holocrystalline basalts, showed that there was a 120 ppm loss of manganese from the holocrystalline basalts and assumed that this was due to hydro-

TABLE 1. CORES USED IN STUDY

Sample	Location lat (S)	Location long (W)	Water depth (m)	Mn accumulation rate (mg/cm²/1,000 yr)	Reference
DSDP site 313 0–2 m	13°01'	101°34'	4,290	1.0	Dymond and Veeh (1975)
V71-2-16#52	10°03'	102°58'	4,541	1.1	Dymond and Veeh (1975)
KK71-34-FFC115	11°58'	103°23'	4,548	2.1*	McMurtry and Burnett (1975)
KK71-106-GC10	9°59'	106°02'	3,647	0.5	Dymond and Veeh (1975)
V71-7-42D	11°05'	110°05'	3,096	5.8*	Dymond and Veeh (1975)
KK71-82-FFC102	12°05'	110°37'	3,069	0.86	McMurtry and Burnett (1975)
GS 7202-35P	14°48'	113°20'	3,030	24	Bostrom (1973)
419-54	17°52'	113°54'	2,830	28*	Bender and others (1971)
419-61	16°57'	116°18'	3,407	2.0*	Bender and others (1971)
419-63	16°56'	121°12'	3,540	0.62*	Bender and others (1971)

* As reported in Dymond and Veeh (1975).

TABLE 2. MANGANESE ABUNDANCES IN HYDROTHERMAL SOLUTIONS

Solution	Mn abundance (ppm)
Seawater (this paper)	1 – 4
Observed:	
Matupi Harbor, New Britain (Ferguson and Lambert, 1972)	2.7 – 111
Atlantis II 56°C brine (Brewer and Spencer, 1969)	82
Heimaey, Iceland (Olafsson, 1975)	0.01 – 0.59
Banu Wuhu, Indonesia* (Zelenov, 1964)	16 – 21
Deception Island, Antarctica (Elderfield, 1972)	0.6 – 2.4
Experimental:	
Bischoff and Dickson (1975)	5
Mottl and others (1974)	0.85 – 284
Nejasn (1975)	0.26 – 90

* Calculated from 100 to 140 mg/l Fe-Mn hydroxides observed, and assuming Fe/Mn ratio of 3, as at East Pacific Rise crest.

thermal leaching. Hajash (1975) showed that basalt reacted with sea water at temperatures between 200 and 500°C and at sea-floor pressures lost between 60 and 180 ppm manganese. If 120 ppm manganese is lost from basalt during hydrothermal activity, leaching of only 0.8 km of newly formed crust is required to produce the hydrothermal manganese estimated in this paper. This is well within estimates of the depth of hydrothermal penetration made by other authors (1 to 2 km—Lister, 1974; 3 km—Williams and others, 1974; 5 km—Wolery and Sleep, 1976).

Hydrothermal solution compositions provide another test of my hydrothermal estimate. Wolery and Sleep (1976) estimated that 2 to 6 × 10^{17} g/yr of sea water circulates through the oceanic crust near spreading centers. My model would require that it have a manganese concentration of 1 to 4 ppm, well within the range of values observed in marine hydrothermal systems and measured in laboratory experiments (Table 2). Exceptions are the low values, seen at Heimaey, Iceland, and Deception Island, Antarctica, which probably reflect significant mixing with normal sea water. Both of these studies were on water collected from open bays near volcanic activity.

SUMMARY

Data on the rate of accumulation of manganese at the East Pacific Rise indicate that approximately 9 × 10^{11} g/yr of manganese is injected into the world ocean by hydrothermal activity at spreading centers. With more accumulation-rate data from the East Pacific Rise and other spreading centers, it may be possible to refine this estimate. This value is further supported by data for the amount of manganese leached from deep-sea basalts and by dissolved manganese contents observed in natural and experimentally derived hydrothermal solutions. Unfortunately, it is impossible to compare the estimate with continental input of manganese, because there is no good measure of detrital manganese input. Because the estimated hydrothermal manganese input is about three times larger than the dissolved load of manganese carried by rivers (2.5 × 10^{11} g/yr), it should be considered an important source of manganese input to the oceans.

REFERENCES CITED

Bender, M. L., 1971, Does upward diffusion supply the excess manganese in pelagic sediments?: Jour. Geophys. Research, v. 76, p. 4212–4215.

Bender, M. L., Ku, Teh-Lung, and Broecker, W. S., 1970, Accumulation rates of manganese in pelagic sediments and nodules: Earth and Planetary Sci. Letters, v. 8, p. 143–148.

Bender, M., Broecker, W., Gornitz, V., Middel, U., Kay, R., Sun, S., and Biscaye, P., 1971, Geochemistry of three cores from the East Pacific Rise: Earth and Planetary Sci. Letter v. 12, p. 425–433.

Bischoff, J. L., and Dickson, F. W., 1975, Seawater-basalt interactions at 200°C and 500 bars: Implications for origin of heavy metal deposits and regulation of seawater chemistry: Earth and Planetary Sci. Letters, v. 25, p. 385–397.

Bischoff, J. L., and Sayles, F. L., 1972, Pore fluid and mineralogical studies of recent marine sediments: Bauer Depression region of the East Pacific Rise: Jour. Sed. Petrology, v. 42, p. 711–724.

Bostrom, K., 1973, The origin and fate of ferromanganoan active ridge sediments: Acta Univ Stockholmiensis, v. 27, p. 149–243.

Bostrom, K., and Peterson, M.N.A., 1966, Precipitates from hydrothermal exhalations on the East Pacific Rise: Econ. Geology, v. 61, p. 1258–1265.

—— 1969, The origin of aluminum-poor ferromanganoan sediments in areas of high heat flow on the East Pacific Rise: Marine Geology, v. 7, p. 427–447.

Brewer, P. G., and Spencer, D. W., 1969, A note on the chemical composition of the Red Sea brines, *in* Degens, E. T., and Ross, D. A., eds., Hot brines and recent heavy metal deposits in the Red Sea: New York, Springer-Verlag, p. 174–179.

Corliss, J. B., 1971, The origin of metal-bearing submarine hydrothermal solutions: Jour. Geophys. Research, v. 76, p. 8128–8138.

Dymond, J., and Veeh, H. H., 1975, Metal accumulation rates in the southeast Pacific and the origin of metalliferous sediments: Earth and Planetary Sci. Letters, v. 28, p. 13–23.

Dymond, J., Corliss, J. B., Heath, G. R., Field, C. W., Dasch, E. J., and Veeh, H. H., 1973, Origin of metalliferous sediments from the Pacific Ocean: Geol. Soc. America Bull., v. 84, p. 3355–3371.

Elderfield, H., 1972, Effects of volcanism on water chemistry, Deception Island, Antarctica: Marine Geology, v. 13, p. M1–M6.

Ferguson, J., and Lambert, I. B., 1972, Volcanic exhalations and metal enrichments at Matupi Harbor, New Britain, T.P.N.G.: Econ. Geology, v. 67, p. 25–37.

Hajash, A., 1975, Hydrothermal processes along mid-ocean ridges: An experimental investigation: Contr. Mineralogy and Petrology, v. 53, p. 205–226.

Heath, G. R., and Dymond, J., 1977, Genesis and transformation of metalliferous sediments from the East Pacific Rise, Bauer Deep, and Central Basin, northwest Nazca plate: Geol. Soc. America Bull., v. 88 (in press).

Krauskopf, K. B., 1956, Factors controlling the concentration of thirteen rare metals in sea-water: Geochim. et Cosmochim. Acta, v. 9, p. 1–32.

Li, Yuan-Hui, Bischoff, J., and Mathieu, G., 1969, The migration of manganese in the Arctic Basin sediment: Earth and Planetary Sci. Letters, v. 7, p. 265–270.

Lister, C.R.B., 1972, On the thermal balance of a mid-ocean ridge: Royal Astron. Soc. Geophys. Jour., v. 26, p. 515.

—— 1974, On the penetration of water into hot rock: Royal Astron. Soc. Geophys. Jour., v. 39, p. 465–509.

Lynn, D. C., and Bonatti, E., 1965, Mobility of manganese in diagenesis of deep sea sediments: Marine Geology, v. 3, p. 457.

McMurtry, G. M., and Barnett, W. C., 1975, Hydrothermal metallogenesis in the Bauer Deep of the southeastern Pacific: Nature, v. 254, p. 42–44.

Mottl, M. J., Corr, R. F., and Holland, H. D., 1974, Chemical exchange between sea water and mid-ocean ridge basalt during hydrothermal alterations: An experimental study: Geol. Soc. America Abs. with Programs, v. 6, p. 879–880.

Muehlenbachs, K., and Clayton, R. N., 1972, Oxygen isotope studies of fresh and weathered submarine basalts: Canadian Jour. Earth Sci., v. 9, p. 172–184.

Olaffson, J., 1975, Volcanic influence on seawater at Heimaey: Nature, v. 255, p. 138–141.

Rea, D. K., Dymond, J., Heath, G. R., Heinrichs, D. F., Johnson, S. H., and Hussong, D. M., 1973, New estimates of rapid sea-floor spreading rates and the identification of young magnetic anomalies on the East Pacific Rise, 6° and 11°S: Earth and Planetary Sci. Letters, v. 19, p. 225–229.

Sayles, F. L., and Bischoff, J. L., 1973, Ferromanganoan sediments in the equatorial East Pacific: Earth and Planetary Sci. Letters, v. 19, p. 330–336.

Scott, M. R., Scott, R. B., Rona, P. A., Butler, L. W., and Nalwalk, A. J., 1974, Rapidly accumulating manganese deposit from the median valley of the Mid-Atlantic Ridge: Geophys. Research Letters, v. 1, p. 355–358.

Talwani, M., Windisch, C. C., and Langseth, M. G., Jr., 1971, Reykianes Ridge crest: A detailed geophysical study: Jour. Geophys. Research, v. 76, p. 473–517.

Turekian, K. K., 1969, The oceans, streams, and atmosphere, *in* Wedepohl, K. H., ed., Handbook of geochemistry (Vol. 1): Berlin-Heidelberg-New York, Springer-Verlag, p. 297–323.

Williams, D. L., and Von Herzen, R. P., 1974, Heat loss from the Earth: New estimate: Geology, v. 2, p. 327–328.

Williams, D. L., Von Herzen, R. P., Sclater, J. G., and Anderson, R. N., 1974, The Galapagos spreading center: Lithospheric cooling and hydrothermal circulation: Royal Astron. Soc. Geophys. Jour., v. 38, p. 587–606.

Wolery, T. J., and Sleep, N. H., 1976, Hydrothermal circulation and geochemical flux at mid-ocean ridges: Jour. Geology (in press).

Zelenov, K. K., 1964, Iron and manganese exhalations of the Banu Wuhu volcano (Indonesia): Akad. Nauk, SSSR Doklady, v. 155, p. 94–96.

ACKNOWLEDGMENTS

Reviewed by D. Z. Piper and M. L. Bender. Supported by National Science Foundation Grant GX-28675 (NSF/IDOE Nazca Plate Project). I thank J. B. Corliss, J. Dymond, E. J. Dasch, G. R. Heath, L. Hogan, and D. Stakes for their comments and criticisms of the manuscript.

MANUSCRIPT RECEIVED APRIL 16, 1976

MANUSCRIPT ACCEPTED SEPT. 27, 1976

APPENDIX 2

The Chemistry of Hydrothermal Sediment Mound Deposits Near the Galapagos Rift

The Chemistry of Hydrothermal Sediment Mound Deposits Near the Galapagos Rift

John B. Corliss, Mitchell Lyle,
and Jack Dymond
School of Oceanography
Oregon State University
Corvallis, Oregon 97331

and

Kathy Crane
Scripps Institution of Oceanography
La Jolla, California 92093

Abstract

Samples dredged from the sediment mounds have a unique chemistry and mineralogy which reveals details of the hydrothermal processes that produce these deposits. The mounds form primarily by deposition of Fe, Mn and Si from hydrothermal fluids which circulate through the basalt crust and the overlying sediments. The Mn, Fe and Si are strongly fractionated in the process; the Fe and Si precipitate within the mounds under slightly reducing conditions as nontronite, while the Mn is deposited as Mn oxyhydroxides at the seawater-sediment interface. The nontronite is exceptionally well crystallized, and contains less than 200 ppm Al. The Mn minerals, todorokite and birnessite, also have exceptional crystallinity and the distribution of trace elements Cu, Ni, Zn, Co, Ca and Ba in these phases agrees with predictions made on the basis of models of their crystal structure. The environment of deposition which produces this suite of minerals - slow percolation of hydrothermal fluids through pelagic sediments - may not be unique to the Galapagos Rift, as the same suite of minerals has been found in similar setting in the Gulf of Aden and on the Mid-Atlantic Ridge.

1.0 Introduction

Although it has been long proposed that ferromanganese nodules and crusts form by volcanic processes (1, 2), recent work suggests that most of these deposits form as a result of slow authigenic and/or diagenetic processes at the sea floor (3, 4). One type of ferromanganese deposit found near active spreading centers, however, exhibits the following characteristics which contrast markedly with typical deposits:

(1) They generally exhibit a very strong fractionation of Fe and Mn and are composed of either nearly pure Mn oxides or Fe oxides and silicates (5, 6, 7).

(2) They appear to accumulate 100-1000 times more rapidly than typical nodules (3).

(3) They have very low trace metal and ^{230}Th contents (5, 8).

(4) Some of these deposits have anomalously high $^{234}U/^{238}U$ values (9).

These characteristics have lead to suggestions that this type of ferromanganese deposits form by precipitation from sea water hydrothermal solutions which have circulated through cooling volcanic rocks and mixed with normal sea water near the sea floor.

We report here on a suite of samples with similar characteristics which were dredged from an area of sediment mounds, located on the south flank of the Galapagos Rift at 86°W, near the spreading center, 200 miles northeast of the Galapagos islands.

2.0 Geologic Setting of the Mound Samples

Detailed descriptions of the sediment mounds based on Deep Tow surveys during expeditions SOUTHTOW and PLEIADES Leg I of Scripps Institution of Oceanography have been published elsewhere (10, 11). These surveys provided both high resolution seismic reflection and side-scanning sonar profiles of the sediment mound area. Williams, et al. (12) reported on an intensive heat flow survey made on

the SOUTHTOW expedition.

The samples described here were dredged on PLEIADES Leg II during a program of heat flow measurements, bottom photography, coring, bottom water and water column sampling, suspended particulate sampling, profiling, bottom water temperature, OBS and sonobuoy measurements which served as a site survey for a deep submersible (ALVIN) study of hydrothermal activity on the Galapagos Rift. Preliminary results of the ALVIN study are reported in Corliss, et al., (13). Comprehensive studies of the results of the ALVIN diving program, which included extensive additional sampling, will be reported in the future.

The mounds are located in a band 20 km south of the Galapagos Rift (Fig. 1) on sediments ranging from 20 to 30 meters in thickness. The spreading half-rate is 35 mm/year (14), so that the basalt crust underlying the mounds ranges from 500,000 to 700,000 years in age. The mean sedimentation rate, derived from observations of sediment thickness and crustal age is approximately 5 cm/1000 years (10).

The topography of the sea floor reflects the underlying basement structure plus increasing sediment thickness to the south. The terrain is dominated by east-west trending normal fault scarps which predominantly face the spreading center to the north (10). The relief on these scarps ranges from greater than 200 meters at the spreading center to less than 100 meters in the sediment mound area.

The mounds themselves reach heights of 15-20 meters and are up to 50 meters in diameter. They occur in linear arrays which are subparallel to the dominant structural and the trend of the spreading axis (11). The distribution pattern of the arrays of mounds and ridges resembles the pattern of small faults and fissures exposed along the spreading axis to the north.

They occur as rows of distinct mounds, and also coalesce to form more or less continuous ridges commonly spaced about 100 m. apart. Some mounds completely buried by sediment were seen in reflection records, and the basalt basement appears to be continuous beneath the mounds.

Bottom photographs and ALVIN observations of the mounds reveal numerous outcrops of resistant material surrounded by sediment. Massive outcrops of dark colored material with occasional bright yellow patches and bands are present as well, contrasting with the normal gray green calcareous-siliceous ooze in the area. During dredging we obtained samples with morphologies and colors representing all types readily visible in the photographs and later seen from ALVIN. Evidence from reflection profiling, the absence of basalt in the dredges, and the direct observations made from ALVIN show that these crusts do not grow on basalt.

The mounds are located within a broad band of high heat flow as described by Williams, et al. (12). Refinement of this work on PLEIADES Leg II has verified the occurrence of the mounds in a high heat flow zone with ranges of heat fluxes of 6 h.f.u. over the whole mound area, several measurements of 12 h.f.u. and two stations with heat flow greater than 30 h.f.u. (15). The measured temperature gradients in the latter case are greater than 2 degrees centigrade per meter.

Recent drilling in the area by the Deep Sea Drilling Project on Leg 54 (16), cored individual sediment mounds. A 10 to 15 meter thick section of Fe-Mn fragments in a green Fe and Si rich, Al poor mud and was recovered from the tops of two mounds.

3.0 Sampling and Analysis

The mound samples described here were collected in three transponder navigated dredges which diagonally crossed lines of mounds noted in the Deep Tow

Survey. In addition to these, one dredge haul was made to the South of the mound area, about 43 km from the spreading center, where the crust is approximately 1.2 million years old. This dredge haul recovered slightly altered basalt, encrusted with a manganese coating on exposed surfaces ranging from 1 to 5 mm thickness.

The dredge hauls were sampled to represent the diversity of the dredged material. Each sample was analyzed by slow-scan x-ray diffractometry (500 sec/deg 2θ), atomic absorption spectrophotometry, and instrumental neutron activation analysis (17). The chemical data are presented in Table 1 and the x-ray results in Table 2 and Figures 2 and 3.

4.0 Comparison of Sediment Mound Deposits and Basalt Coatings

The samples dredged in the PLEIADES II cruise can be separated into two distinct groups, relatively thick crusts deposited on sediment mounds and the thin and presumably more slowly deposited crusts on basalt which were dredged from a scarp south of the mounds area (samples DM1 and DM2). These latter samples have δMnO_2, following the usage of (18), as the only Mn mineral present (Figure 1). This mineral has been reported as Fe-Mn coatings on altered basalt from the Nazca plate (21) and nodules in oxidizing environments (4). Growth rates of these Fe-Mn basalt coatings calculated from the crustal age at the dredge site are approximately 4 mm/10^6 years, within the range of typical ferromanganese deposits (3).

The samples from the mounds area show mineralogical and morphological features which contrast strongly with these slowly deposited Fe-Mn coatings. They fall into 3 categories: crusts that are mixtures of the two well crystallized manganese minerals, todorokite and birnessite (samples TB1 - TB7, Figure 3), pieces of well crystallized nontronite smectite (N1 - N5), and coatings of x-ray amorphous material (A1 - A2, Figure 2).

The Mn crust samples range from thin flat plates, often smooth, hard and dense on one side and soft on the other (TB1, TB2, and TB3) to veins of hard Mn mineral (TB4) in a porous soft black groundmass (TB6), to thin plates (3-15mm) with chalky, irregular surfaces on both sides (TB5 and TB7). Most of the todorokite-birnessite samples are about 1 cm thick, but some massive crusts are more than 6 cm thick. Given the age of the crust they overlie, these samples must have a growth rate greater than 2 cm/10^6 year, or at least an order of magnitude greater than typical ferromanganese deposits (3). The amorphous Fe-oxide samples (A1 and A2) occur as red- or yellow-orange coatings on some of these todorokite-birnessite Mn crusts.

The nontronite samples occur either as dark green to yellow-green irregular crusts with a thin black surface coating, N1 and N2, or roughly equidimensional lumps of semi-lithified mud, 3-6 cm in diameter with colors ranging from dark green to a rich dark orange (N3, N4 and N5). Some pieces grade continuously in color from green to orange from one side to the other.

The samples dredged from the sediment mounds exhibit a strong fractionation of Fe and Mn. Iron is found almost exclusively in an Fe-rich nontronite (N) containing approximately 25% Fe and essentially no Mn, or in amorphous iron oxides (A). Manganese forms separate phases (TB) composed of todorokite, birnessite, or mixtures of these two minerals, containing 50% Mn and less than 0.6% Fe (Table 1, Figure 4). The crusts (TB), the nontronite (N), and the amorphous Fe-oxides (A) because of their low trace metal abundances, have compositions that Bonatti et al., (5) have defined as hydrothermal (Figure 5).

The Fe-Mn coatings on basalts (BM) have much higher trace element contents than the mounds deposits. For example, Co and Th are 100X, Ni and As from 10X to 100X and the rare earth elements (REE), Hf and Sc are 50X more abundant in the Fe-Mn coatings on basalt compared to the mounds crusts. Consequently the Fe-Mn

coatings fall in the "hydrogenous" ferromanganese field on Figure 5 and have Fe, Mn and Si contents in the range of typical Pacific manganese nodules (4, 19).

Antimony and barium exhibit behavior unlike the other trace elements in the Mn deposits. Although most trace elements are consistently enriched in the slowly growing Fe-Mn coatings on basalt (DM), Sb and Ba have approximately the same concentration in both types of deposit. This suggests either more active uptake of Sb and Ba by the Mn minerals in the mounds deposits, or an additional source in the mounds area, presumably the hydrothermal fluids.

The REE distribution patterns (Fig. 6) of all samples dredged from the sediment mounds (TB, N, and A) exhibit only slight cerium depletions relative to chrondritic abundances, less than those in the seawater REE pattern. The ferromanganese coatings on basalt (DM), in contrast, have REE abundances 100X greater than the mounds deposits and no cerium depletions. Although the DM samples have a total REE content similar to normal ferromanganese nodules, they do not display the strong Ce enrichments that are characteristic of nodules (20, 21).

5.0 Mineralogy and Trace Element Distribution in the Hydrothermal Manganese Phases

Burns and Burns, in a recent summary (18) suggest that both the birnessite and todorokite structures accommodate Mn^{+2}, and that the divalent cations Ni^{+2}, Cu^{+2}, Zn^{+2} replace this Mn^{+2}. Co^{+3} and Ce^{+4} replace Mn^{+4} in the octahedral sites. They also suggest that Ca^{+2} and Na^{+} can be accomodated in the layered birnessite structure and that the large cations Ba^{+2} and K^{+} may be accommodated in cavities in a framework structure tentatively hypothesized for todorokite.

Two features of the chemistry of the mounds Mn crusts seem to support these ideas. The concentration of Cu, Ni, and Zn are independent of the relative

abundance of todorokite and birnessite. The todorokite (9.8Å) to birnessite peak (7.2Å) ratio (T/B) varies from 20 in TB1 to less than .01 in TB7, but it is apparent that the distribution of samples in the plots of Cu, Ni and Zn (Figure 6a,b) bears no relationship to variations in mineralogy. The samples with the highest Cu, Ni, and Zn concentrations (TB6) is essentially pure birnessite (T/B = .01), while the sample with the next highest abundances of these metals is predominantly todorokite (T/B = 2). The purest todorokite (TB1) is similar in Cu-Ni-Zn composition to samples with only traces of todorokite (TB3 and TB5). Co is most abundant in the todorokite rich samples (TB1 and 2) but also is high in a nearly pure birnessite sample (TB6).

While the Cu, Ni, and Zn are not correlated with the T/B ratio, they are highly correlated with one another (Figure 7a,b). The reason for the covariance may relate to the availability of Mn^{+2} sites, but this seems unlikely as it requires that the number of Mn^{+2} sites is a limiting factor. Since it is likely that sufficient Mn^{+2} sites are available, the fluctuations in Cu, Ni and Zn may result from variations in the rate of growth of the crusts. In contrast the Co abundance in these crusts does not correlate with Cu, Ni, or Zn. The correlation coefficients (r^2) for Co with Cu, Ni, and Zn range from .38 to .43. This contrast in the distribution of Co and Cu, Ni, and Zn tends to support the notion of Burns and Burns that Co can have two valence states and replace both Mn^{+2} and Mn^{+4} while Cu, Ni, and Zn substitute only for Mn^{+2} in both birnessite and todorokite.

Ca and Ba may show fractionation between todorokite and birnessite, however. Burns and Burns suggest that birnessite accommodates Ca^{+2} in interlayer sites suitable for an ion of its size and that todorokite will take up the large Ba^{+2} ion in large cavities in its proposed tubular structure. The plot of Ca vs.

Ba (Figure 8) shows that the distribution of these elements agrees with this prediction. Burns and Burns also suggest that the monovalent cations K^{+} and Na^{+} which have similar ionic radii to Ba^{+2} and Ca^{+2} respectively, could also substitute in the same sites. Our data does not support this (Table 1). We can only speculate that the difference in charge may be important.

6.0 Formation of Hydrothermal Nontronite

The nontronite from the sediment mounds is another important component of these deposits. The data on the nontronite samples reveals a trend from nearly pure Fe-nontronite (N1 and N2) with extremely low Al, Ca, Mn and trace elements through N3, N4 and N5 which contain increasing abundances of these elements. The purest samples, N1 and N2, are from crust like fragments while the contaminated samples occur as formless lumps. The presence of calcite and quartz in the x-ray patterns of N4 and N5, and the appearance of foraminiferal fragments in N5 indicate that this trend results from increasing contamination of the nontronite in these samples with the normal pelagic sediment depositing in the sediment mound area.

The green Al-poor Fe-Si-rich mud recovered by the DSDP Leg 54 drilling (16) presumably is dominantly nontronite. Bischoff (22) also reports on an occurrence in the Red Sea brine deposits. Because the Galapagos Rift Mound samples are essentially Al free (Table 3), Fe must be present in both the octahedral and tetrahedral layer as proposed by Bischoff and clearly shown by Goodman et al. (23) in Mossbauer spectroscopy studies. As noted in the descriptions, the nontronite varies in color from yellow to green. Oxidation-reduction experiments (24, 25, 26, 27) show that this color change accompanies

a change in oxidation state of some octahedral Fe from Fe^{+3} in the yellow nontronite to Fe^{+2} in the green with the charges balanced by addition of a second hydrogen, derived from interlayer water, to the OH groups adjacent to the Fe^{+3}. In the experimental synthesis (28), nontronite formed by precipitation and subsequent aging of Fe hydroxides and Si co-precipitated silica from solutions containing these elements. Precipitation occurred in solutions that contained 20 ppm monomeric SiO_2 and 4 to 7.5 ppm Fe, at temperatures of 3°C and 20°C under reducing conditions (Eh = -0.1 to -0.8 v.) with pH in the range 7-9. Two features of the experimental conditions which Harder cites as critical to the formation of nontronite are the relatively low Si concentration and the presence of reduced iron (Fe^{+2}) in the solutions. Higher Si concentrations lead to polymerization of the silica, which inhibits clay mineral formation so that the precipitates remain amorphous on aging. The presence of Fe^{+2}, Harder suggests, stabilizes the formation of a brucite-gibbsite-type octahedral layer which in turn is necessary for orientation of the SiO_4 tetrahedra into a clay mineral lattice. With positive Eh, the Fe^{+3} precipitates rapidly to form goethite and the silica precipitates as quartz. At lower Eh, some proportion of the Fe occurs as Fe^{+2}, and the layer silicate structure of nontronite can form. The occurrence of coexisting yellow and green nontronite and amorphous silica-rich Fe oxide in the mounds suggest that the interstitial fluids of the mounds contain iron and silica contents in the general range of the nontronite synthesis experiments, with Eh ranging from slightly oxidizing to reducing.

7.0 The Site of the Convective System which Could Produce the Mound Deposits

There are two models, calling on hydrothermal activity, that could explain the presence of the mounds. In one model, hydrothermal convection

cells are established with the fractured permeable basalt crust beneath the sediment layer. Channels for hydrothermal flow may be established through the sediment, stabilized by alteration and deposition in the sediments around them or the fluids may simply percolate through the sediment. The vertical flow is concentrated along fissures and fractures within the basalt, so that the pattern of mounds reflects the distribution of fractures in the basalt.

The second model involves the establishment of a secondary convection cell within the sediments. If the sediment is sufficiently permeable, slow convection of pore waters could be established through heat delivered to the base of the sediment by the convection system within the basalt. The hydrothermal fluids in this case would be influenced only slightly by basalt alteration reactions, since most of the fluids debouching would be pore waters.

The prime geochemical distinction between these two models, is that the first model calls for extensive influence of basalt alteration reactions on the chemistry of the hydrothermal fluid while the second demands that the hydrothermal fluid chemistry be governed primarily by reactions within the sediment. The first model also implies large scale transfer of material from the mantle into the mounds and seawater. In the second model, this material is derived from the underlying sediments.

We can examine the relative importance of these two processes by considering a mass balance for manganese assuming it is all derived from the sediment. Manganese is known to be mobilized and transferred upward in the sediments of the Galapagos Rift area by reduction at depth and oxidation at the surface (29), as was observed in cores taken adjacent to the mound areas. Conceivably, large scale enrichments of manganese could occur by the enhancement of this process. Preliminary analyses of the 45 cores from the area between the spreading center and the mounds reveal a surface oxidized layer of about 10 cm thickness which

contains 1.6% Mn. The sediments below contain about 0.1% Mn. Given the concentration of Mn in the sediment (0.1%), in the Mn crust (50%), the dry bulk density of the sediment (0.7 g/cm^3), and the bulk density of the crust ($\sim$ 2.5 gm/cm^3), a crust about 2 cm thick would be deposited if all the sedimentary manganese from a 30 meter column were mobilized to the surface and deposited. If the convective systems in the sediment extended laterally to flush the sediment between the chains of sediment mounds then, given that the mound chains are spaced about 100 m apart, according to the Deep Tow Survey (8) and are from 20 to 50 meters wide, this should provide at most a 2-5 fold increase in thickness, so that something on the order of 10 cm of Mn could possibly be deposited on the mound ridges by this process. Sampling of the mounds by coring and visual observations suggest that the Mn crusts are predominantly formed at the surface of the mounds in contact with oxygenated bottom water, and that their total average thickness, over the mounds may not be significantly greater than this.

The situation is complicated by the observation that there seems to be a considerable flux of Mn into the bottom water above the mounds. On Leg II of the PLEIADES Cruise on the R/V Melville, we collected near bottom water samples in contamination-free 30 liter bottles mounted both on the wire and on a Kamikaze bottom water sampler. The samples have been analyzed for total dissolvable manganese by G. Klinkhammer and M. Bender (30). Figure 9, from Klinkhammer et al. (30), reveals a strong gradients in total dissolvable Mn in the bottom water reaching maximum values in Kamikaze samples taken less than 5 meters above the sediment water interface.

This gradient implies a considerable flux of Mn out of the sediments and supports the suggestion that the hydrothermal fluids derive significant Mn from interaction with the basalt rather than the sediment alone.

The most likely situation is that the interstitial fluids in the basalt can migrate across the sediment rock boundary and thus do interact with the pore waters of the sediments to form a continuous chemical system. Thus, it is probable that the chemistry of the fluids forming the mound deposits is influenced both by reactions within the basalt and interaction with the overlying sediment. The actual situation will be clarified by studies of sediment cores and both squeezed and in situ sampled interstitial fluids from the mounds currently underway.

8.0 The Formation of Submarine Hydrothermal Deposits

One important question regarding these mounds samples is whether they are a common occurrence on the sea floor or are the result of a unique set of conditions existing only near the Galapagos Rift. In this regard, a recent report by Cann and others (6) of a very similar deposit dredged 3 km from a spreading axis in the Gulf of Aden is of some interest. They describe a dredge haul containing (1) soft to hard manganese crusts of todorokite and birnessite, (2) a low Al nontronite and (3) X-ray amorphous iron oxides, with the Mn oxides forming a carapace over the nontronite and Fe-oxide. This assemblage is strikingly similar to that of the Galapagos Rift mounds. The dredge site was described by Glasby (31) as the side of a narrow shallow median valley, containing a considerable thickness of rapidly accumulating, highly reduced green sediment which results from the high biologic productivity in the area. Thus, the setting at the Gulf of Aden is also similar to that of the Galapagos mounds.

A similar deposit was also reported from transform fault A in the FAMOUS

area on the Mid-Atlantic Ridge (7). Two vent areas, 100 meters apart, deposited concentric bands of green, yellow, red and then black crusts from 1 meter thick at the vents and 10- 50 cm thick away from the vents. They are low in Co, Ni and Cu and have Fe/Mn ratios from 0.2 to 237. The X-ray patterns show that the Mn rich phases are todorokite and birnessite, and the Fe-rich samples are primarily nontronite (32). The deposits rest on consolidated carbonate ooze; some samples of the crusts contain coccoliths and foraminifera in various stages of alteration and replacement by hydrothermal fluids.

The similarity of these three occurrences of this mineralogically and chemically unique suite of samples indicates that the hydrothermal processes in each area are also similar. The experimental data on nontronite synthesis (28) suggests that the solutions were at low temperatures (3-20°C), nearly neutral pH (7-9) and slightly reducing (Eh= -.2 to -.8). The presence of sediment underlying the deposits is interesting, and one can speculate that the percolation of fluids through the sediment is an important part of the process leading to this particular suite of minerals.

Samples attributed to hydrothermal activity containing Mn oxyhydroxides but without nontronite, accompanied by silica-rich Fe oxides have been recovered from many localities in the oceans; for example, the TAG area (26°N) on the Mid-Atlantic Ridge (33, 9) the De Steiger Deep on the Galapagos Rift (34), 11°S on the East Pacific Rise (35), Dellwood Seamount in the Northeast Pacific (36), etc. The experimental data suggest that these deposits form under oxidizing conditions with the Fe^{+3} precipitating rapidly as Fe hydroxides and silica, aging to goethite in some cases and followed by precipitation of the low temperature Mn phases with no low temperature reducing zone suitable for nontronite formation.

When there is sufficient sediment present so that the hydrothermal fluids cool slowly under reducing conditions while percolating through the sediment, the Fe and Si precipitate as nontronite.

Approaching the surface of the mounds, the sequence of nontronite-iron oxide-manganese oxides may reflect a stable steady-state oxidation gradient. Near the surface of the mound the interstitial fluids become slightly more oxidized and Fe-oxides and amorphous silica are precipitated instead of nontronite. At the interface with the oxygenated bottom water, the Mn oxides precipitate, perhaps initiated by epitaxial intergrowth with the Fe-oxides, as suggested by Burns and Burns (37).

Conclusions

(1) The Galapagos Rift sediment mounds are formed by deposition of Fe, Mn and Si from hydrothermal fluids percolating through sediments overlying basaltic crust. The fluids are sea water which has circulated through and interacted with the basaltic crust and the sediments. The relative contribution of interactions with the basalt and the sediment to the composition of the fluids is not clear, but it is likely that the basalt is the primary source of the Fe, Mn and Si which form the bulk of the deposits.

(2) The chemistry and mineralogy of the deposits reflect a change from reducing conditions within the mounds, where Fe and Si are deposited as a nearly Al-free nontronite, to oxidizing conditions at the bottom water interface, where Si-rich Fe-oxides and Mn-oxide crusts form the exposed surface of the mounds. These conditions lead to nearly quantitative separation of Fe and Mn.

(3) These Mn crusts are well crystallized todorokite or birnessite or mixtures of these phases. The trace element abundances in these samples reveal that the Cu, Ni and Zn are strongly covariant independent of mineralogy, that

Co is not covariant with Cu, Ni, and Zn, and that in contrast to the metals, mineralogy does influence the distribution of Ba and Ca in the crusts. These rapidly deposited hydrothermal Mn crusts have a much lower Cu, Ni, Zn and Co content than a slowly accumulating Mn-coating composed of δMnO_2 on basalt dredged from older oceanic crust south of the sediment mounds.

(4) The combination of nontronite with Fe and Mn oxides in submarine hydrothermal deposits has been observed in the Gulf of Aden and on the Mid-Atlantic Ridge in the FAMOUS area as well as in these Galapagos Rift mounds. This suite of minerals may result from the presence of sediment, which allows the fluids to cool and precipitate Fe and Si, under reducing conditions as nontronite, in contrast to conditions where hydrothermal fluids flow directly from basalt into bottom waters and deposit only oxides.

Acknowledgments

The activation analysis was performed by Roberta Conard, the atomic absorption spectrometry by Christine Chow. The samples were dredged on PLEIADES Leg II Cruise of the R/V MELVILLE with the cooperation of Capt. Finney and the scientific party and crew. Useful reviews of the manuscript were provided by Roger Burns, Peter Lonsdale, and Martha Scott.

REFERENCES

(1) Murray, J. and A. F. Renard, 1891, Deep-sea deposits: Challenger Expedition Report, London, 525 p.

(2) Bonatti, E. and Y. R. Nayudu, 1965, The origin of manganese nodules on the ocean floor, Am. J. Sci. 263, 17-39.

(3) Ku, T. L., and W. S. Broecker, 1969, Radiochemical studies of manganese nodules of deep sea origin, Deep Sea Res., 16, 625-637.

(4) Price, N. B. and S. E. Calvert, 1970, Compositional variation in Pacific Ocean ferromanganese nodules and its relationship to sediment accumulation rates, Mar. Geol., 9, 145-171.

(5) Bonatti, E., T. Kraemer, and H. Rydell, 1972, Classification and genesis of submarine iron-manganese deposits. In: Ferromanganese deposits on the Ocean Floor, ed. D. Horn, IDOE, Nat. Sci. Found., 149-165.

(6) Cann, J. R., D. K. Winter, and R. G. Pritchard, 1977, A hydrothermal deposit from the floor of the Gulf of Aden, Mineralogical Magazine, 41, 193-9.

(7) Hoffert, M., A. Perseil, R. Hekinian, P. Choukroune, H.D. Needham, J. Francheteau, X. Le Pichon, 1978, Hydrothermal deposits sampled by diving saucer in Transform Fault "A" near 37°N on the Mid-Atlantic Ridge, Famous area, Oceanologica Acta 1, 72-86.

(8) Scott, M. R., R. B. Scott, P. R. Rona, L. W. Butler, and A. J. Nalwalk, 1974, Rapidly accumulating manganese deposits from the median valley of the Mid-Atlantic Ridge, Geophys. Res. Lett., 1, 355-358.

(9) Piper, D. Z., H. H. Veeh, W. G. Bertrand, and R. L. Chase, 1975, An iron-rich deposit from the Northeast Pacific, Earth Planet. Sci. Lett., 26, 114-120.

(10) Klitgord, K. D. and J. D. Mudie, 1974, The Galapagos Spreading Center: a near-bottom geophysical survey, Geophys. Jour. Roy. Astr. Soc., 38, 563-588.

(11) Lonsdale, P., 1977, Deep tow observations at the mounds abyssal hydrothermal field, Galapagos Rift, Earth Planet. Sci. Lett., 36, 92-110.

(12) Williams, D. L., R. P. von Herzen, J. G. Sclater, and R. N. Anderson, 1974, the Galapagos spreading center: lithospheric cooling and hydrothermal circulation, Geophys. Jour. Roy. Astr. Soc., 38, 587-608.

(13) Corliss, J. B., J. Dymond, L. Gordon, J. Edmond, R. P. von Herzen, R. D. Ballard, K. Green, D. Williams, K. Crane, A. Bainbridge, Tj. H. van Andel, SCIENCE, (submitted).

(14) Sclater, J. G., and K. D. Klitgord, 1973, A detailed heat flow, topographic and magnetic survey across the Galapagos spreading center at 86°W, J. Geophys. Res. 78, 6951-6975.

(15) Von Herzen, R., K. Green, and D. Williams, Hydrothermal Circulation at the Galapagos Spreading Center, 1977, Geol. Soc. Amer. Abstracts with Programs, 9, 1212.

(16) Deep Sea Drilling Project, 1977, Glomar Challenger completes 54th Cruise, Geotimes 22, 19-22.

(17) Dymond, J., J. Corliss, G. R. Heath, C. W. Field, E. J. Dasch, H. H. Veeh, 1973, Origin of metalliferous sediments from the Pacific Ocean, Geol. Soc. Amer. Bull. 84, 3355-3372.

(18) Burns, R. G. and V. M. Burns, 1977, Mineralogy of ferromanganese nodules, in G. P. Glasby (ed.), Marine Manganese Deposits, Elsevier.

(19) Lyle, M. J. Dymond, and G. R. Heath, 1977, Copper-enriched ferro-manganese nodules and associated crusts from the Bauer Deep, Northwest Nazca Plate, Earth Planet. Sci. Lett., 35, 55-64.

(20) Goldberg, E. D., Koide, M., Schmitt, R., Smith, R., 1963. Rare earth distributions in the marine environment. J. Geophys. Res., 68, 4209-4217.

(21) Piper, D. Z., 1974, Rare earth elements in ferromanganese nodules and other marine phases. Geochim. Cosmochim. Acta., 38, 1007-1022.

(22) Bischoff, James L., 1972, A ferroan nontronite from the Red Sea geothermal system, Clays and Clay Minerals, 20, 217-223.

(23) Goodman, B. A., Russell, J. D., and A. R. Fraser, 1976, A Mössbauer and I. R. spectroscopic study of the structure of nontronite, Clays and Clay Minerals, 24, pp. 53-59.

(24) Stucki, J. W. and C. B. Roth, 1976, Interpretation of infrared spectra of oxidized and reduced nontronite, Clays and Clay Minerals, 24, 293-296.

(25) Stuki, J. W., Roth, C. B. and W. E. Baitinger, 1976, Analysis of iron-bearing clay minerals by electron spectroscopy for chemical analysis (ESCA), Clays and Clay Minerals, 24, 289-292.

(26) Rozenson, I. and L. Heller-Kallai, 1976, Reduction and Oxidation of Fe^{3+} in dioctahedral smectites --1: reduction with hydrazine and dithionite, Clays and Clay Minerals, 24, 271-282.

(27) Rozenson, I. and L. Heller-Kallai, 1976, Reduction and oxidation of Fe^{3+} in dioctahedral smectites--2: Reduction with sodium sulphide solutions, Clays and Clay Minerals, 24, 283-288.

(28) Harder, Hermann, 1976, Nontronite synthesis at low temperatures, Chemical Geology, 18, 169-180.

(29) Bonatti, E., D. E. Fisher, O. Joensun, and H. S. Rydell, 1971, Postdepositional mobility of some transition elements, phosphorous, uranium and thorium in deep sea sediments, Geochim. Cosmochim. Acta, 35, 189-201.

(30) Klinkhammer, G., R. F. Weiss, and M. Bender, 1977, Hydrothermal manganese in the Galapagos Rift, Nature, 269, 319-320.

(31) Glasby, G. P., Tooms, J. S., and Cann, J. R., 1971, The geochemistry of manganese encrustations from the Gulf of Aden, Deep-sea Research, 18, 1179-1187.

(32) Toth, John R., 1977, Deposition of submarine hydrothermal manganese and iron, and evidence for hydrothermal input of volatile elements to the ocean, unpub. M. S. thesis.

(33) Scott, Robert B., Rona, Peter A., McGregor, Bonnie A., Scott, Martha R., 1974, the TAG hydrothermal field, Nature, 251, 301-302.

(34) Moore, Willard S., and Peter R. Vogt, 1976, Hydrothermal manganese crusts from two sites near the Galapagos spreading axis, Earth and Planet Sci. Lett. 29, 349-356.

(35) Bonatti, E. and O. Joensuu, 1966, Deep-sea iron deposit from the South Pacific, Science 154, 643-645.

(36) Piper, D. Z., Veeh, H. H., Bertrand, W. G., and Chase, R. L., 1975, An iron-rich deposit from the northeast Pacific. Earth Planet Sci. Lett. 26, 114-120

(37) Burns, Roger G., and Virginia Mee Burns, 1975, Mechanism for nucleation and growth of manganese nodules, Nature, 255, 130-131.

(38) Wadsley, 1950, A hydrous manganese with exchange properties, J. Am Chem. Soc., 72, 1782-1784.

Table 1 Composition of Dredged Samples

Major Elements (%)	TB1	TB2	TB3	TB4	TB5	TB6	TB7	DM1	DM2	A1	A2	N1	N2	N3	N4	N5
Na	2.29	2.1	3.8	2.98	3.46	2.28	4.03	--	1.11	--	--	1.19	1.03	1.21	.09	.20
Mg	1.97	1.81	.85	1.42	.75	2.07	.67	--	.88	--	--	1.44	1.71	1.27	1.01	1.01
Al	.20	.27	.27	.01	.28	.16	.16	1.33	1.32	.09	.55	.01	.02	.26	1.12	.83
Si	.65	.92	1.2	.11	1.06	.91	.70	5.17	17.5	15.1	11.4	22.4	24.8	18.8	20.8	13.4
K	.55	.62	.32	.92	.36	1.17	.27	--	.46	--	--	1.74	1.86	.83	.64	.50
Ca	1.19	1.34	1.6	1.31	1.69	1.82	1.72	2.46	2.1	1.07	1.7	.49	.08	1.02	6.7	17.2
Mn	51.1	50.1	50.2	50.8	50.3	46.7	51.	22.6	15.1	7.29	8.41	.20	.18	.35	.34	1.14
Fe	.31	.33	.19	.03	.26	.57	.14	17.3	10.2	27.3	27.6	25.7	23.2	27.4	11.8	8.33
Minor Elements (ppm)																
Sc	.76	.97	.95	.18	.86	.54	.62	11.5	7.1	.48	1.8	.20	.19	.84	3.9	2.6
Cr	5.1	5.1	2.8	3.6	3.2	2.6	4.0	40.8	16.3	5.9	10.7	3.4	4.1	6.8	18.9	12.
Co	8.7	8.1	2.9	1.3	3.5	5.9	2.4	503.	247.	1.6	4.8	.35	.91	1.6	11.7	7.0
Ni	496.	850.	122.	76.	158.	1480.	103.	7770.	4540.	71.	54.	3.0	14.	27.	101.	58.
Cu	99.	186.	48.	30.	65.	264.	29.	400.	380.	36.	60.	2.3	8.0	2.9	152.	86.
Zn	301.	753.	245.	38.	163.	1070.	75.	774.	524.	150.	151.	28.	29.	55.	375.	244.
As	4.3	3.7	27.	40.	4.9	18.	2.5	180.	120.	59.	24.	5.2	2.9	11.8	2.1	1.0
Sb	32.	54.	9.	21.	20.	42.	5.5	23.	13.	8.1	3.9	1.3	.90	1.9	1.4	3.5
Ba	2490.	3160.	1230.	2310.	1530.	1300.	1000.	1440.	760.	320.	1090.	75.	68.	600.	1930.	2090.
Hf	--	.19	.10	.06	.15	--	--	11.	7.2	.19	.55	.11	--	.11	.68	.29
Th	.12	.14	.14	.02	.18	.09	.11	13.	7.7	--	.03	--	--	.12	.58	.55
Rare Earths (ppm)																
La	3.2	3.9	2.5	.8	3.1	3.7	1.8	175.	92.	6.8	6.6	2.9	2.2	5.2	5.3	4.6
Ce	3.4	4.4	1.8	1.0	2.5	1.5	1.3	207.	113.	--	4.2	2.9	2.3	2.2	4.8	4.2
Nd	.4	--	--	--	--	--	--	--	73.	--	--	--	--	--	--	--
Sm	.39	.43	.40	.07	.56	.75	.26	26.9	15.5	.61	.96	.66	.49	.54	1.2	.89
Eu	.16	.14	.12	.12	.10	.16	.09	8.6	4.3	.21	.32	.18	.15	.16	.25	.23
Tb	.08	.08	.07	.01	.07	.09	.06	5.4	2.7	.13	.16	.04	--	.05	.20	.14
Yb	.51	.70	.56	.22	.53	.66	.43	27.6	14.	--	.99	.38	.30	.83	1.2	1.2
Lu	.13	.17	.10	.05	.13	.17	.09	4.1	2.4	.09	.15	.03	.03	.20	.22	.16
Todorokite/ Birnessite	20.	2.	0.1	0.1	0.1	.01	< .01									

TABLE 2. Mineralogical Description of Samples

Sample	Dredge	T/8*	Mineralogy of Sample
TB1	5	20	Almost pure todorokite, very well crystallized, with slight amount of birnessite. There is a well defined 1.47 Å peak, not related to known todorokite or birnessite peaks (see note **)
TB2	5	2	Well crystallized todorokite with some birnessite. Possible nontronite and barite present. Well defined 1.47 Å peak appears again.
TB3	7	.1	Well crystallized birnessite with a minor amount of todorokite. 1.47 Å peak is well defined again, and 'associated' 1.82 Å and 2.15 Å peaks also are present.
TB4	3	.1	Well crystallized birnessite with a minor amount of todorokite. A small 1.47 Å peak is present.
TB5	5	.1	Well crystallized birnessite with a minor amount of todorokite. 1.47 Å, 1.82 Å, 2.15 Å peaks all again present.
TB6	3	.01	Almost pure birnessite, well crystallized, with very minor todorokite calcite and quartz.
TB7	7	< .01	Almost pure birnessite, well crystallized, with only hints of todorokite. 1.47 Å peak has returned in strength, and 1.82 Å, 2.15 Å peaks are again present.
DM1	4	-	Essentially pure δMnO_2, with minor quartz present. Slight hump at ~ 6.9 Å possible phillipsite or birnessite.
DM2	4	-	δ MnO_2 with slight amount of plagioclase.
A1	5	-	Generally X-ray amorphous, with slight amounts of birnessite and nontronite.
A2	7	-	Generally X-ray amorphous, but with slight amount of a plagioclase.
N1	5	-	Nontronite, very well crystallized. A strong 060 peak at 1.518 Å in the random mount shows that it is primarily a dioctahedral clay.
N2	5	-	Well crystallized nontronite, as in N1.

TABLE 2. continued

Sample	Dredge	T/B*	Mineralogy of Sample
N3	7	-	Almost pure nontronite, not quite so well crystallized as N1. Hint of birnessite.
N4	7	-	A mixture of calcite and fairly well crystallized nontronite.
N5	5	-	A mixture of calcite and fairly well crystallized nontronite.

*T/B refers to the peak area ratio of the 9.7 Å todorokite peak to the 7.2 Å birnessite peak.

**The 1.47 Å, 1.82 Å and 2.15 Å peaks resemble a synthetic Na-Mn mineral reported by Wadsley (38)

Table 3. Atomic Proportions and Site Occupancy of Montronite Assuming all Fe as Fe^{+3}

		N1	N2
Tetrahedral Layer	Si^{+4}	7.30	7.74
	Al^{+3}	.003	.007
	Fe^{+3}	.70	.25
		8.00	8.00
Octahedral Layer	Fe^{+3}	3.50	3.39
	Mg^{+2}	.54	.62
Interlayer	Ca^{+2}	.11	.02
	Na	.47	.39
	K	.41	.42
		.99	.83
	Interlayer Charge	1.10	.85

Figure Captions

Figure 1. Maps showing the location of the survey area, the distribution of the hydrothermal mounds (from Londsdale, 1977) and the tracks of the dredge hauls (Dredge 4 is located off the map at 0°25'N, 86°06'W).

Figure 2. Ultra slow scan X-ray diffraction patterns of three samples studied. Upper trace (DM1) is δ MnO_2, a basalt coating, dredged south of the mounds area, the middle scan (A2) is amorphous iron oxide from the sediment mounds, and lower scan (N1) is a very well crystallized nontronite from the mounds. Peaks labeled Zn are zinc backing used in the X-ray mount.

Figure 3. X-ray diffraction patterns of the ferromanganese sequence from the mounds. The upper trace (TB7) is nearly pure birnessite and the lower trace (TB1) is well crystallized todorokite with only traces of birnessite. Middle trace (TB4) is a sample containing significant portions of both birnessite and todorokite.

Figure 4. Ternary diagram of Fe-Mn-Si. The basalt crusts fall in the field of manganese nodules. The mounds samples show the strong fractionation of Mn into oxide phases and Fe into nontronite, the dilution of the pure Fe-rich nontronite samples with normal sediment, and the intermediate composition of the amorphous Fe-oxides between the Mn oxides and the purest nontronite.

Figure 5. Ternary diagram of Fe vs. Mn vs. (Co + Cu + Ni)X10 after Bonatti et al (5). The mounds samples fall in the hydrothermal field, the basalt crusts in the hydrogenous field.

Figure 6. Rare earth element abundances normalized to the rare earth element concentration in chondrites. The seawater abundances are from (20) ($X10^4$). The δ MnO_2 basalt coatings (DM) are strongly enriched in the REE relative to the hydrothermal mound samples.

Figure 7. (a) Cu vs. Ni and (b) Cu vs. Zn in Mn oxide crusts (TB) from the mounds showing strong correlation of Cu-Ni-Zn but no correlation of metal content with the mineralogy expressed as the todorokite/birnessite X-ray peak ratio. (T/B).

Figure 8. Ba vs. Ca in Mn-crusts from the mounds suggesting that Ba enters the todorokite lattice and Ca the birnessite lattice, as suggested by Burns and Burns (18).

Figure 9. Total dissolvable manganese in the water column over the mounds, compared to a profile free of direct hydrothermal influence. The Kamikazi samples are collected from 1 to 6 meters above the sediment-water interface. The samples were analyzed by G. Klinkhammer (30).

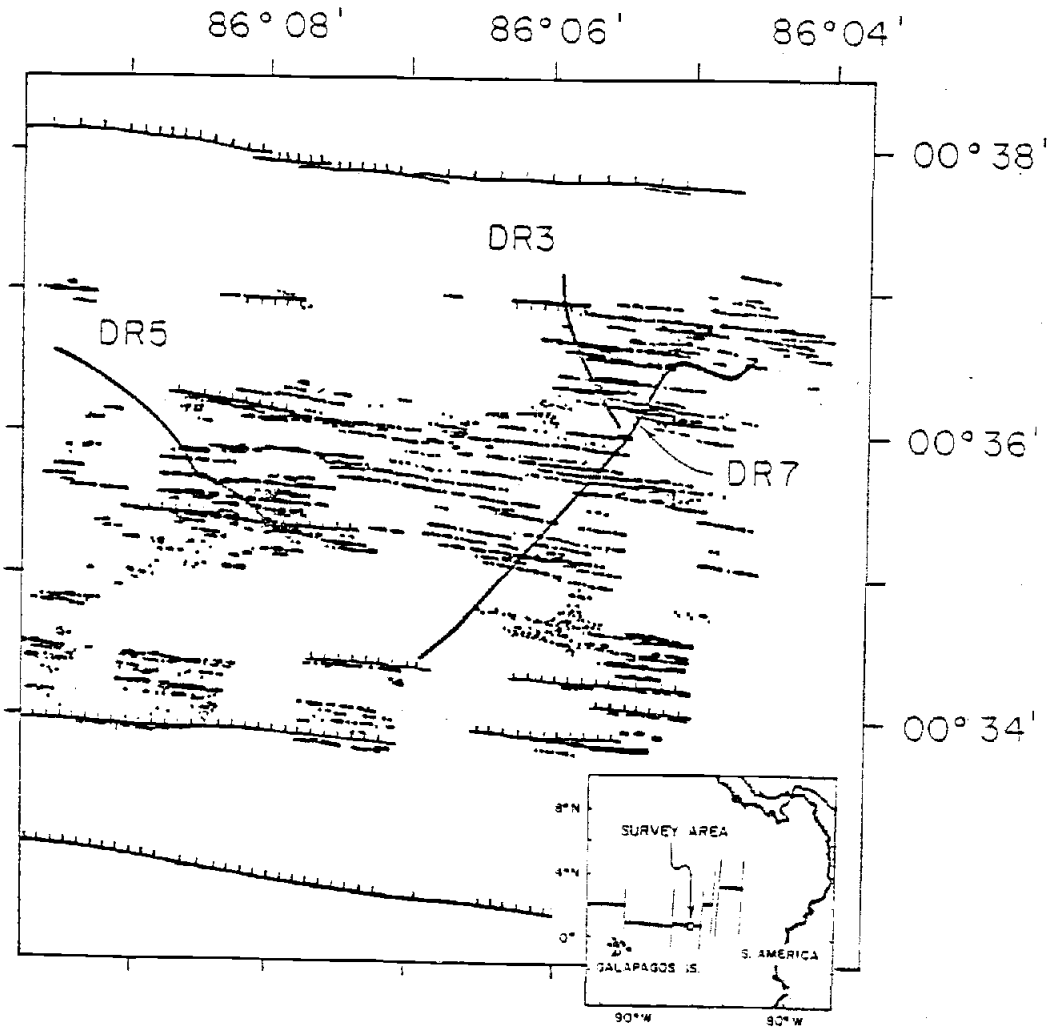
86°08'
86°06'
86°04'
00°38'
00°36'
00°34'
DR3
DR5
DR7
SURVEY AREA
GALAPAGOS IS.
S. AMERICA
90°W

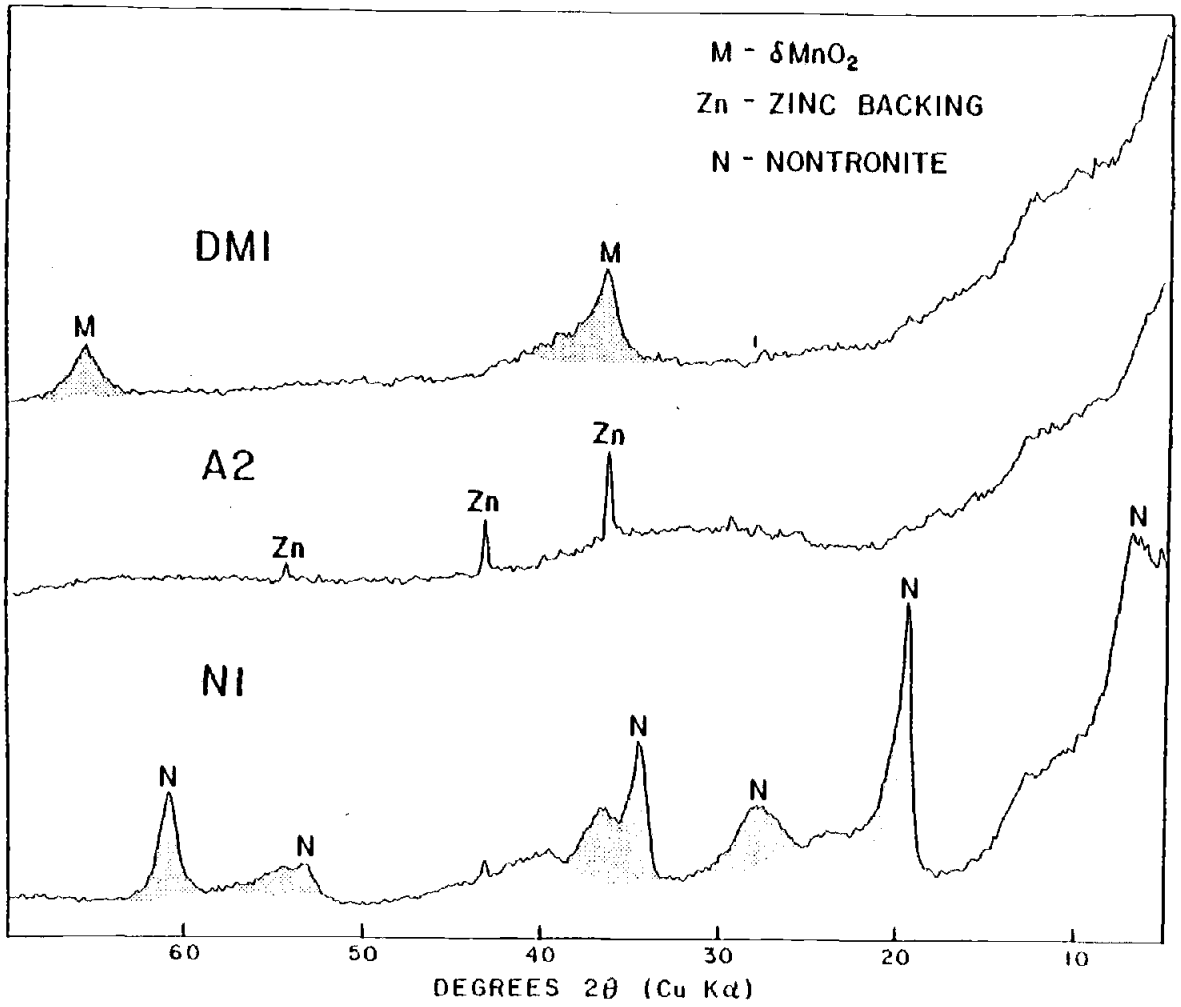
M - δMnO2
Zn - ZINC BACKING
N - NONTRONITE
DMI
M
M
A2
Zn
Zn
Zn
N
NI
N
N
N
N
60
50
40
30
20
10
DEGREES 2θ (Cu Kα)

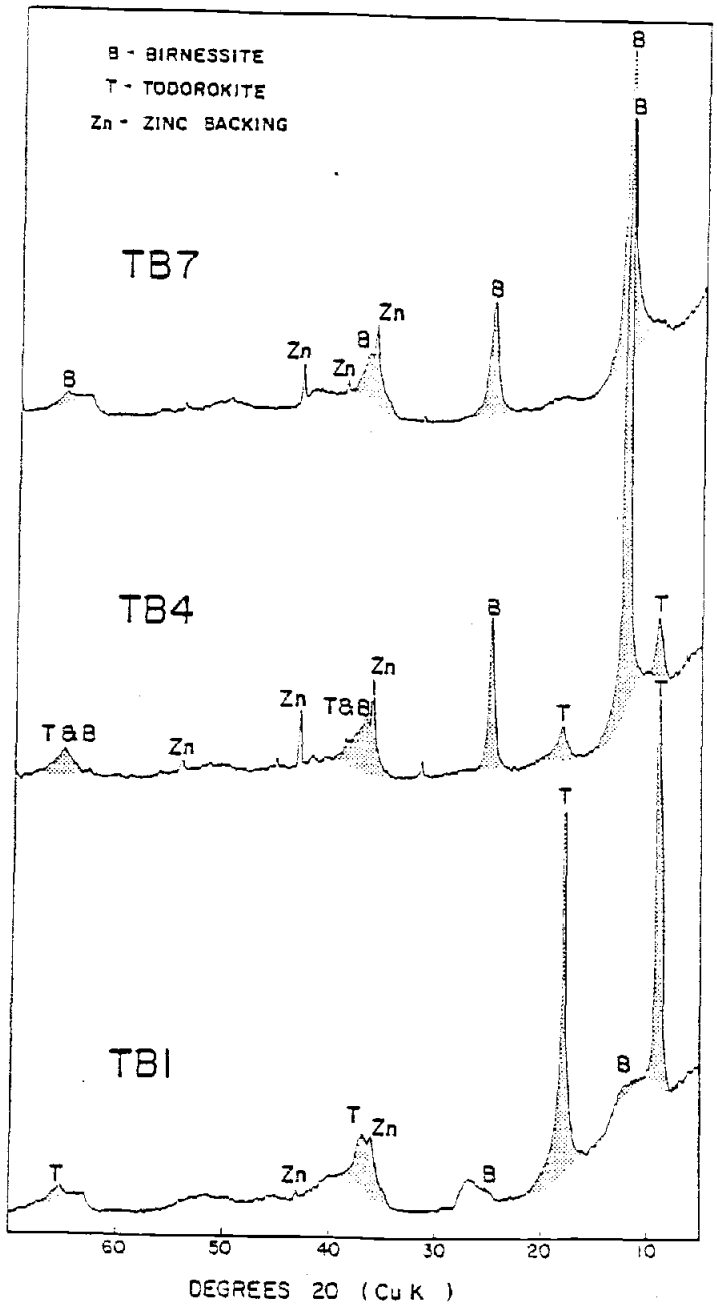
B - BIRNESSITE
T - TODOROKITE
Zn - ZINC BACKING
TB7
TB4
TB1
B
T
Zn
T&B
60
50
40
30
20
10
DEGREES 2θ (Cu K)

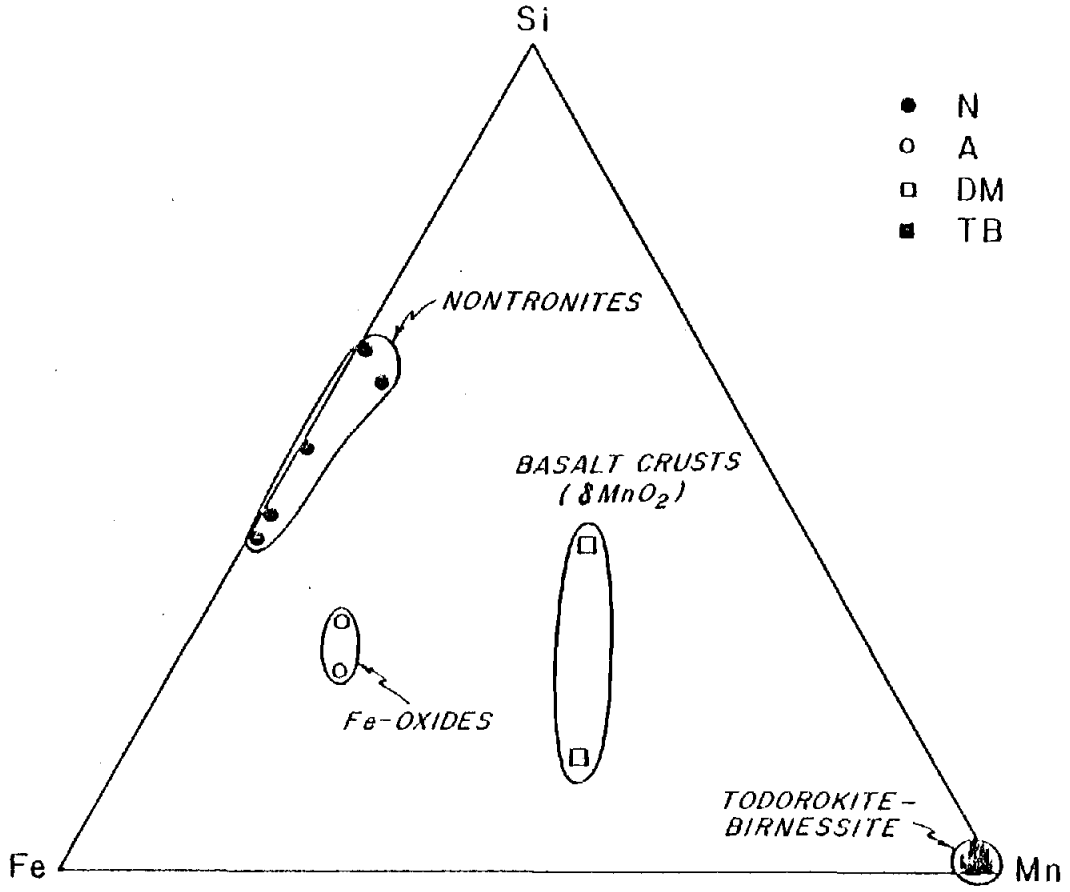
Si
N
A
DM
TB
NONTRONITES
BASALT CRUSTS
(δMnO2)
Fe-OXIDES
TODOROKITE-
BIRNESSITE
Fe
Mn

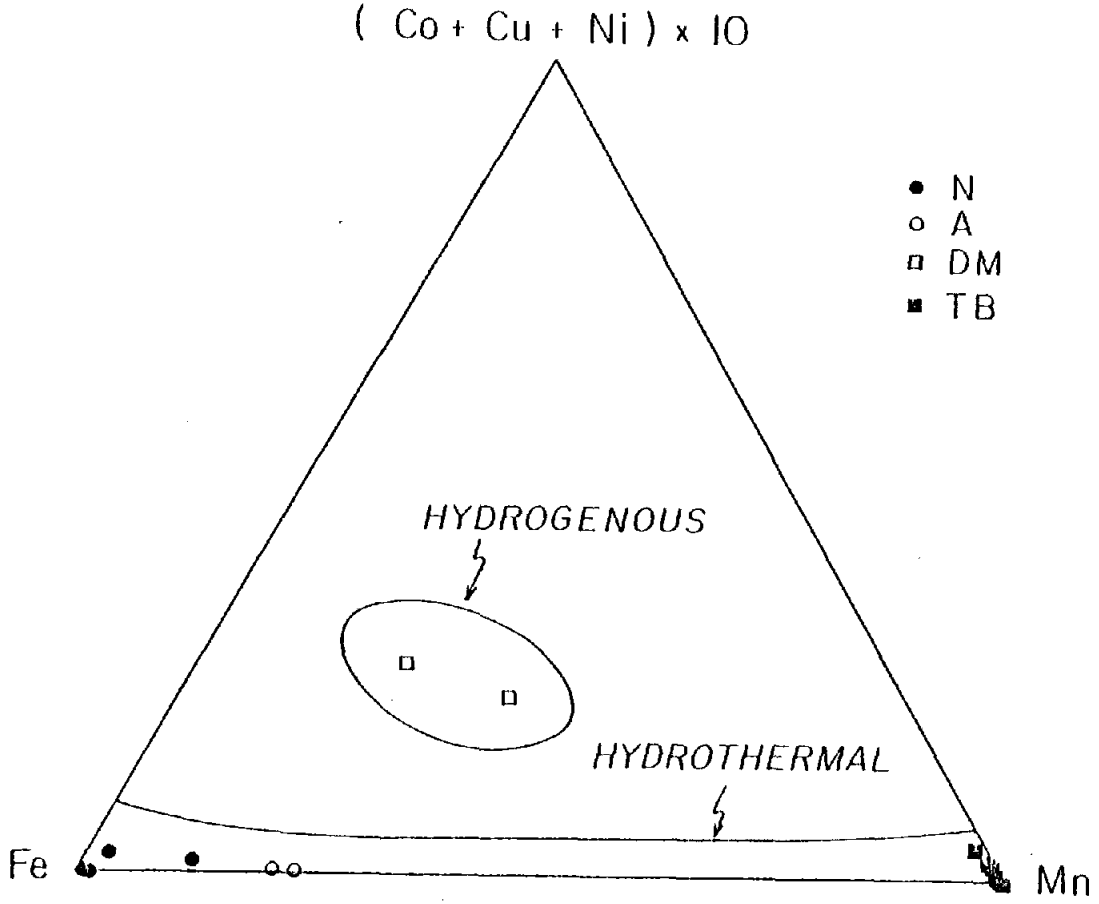
(Co + Cu + Ni) x 10
N
A
DM
TB
HYDROGENOUS
HYDROTHERMAL
Fe
Mn

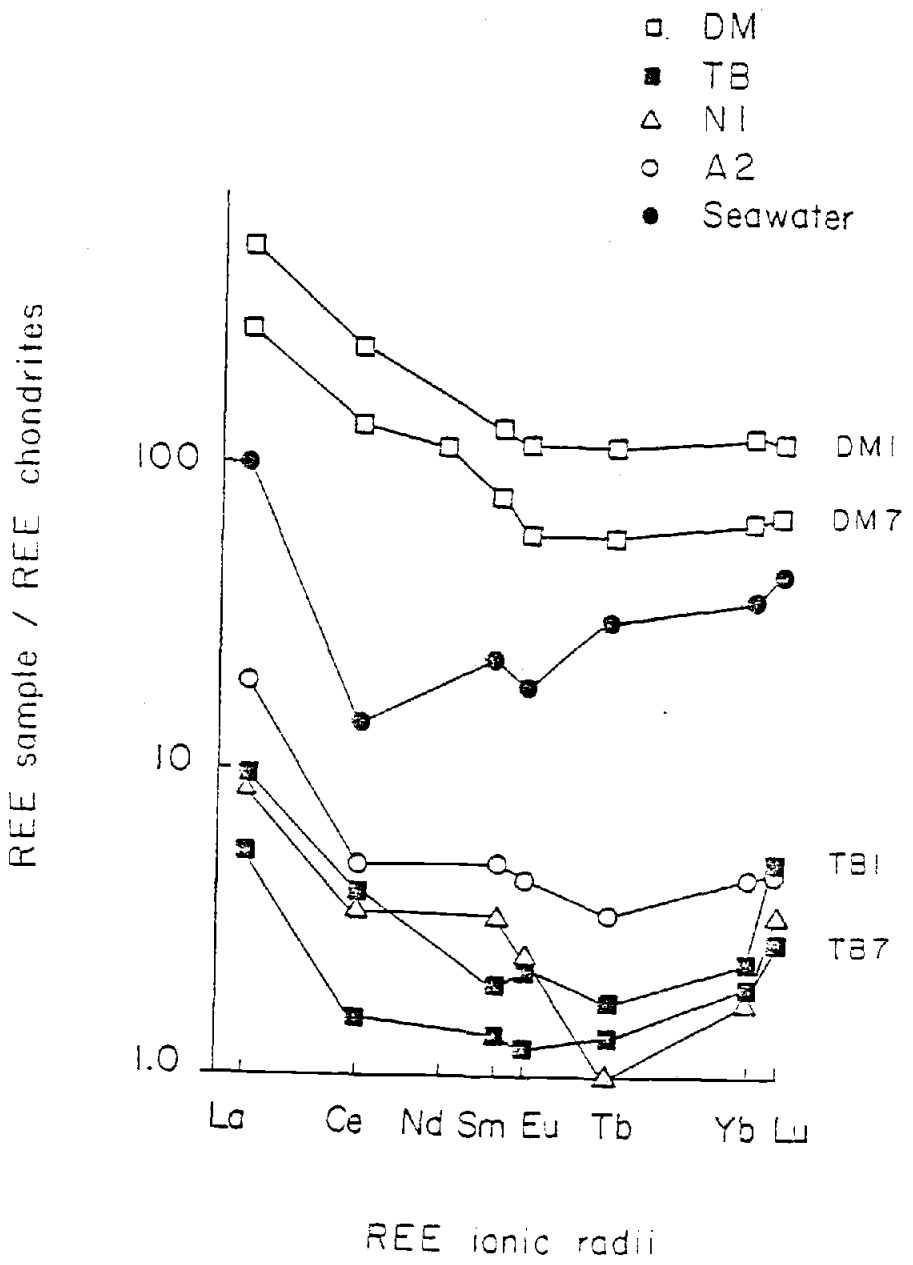
DM
TB
N1
A2
Seawater
REE sample / REE chondrites
100
10
1.0
DM1
DM7
TB1
TB7
La
Ce
Nd
Sm
Eu
Tb
Yb
Lu
REE ionic radii

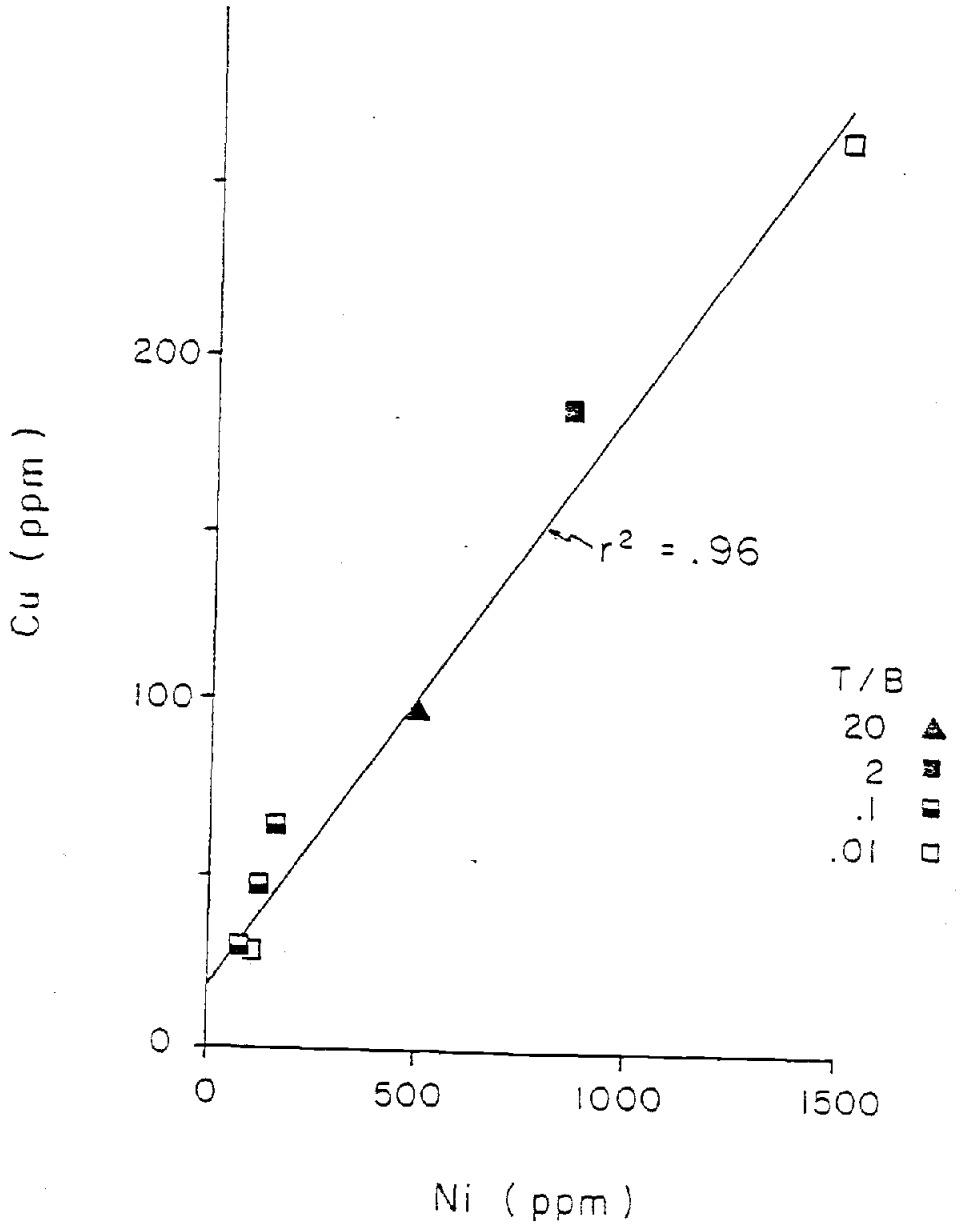
Cu (ppm)
200
100
0
0
500
1000
1500
Ni (ppm)
r² = .96
T/B
20
2
.1
.01

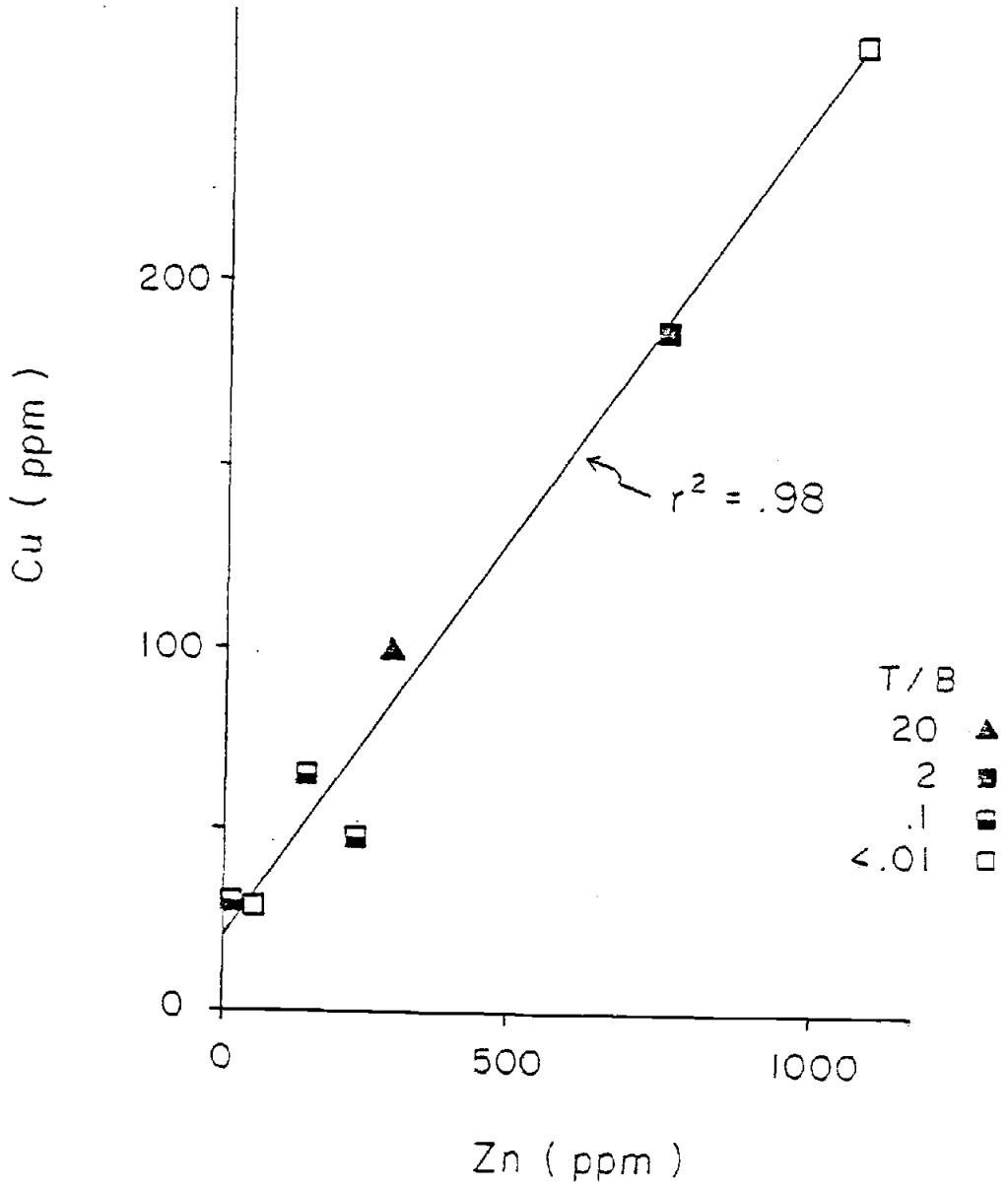
Cu (ppm)
200
100
0
0
500
1000
Zn (ppm)
r^2 = .98
T / B
20
2
.1
<.01

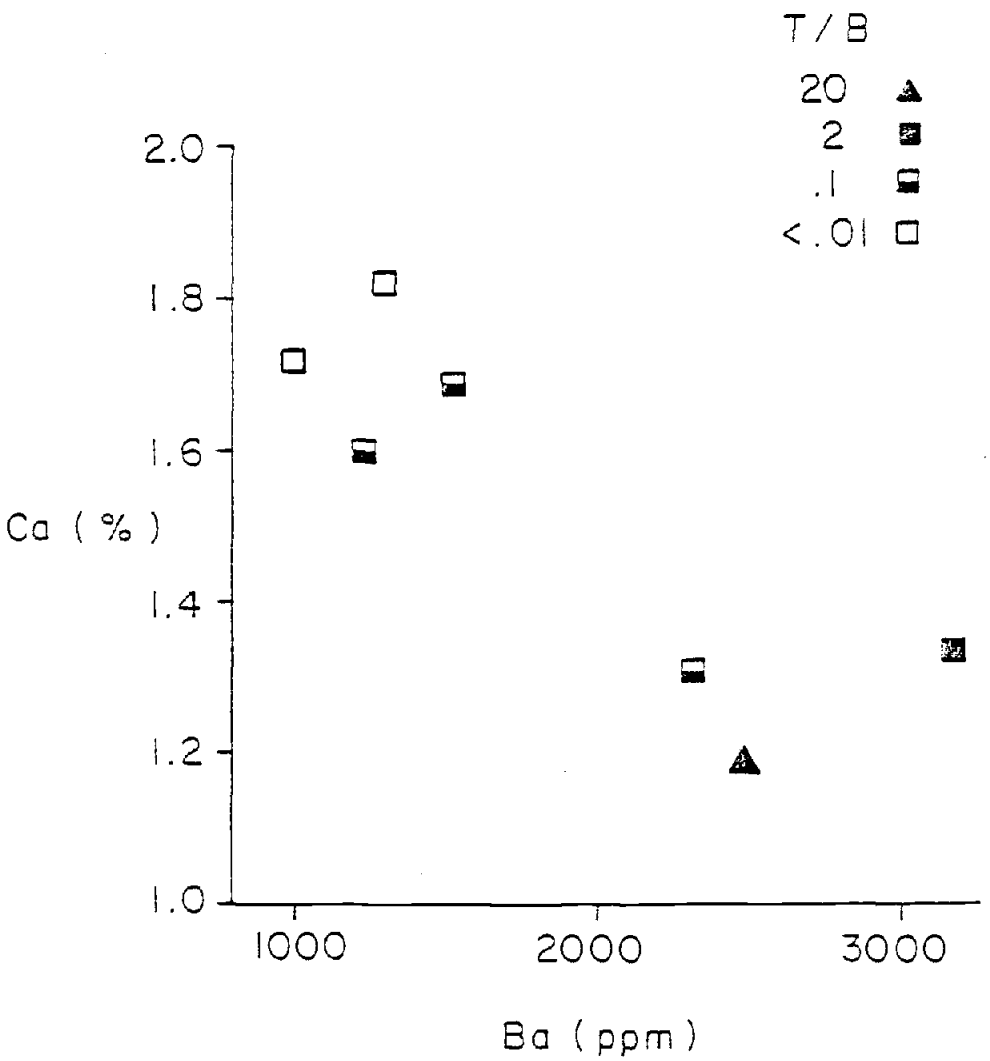
T / B
20
2
.1
< .01
2.0
1.8
1.6
1.4
1.2
1.0
Ca (%)
1000
2000
3000
Ba (ppm)

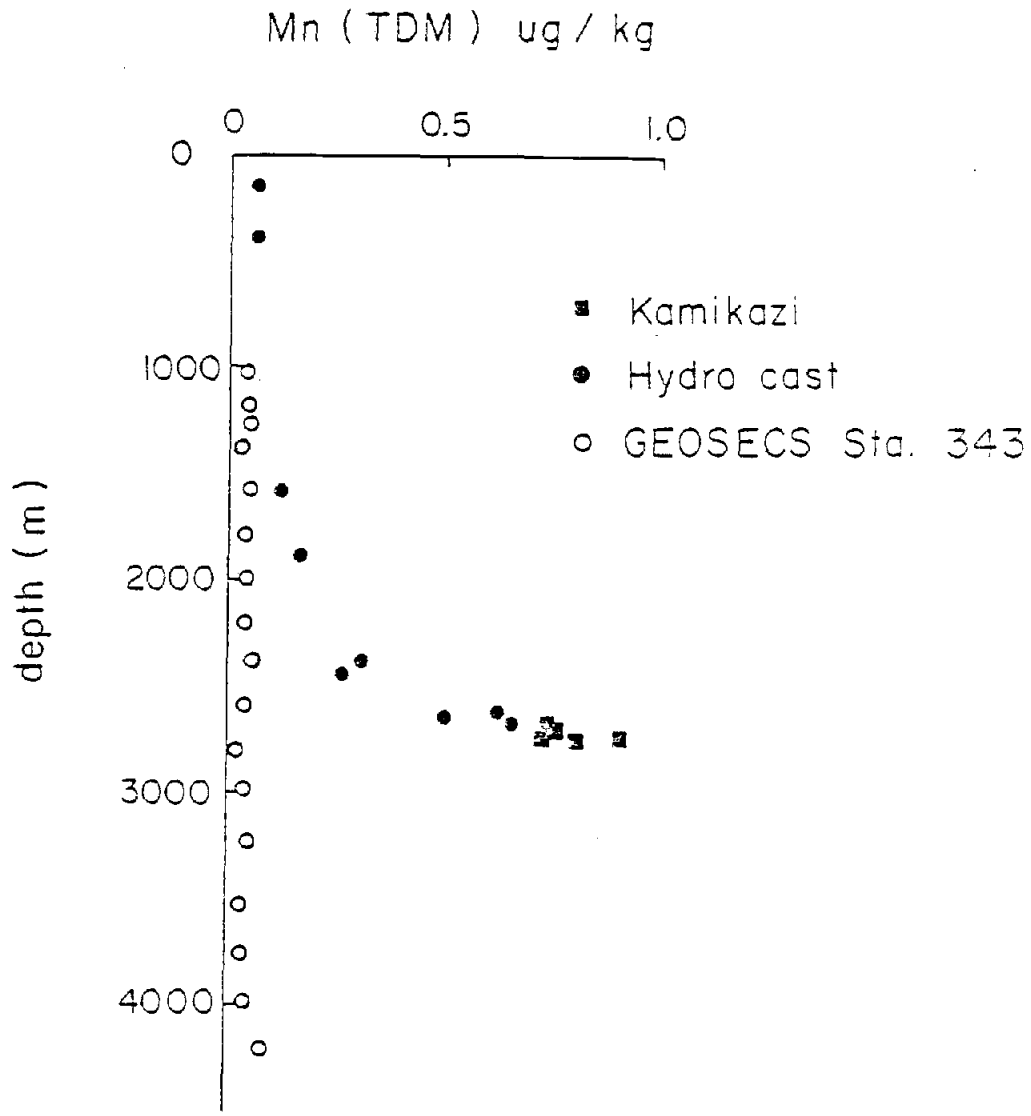
Mn (TDM) ug / kg
0
0.5
1.0
0
1000
2000
3000
4000
depth (m)
Kamikazi
Hydro cast
GEOSECS Sta. 343

APPENDIX 3

Ferromanganese Nodule, Fe-Mn Basalt Coating, and Sediment Coarse Fraction Descriptions

APPENDIX 3

Ferromanganese Nodule, Fe-Mn Basalt Coating, and Sediment Coarse Fraction Descriptions

Ferromanganese Nodules

Y71-9-86 5°05'S 90°47'W 3877 m

Nodule: 4 x 3 cm subspherical nodule, vary friable. Surface is grainy, botyroidal. No core can be distinguished, while thick indistinct layers can be seen.

>44 μ sediment fraction: Forams and other calcite microfossils abundant. Micronodules rare, even after acetic acid cleaning. All are growing inside radiolaria or are of the size to have done so. Radiolaria are abundant, with rare fish debris. Some of the radiolaria are Fe-stained.

C136 8°47'S 89°26'W 4252 m

Nodule: Small multicentered nodule, 3 x 1.5 cm. Smooth to slightly grainy surface. Two major cores, both nodule fragments; one minor core of altered basalt. Layering is well developed.

>44 μ sediment fraction: Original sediment red-brown. Large numbers of microfossil fragments, biotite flakes. Micronodules are about 20% of coarse fraction, small, subangular.

C151 8°58'S 86°22'W 4253 m

Nodule: Large ellipsoidal nodule, 6 x 3 cm. Surface very knobby, porous. Layering indistinct, no distinguishable core.

>44 μ sediment fraction: Micronodules ~10% of coarse fraction, generally small, rounded. Some are growing in radiolaria, others are of the size to fit in cavity. Larger micronodules are rare. Radiolaria are abundant - many Fe-stained or filled with smectite (?). Rare sponge spicules.

C141 14°55'S 87°43'W 4171 m

Nodule: Large subspherical ellipsoidal nodule, 4 x 7 cm. Botyroidal equatorial rim, smooth top, more grainy underside. ~1 cm^3 piele of

altered basalt forms the core of the nodule. Layering is distinct, smooth on upper side, botyroidal on the lower.

>44 μ sediment fraction: Micronodules ~25% of the coarse fraction, regular to botyroidal, small. Forams and foram fragments abundant, some Fe-stained or Si-replaced (do not dissolve in acetic acid). Radiolaria common. Phillipsite common but as an hedral to subhedral crystals.

C165 13°29'S 83°40'S 4634 m

Nodule: Large subspherical nodule, 4.5 x 6 cm. Upper surface smooth but grades to very grainy at the bottom. 'Equatorial' rim of botyroids about 2/3 of the distance of the upper surface. Layering indistinct, no observable core.

>44 μ sediment fraction: Many large micronodules, up to 2 mm, botyroidal. Smaller micronodules rounded. Micronodules ~20% of sample. Abundant radiolaria, common replaced forams, some of which are Fe-stained. Several large, orange, palagionitic grains ~5 mm, some with Mn veins. One greenish quartz grain, rounded. Two .5 km nodules picked out of the coarse fraction. Both were rounded.

C169 14°24'S 81°83'W 4634 m

Nodule: Large nodule, 6 x 4 cm. Originally spherical, but 1/2 broken away. Broken surface has been overgrown by new Mn precipitation. Indistinct top and bottom - upper surface smooth with large botyroids, lower surface grainy on large botyroids. Layering distinct, no observable core.

>44 μ sediment fraction: Micronodules consist of ~20% of this small sample. Radiolaria abundant, forams present, but all appeared Fe-stained and/or Si replaced. Micronodules are generally small, botyroidal to subrounded.

W7706-19 22°14'S 79°31'W 4416m

Nodule: Spherical nodule, 2 cm in diameter. Surface is grainy but competent. Small piece of altered basalt forms core, cross cut by Mn-oxide vein filling. Layering within the nodule is indistinct - has 'chrysanthemum' texture of small petal-like botyroids growing from the center.

>44 μ sediment fraction: Approximately 70% micronodules. There were nodule fragments in core, so some may be from nodule. About 90% of

the micronodules are rounded, however, Common quartz grains, common rock fragments, common biotite.

DM994 48°19'S 96°28'W 4540 m

Nodule: Multicentered nodule ~6 cm in diameter. The surface is smooth to grainy with botyroids ~1 cm in diameter. Multiple cores of altered basalt, up to 5 mm in diameter. FeMn-oxide layering is distinct.

>44 μ sediment fraction: Almost entirely forams in coarse fraction. Radiolaria are abundant in the acetic and cleaned sample, as well as large amounts of detrital material. Detritus includes large rounded quartz grains, rock fragments. Micronodules make up ~20% of cleaned coarse fraction. Most of them are rounded or botyroidal, but there are many angular ones. Occasional fish debris is seen. Miocene-pliocene boundary was seen at 240 cm in this core.

DM1006 38°08'S 125°21'W 4890 m

Nodule: Ellipsoidal multicentered nodule, ~5 cm. Surface is smooth, made up of botyroids ~1 cm in diameter. Large altered basalt core. FeMn oxides layering is distinct.

>44 μ sediment fraction: Micronodules make up ~80% of sample, mostly small, subrounded, but some are angular. Rare fish debris. Phillipsite (?) particles present. Si replaced forams and siliceous biogenic debris common. Rare sponge spicules.

DM981 22°40'S 160°47'W 4800 m

Nodule: Spherical nodule, 4 cm in diameter. Surface is grainy. The core is a ~1 cm multicentered nodule. Indistinct layering - shows 'chrysanthemum' texture as in W7706-19. Outer 5 mm is a dense Fe-Mn oxide, with no layering.

>44 μ sediment fraction: Micronodules are ~30% of the sample, generally small, angular to subrounded. Some reach 1 mm in size. Forams and foram fragments are common. Large phillipsite crystals, many of which are twinned, are also common. Yellowish phillipsite (?) aggregates and red-brown grains present. Occasional quartz grains, fish debris and sponge spicules are seen, as well as rare radiolarian.

Y73-3-20P 13°38'S 102°34'W 4396 m

Nodule: Subspherical nodule, 5 x 4 cm. Surface grainy, consists of small botyroids up to 1 cm in diameter. Layering inside indistinct, no distinguishable core.

>44 μ sediment fraction:

0-20 cm (Y73-3-20MGZ) - Small rounded to subspherical micronodules make up ~40% of the sample. Foram fragments and siliceous biogenic debris is common; many Fe-stained Si-replaced forams. Phillipsite (? yellowish-white subrounded grains) common. Rare whole radiolaria.

25-45 cm (Y733-20P) - Large nodule fragments ~5 mm in sieved sample. These were removed. Micronodules make up about 40% of coarse fraction. Large micronodules (or nodule fragments) more common. Foram fragments are present, rare whole tests. Fe-stained, Si-replaced foram tests common, sponge spicules, whole radiolaria, fish debris, are rare. There are some phillipsite laths.

160-180 cm - Micronodules are about 50% of the coarse fraction - some show evidence of layering. Large micronodules common, generally subrounded to botyroidal. Euhedral phillipsite crystals common, mostly twinned. Fe-stained, Si-replaced forams or casts of forams common. Fish debris is present.

260-280 cm - Micronodules are about 30% of the sample, are small and subrounded. Yellow phillipsite (?) grains common. Common Fe-stained, Si-replaced foram fragments; other biogenic debris is rare. Fish debris is present.

360-380 cm - Micronodules make up about 30% of the coarse fraction, are small to medium-sized, subrounded. Fe-stained, Si-replaced forams present. Fish debris present to common. Phillipsite (?) aggregates present. Occasional quartz grains seen.

440-460 cm - Micronodules make up about 20% of the coarse fraction; are small, subrounded. Fe-stained, Si-replaced forams common, fragments of sponge spicules common, phillipsite (?) grains present. Fish debris common to abundant.

510-530 cm - Forams and foram fragments abundant. After the acetic acid leach, micronodules make up ~10% of the sample. Some appear to be pseudomorphs of forams. Some Fe-stained, Si-replaced forams. Phillipsite (?) aggregates present, as are spicule fragments, fish debris.

650-670 cm - Forams and foram fragments are abundant. Micronodules comprise about 10-20% of acetic acid cleaned sample; are small to medium, subrounded. Phillipsite (?) particles present, replaced forams common.

680-700 cm - Forams and foram fragments are extremely abundant. Micronodules comprise ~10% of cleaned sample and tend to be larger, subrounded. Replaced forams and fish debris are common in the clean sample.

760-780 cm - Forams and foram fragments as well as other biogenic debris is abundant. Micronodules are about 20% of the acetic acid cleaned fraction. Fe-stained, Si-replaced forams are abundant in the cleaned fraction.

Ferromanganese Coatings on Basalt

FDRAKE 75 3-10-45 17°09'S 75°15'W 4911 m

5 cm thick ferromanganese crust on extremely altered basalt. Red-brown color, no distinct layering.

DM1028-3-2 to 4 21°07'S 80°50'W 2953 m

Dark brown-black ferromanganese coating, 3-5 mm thick growing on extremely altered basalt.

DM1016 25°24'S 98°47'W 3813 m

Black ferromanganese coating, 5-7 mm thick on white altered basalt (?). Coating is hard but very porous.

DM1011 33°00'S 109°30'W 4384 m

~1 mm thick brown-black coating on fresh basalt.

KK72-33-2 23°02'S 113°56'W 2285 m

~1 mm thick red-brown coating on fresh basalt.

APPENDIX 4

Chemical Compositions of Bulk Sediment, Oxalic Acid Leachable Fraction of Sediment, and Micronodules in Core Y73-3-20P

(Data for Chapter 2)

APPENDIX 4. Data for Chapter 2.
(ALL VALUES IN PPM.)

BULK SEDIMENT
COMPOSITION

NAME	MG	AL	SI	CA	SC	MN	FE	CO	NI	CU	ZN
Y73-20	18000.	25000.	120000.	73500.	24.20	43100.	116000.	220.	962.	957.	321.
25-45	19100.	26000.	116000.	52300.	25.40	47700.	123000.	226.	1110.	1040.	344.
61-80	21500.	29400.	133000.	20100.	28.90	48700.	135000.	258.	1070.	1140.	360.
160-90	19900.	27500.	122000.	23200.	25.90	68600.	156000.	263.	1340.	1330.	426.
260-80	20600.	24200.	116000.	25900.	22.50	62600.	180000.	248.	1230.	1250.	511.
360-80	22100.	26300.	144000.	32100.	21.10	46200.	142000.	221.	781.	976.	379.
440-60	29300.	9890.	146000.	46700.	8.92	28700.	135000.	86.	283.	794.	361.
510-30	15500.	5570.	80100.	190000.	5.23	15000.	74000.	50.	137.	457.	191.
650-70	10400.	3640.	77700.	285000.	4.11	14700.	64700.	40.	117.	430.	175.
680-00	6160.	1770.	18100.	334000.	1.37	4660.	21500.	13.	39.	152.	58.

LEACHABLE FRACTION
OF SEDIMENT*

Y73-20	9900.	6120.	13700.		40100.	55300.	260.	912.	652.	245.
25-45	10300.	6730.	17700.		45000.	58700.	260.	1100.	740.	348.
60-80	11400.	6460.	19300.		46700.	61400.	272.	1040.	794.	282.
160-90	9380.	3750.	13800.		65400.	61000.	277.	1450.	884.	268.
260-80	10400.	3130.	13200.		61300.	69200.	253.	1310.	731.	314.
360-90	9890.	2380.	10500.		46000.	50000.	213.	765.	566.	202.
440-60	12000.	1350.	9560.		27900.	34500.	99.	251.	291.	168.
510-30	6520.	768.	3880.		14200.	18400.	62.	130.	188.	79.
650-70	5760.	592.	7050.		13100.	14200.	48.	101.	162.	63.
680-00	2150.	239.	1840.		3490.	5550.	10.	24.	65.	32.

MICRONODULE
COMPOSITION

Y73-20	10400.	26100.	25700.	378000.	239000.	1090.	12700.	6960.	1880.
25-45	9950.	20900.	20400.	383000.	125000.	876.	13300.	7290.	1910.
160-80	11200.	16500.	11800.	384000.	104000.	741.	14400.	7750.	2420.
260-80	11300.	33000.	36300.	282000.	253000.	740.	11900.	6170.	1980.
360-80	14000.	32100.	33100.	285000.	243000.	1070.	5770.	5230.	3640.
440-60	18500.	26400.	61900.	351000.	311000.	540.	7050.	5070.	5040.
680-00	13700.	36900.	50200.	224000.	282000.	656.	2450.	3620.	1960.
760-80	12000.	51700.	43500.	152000.	184000.	293.	1900.	3210.	1320.

*Reported in mg of element leached/kg of original sample weight

APPENDIX 4 (CONTINUED)

BULK SEDIMENT COMPOSITION	AS	AG	SB	BA	LA	CE	ND	SM	EU	TB	YB	LU	HF	TH	U
Y73-20	56.8	9.55	9.3	16700.	151.0	78.0	168.0	29.20	7.99	5.41	26.20	3.97	4.69	4.41	2.38
25-45	76.5	12.80	10.3	16600.	152.0	80.8	192.0	29.70	8.25	5.68	25.10	4.07	4.99	4.14	3.12
60-80	104.0	9.32	11.3	20000.	182.0	96.9	139.0	36.50	9.69	6.75	31.40	5.08	5.74	5.43	3.38
160-180	152.0	14.20	13.9	17300.	184.0	85.1	205.0	34.30	9.33	6.29	32.20	5.01	4.41	3.26	4.05
260-280	226.0	11.90	16.8	12200.	141.0	62.9	158.0	31.30	8.45	5.91	33.60	5.20	4.94	2.18	4.30
360-380	124.0	15.60	11.0	16400.	299.0	53.9	204.0	31.30	8.80	6.58	34.50	5.61	4.01	2.56	3.50
440-460	56.5	10.60	6.3	10300.	104.0	30.7	129.0	15.10	3.99	2.37	12.80	2.06	1.24	1.11	2.38
510-530	26.9	7.30	3.1	5880.	54.4	14.8	61.0	7.94	2.22	1.25	7.18	1.15	1.07	.56	1.38
650-670	15.9	10.80	2.2	4920.	42.5	13.8	46.2	6.24	1.77	1.18	5.37	.86	.91	.56	.35
680-700	9.8	8.53	.9	1760.	18.4	4.6	20.7	2.11	.61	.47	2.28	.35	.21	.14	.55

SEDIMENT COMPONENTS	$CaCO_3$%	H_2O%	OPAL%[1]	QUARTZ%[1]	MICRONODULE%[1]
Y73-20	16.7	79.6	9.7	2.37	13.
25-45	11.3	80.7	9.8	2.34	12.
60-80	3.1	81.7	9.8	1.55	—
160-80	3.9	77.2	9.4	1.15	13.
260-280	4.6	76.1	9.4	.83	13.
360-380	6.2	79.2	14.8	1.09	7.0
440-460	9.6	83.0	19.6	1.18	6.8
510-530	46.3	74.3	25.0	1.21	—
650-670	50.1	72.6	25.4	1.40	—
680-700	83.6	50.7	20.3	1.60	1.5
760-780	55.5	66.4	—	1.47	—

[1]All reported as $CaCO_3$ and salt free percentages. Opal is estimated by the technique of Leinen (1977), quartz by X-ray diffraction analysis, and micronodule abundance is estimated by leach fraction abundance and composition.